Predictive Dynamic Simulation of Healthy Sit-to-Stand Movement

by

Valerie Theresa Norman-Gerum

A thesis
presented to the University of Waterloo
in fulfillment of the
thesis requirement for the degree of
Doctor of Philosophy
in
Systems Design Engineering

Waterloo, Ontario, Canada, 2019

Examining Committee Membership

The following served on the Examining Committee for this thesis. The decision of the Examining Committee is by majority vote.

External Examiner:	Katja Mombaur, Professor Institut für Technische Informatik Universität Heidelberg
Supervisor:	John McPhee, Professor Department of Systems Design Engineering University of Waterloo
Internal Member:	Jonathan Kofman, Associate Professor Department of Systems Design Engineering University of Waterloo
Internal Member:	Bryan Tripp, Associate Professor Department of Systems Design Engineering University of Waterloo
Internal-External Member:	Andrew Laing, Associate Professor Department of Kinesiology University of Waterloo

Author's Declaration

I hereby declare that I am the sole author of this thesis. This is a true copy of the thesis, including any required final revisions, as accepted by my examiners.

I understand that my thesis may be made electronically available to the public.

Abstract

This thesis situates itself at the intersection of biomedical modelling and predictive simulation to synthesize healthy human sit-to-stand movement. While the importance of sit-to-stand to physical and social well-being is known, the reasons for why and how people come to perform sit-to-stand the way we do is largely unknown. This thesis establishes the determinants of sit-to-stand in healthy people so that future researchers may investigate the effects of compromised health on sit-to-stand and then explore means of intervening to preserve and restore this motion. Previous researchers have predicted how a person rises from seated. However aspects of their models, most commonly contact and muscle models, are biomechanically inconsistent and restrict their application. These researchers also have not validated their prediction results.

To address these limitations and further the study of sit-to-stand prediction, the underlying themes of this thesis are in biomechanical modelling, predictive simulation, and validation. The goal of predicting sit-to-stand inspired the creation of three new models: a model of biomechanics, a model of motion, and performance criteria as a model of preference. First, the human is represented as three rigid links in the sagittal plane. As buttocks are kinetically important to sit-to-stand, a new constitutive model of buttocks is made from experimental force-deformation data. Ten muscles responsible for flexion and extension of the hips, knees, and ankles are defined in the model. Second, candidate sit-to-stand trajectories are described geometrically by a set of Bézier curves, for the first time. Third, with the assumption that healthy people naturally prioritize mechanical efficiency, disinclination to a motion is described as a cost function of joint torques, muscle stresses, and physical infeasibility including slipping and falling.

This new dynamic optimization routine allows for motions of gradually increasing complexity, by adding control points to the Bézier curves, while the model's performance is improving. By comparing the predictive simulation results to normative sit-to-stand as described in the literature, for the first time, it is possible to say that the use of these mod-

els and optimal control strategy together has produced motions characteristic of healthy sit-to-stand. This work bridges the gap between predictive simulation results and experimental human results and in doing so establishes a benchmark in sit-to-stand prediction. In predicting healthy sit-to-stand, it makes a necessary step toward predicting pathological sit-to-stand, and then to predicting the results of intervention to inform medical design and planning.

Acknowledgements

First, I acknowledge my supervisor, Professor John McPhee. For the last [redacted] years, John has been my primary source of technical consultation, feedback, and funding. I am most grateful for the times when John expressed faith in my abilities greater than my own: in pursuing a PhD, for example. He was also the one who insisted that I learn LaTeX to format this thesis and I would like to formally acknowledge that he was right — it looks better this way and I am glad that I made the change.

I have had the pleasure of meeting and sharing with many extraordinary people in the course of my PhD. There are two more Professors I must acknowledge for their substantial contribution to the growth of my research work. First, I wish to recognize Professor Andrés Kecskeméthy, my host during an exchange to the Universität Duisburg-Essen, who opened his lab and shared his time with me, allowing me to test my ideas about human motion prediction. Second, I wish to express my appreciation to Professor Steve Prentice, a researcher from the Biomechanics of Human Mobility Lab and a member of my committee for most of my degree, who helped me work through many of my questions about measuring and modelling human phenomena.

There are additional members of the Biomechanics of Human Mobility Lab that have supported my experimental data collection work; specifically, Professor Stacey Acker, Dave Kingston, and Tyler Chuang. I would also like to recognize Shu Jiang from the Statistical Consulting and Collaborative Research Unit for her guidance in analysing and interpreting my experimental results. I must also acknowledge my sister, Joanna, who acted as the patient participant while I piloted my experimental work.

As a long-time member of the Motion Research Group (the MoRG) I have had the privilege of working with many remarkable lab mates. I would like to acknowledge the members of the MoRG, past and present, who have challenged me and inspired me to do better work. I especially want recognize Matthew Millard, Thomas Uchida, Willem Petersen, and Mahdokht Ezati, who have each, in their own ways, enriched and broadened

my academic experience. Although she is not a member of the MoRG, but of the Digital Industrial Ergonomics and Shoulder Evaluation Laboratory, I am forever grateful to Tea Lulic-Kuryllo for her support as a gifted scientist and generous friend.

I am proud to share my research through this thesis and, for their help in transforming my ideas to text, I am thankful to Nicole Westlund Stewart and Nadine Fladd of the Writing and Communication Centre.

Finally, I would like to acknowledge my family and friends who have comforted me and emboldened me over these years. I especially want to thank David, who has read this thesis more times than any one person should, and cared for the home front while I concluded this work.

Dedication

To Frederick and Adelaide — two of my favourite people.

Table of Contents

Examining Committee Membership ii

Author's Declaration iii

Abstract iv

Acknowledgements vi

Dedication viii

List of Figures xiii

List of Tables xvii

1 Introduction 1

1.1 The problem, the challenge, and the approach 2

1.2 Contributions 5

1.3 Applications 6

1.4 Thesis Structure 8

2 Literature Review 10

2.1 Biomechanical descriptions of sit-to-stand 11

2.2 Biomechanical modelling for sit-to-stand . . . 18
2.3 Motion prediction in biomechanics . . . 24
2.3.1 Controls . . . 24
2.3.2 Performance criteria . . . 26
2.4 Previous work in sit-to-stand prediction . . . 27
2.4.1 Garner, 1992 . . . 28
2.4.2 Daigle, 1994 . . . 30
2.4.3 Domire, 2004 . . . 31
2.4.4 Ozsoy, 2014 . . . 32
2.4.5 Mombaur and Ho Hoang, 2017 . . . 33
2.4.6 Summary . . . 34
2.5 Conclusion . . . 38

3 Predictive Sit-to-Stand of a Three-Link Torque-Driven Model 41

3.1 Biomechanical model construction . . . 42
3.1.1 Model components and parameters . . . 42
3.1.2 Fixed foot implications . . . 44
3.2 Optimal control framework . . . 46
3.2.1 The controls . . . 47
3.2.2 Objective function construction . . . 50
3.2.3 Computation of optimal controls . . . 50
3.3 Resulting motion . . . 52
3.4 Comparison with healthy sit-to-stand . . . 54
3.5 Discussion . . . 58

4 Better Buttocks for Sit-to-Stand Simulation **61**

4.1 Mechanical behaviour of the buttocks . . . 62

4.1.1 Experimental procedure . . . 63

4.1.2 Experiment set-up . . . 63

4.1.3 Data processing . . . 64

4.1.4 Experimental results . . . 68

4.2 Characterizing the buttocks . . . 71

4.2.1 Constructing the model . . . 72

4.2.2 Parameter identification . . . 74

4.2.3 Statistical analysis . . . 78

4.3 Sit-to-stand prediction with better buttocks . . . 80

4.3.1 Comparison with the prediction using the Chapter 3 model . . . 81

4.3.2 Comparison with healthy sit-to-stand . . . 83

4.4 Updating the description of sit-to-stand . . . 85

4.5 Discussion . . . 87

5 Contributions of Muscles to Sit-to-Stand **90**

5.1 Modelling musculoskeletal geometry . . . 91

5.1.1 Musculoskeletal model mapping . . . 93

5.1.2 Geometric constraints and muscle wrapping . . . 93

5.1.3 Optimization of musculoskeletal geometry . . . 99

5.2 Optimal control framework . . . 104

5.2.1 The inverse muscle force approach . . . 104

5.2.2 Objective function construction for optimal sit-to-stand . . . 106

5.2.3 Computation of optimal controls . . . 107

5.3 Sit-to-stand prediction for a musculoskeletal model 109
5.3.1 Comparison with the prediction using the Chapter 4 model 110
5.3.2 Comparison with healthy sit-to-stand 112
5.4 Discussion 117

6 Conclusion **121**
6.1 Previous state of the field 121
6.2 Summary of thesis work 123
6.3 Contributions to the field 125
6.4 Recommendations for future research 126

References **129**

Appendix A Experiments Performed **149**

Appendix B Hyperelastic Spring Equations **154**

Appendix C Details of Musculoskeletal Geometry Optimization **159**

Appendix D Geometry of Wrapping a Cylindrical Constraint **178**

Appendix E The Routine to Determine an Optimal Sit-to-Stand **184**

List of Figures

2.1 Sit-to-stand angles of inclination. 13

2.2 Sit-to-stand joint angles. 14

2.3 Schematic of experimental set-up by Kralj et al. 17

2.4 Sit-to-stand event timings. 17

2.5 A planar link-segment model of a human body. 19

2.6 The dynamics of human motion. 20

2.7 Garner's human model. 29

3.1 A schematic of the three-link sagittal plane model while seated. 43

3.2 Free body diagram of the foot. 45

3.3 Three Bézier curves describing the initial motion paths. 48

3.4 The iterative routine to determine an optimal sit-to-stand. 51

3.5 Joint torques for optimal sit-to-stand from a 46 cm chair. 52

3.6 Optimal sit-to-stand from a 46 cm chair. 53

3.7 Evenly spaced snapshots of predicted sit-to-stand. 53

3.8 Sit-to-stand joint angle profiles as predicted from three chairs. 56

3.9 Maximum flexion angular velocity of the hip. 57

3.10 Predicted sit-to-stand event timing from three chairs. 57

4.1 The set-up of the sit-to-stand experiment. 64
4.2 Magnetic resonance image of buttocks while lying down and sitting. 66
4.3 Procedure of approximating the locations of the ischial tuberosities. 67
4.4 Average force profiles at the chair in the second leading to seat-off. 68
4.5 The buttocks deformed and undeformed. 69
4.6 Average deformation of the buttocks and velocity of the ischial tuberosities. 70
4.7 Average force-deformation and force-velocity behaviour of the buttocks. . . 71
4.8 Deformation of a spring. 73
4.9 Example effects of the elastogap model. 74
4.10 Experimental forces versus simulated forces from the buttocks models. . . . 77
4.11 Errors of the candidate buttocks models. 79
4.12 Force-deformation behaviour of the candidate spring models. 80
4.13 Evenly spaced snapshots of predicted sit-to-stand. 81
4.14 Optimal sit-to-stand from a 46 cm chair. 82
4.15 Joint torques for optimal sit-to-stand from a 46 cm chair. 83
4.16 Predicted sit-to-stand joint angles profiles. 84
4.17 Predicted sit-to-stand event timing. 85

5.1 Major flexors and extensors of the lower extremity. 91
5.2 Points describing musculoskeletal geometry initially. 94
5.3 Femoral reference frame for patellar pulley model. 95
5.4 Patellar pulley location assuming typical female skeletal geometry. 96
5.5 Patellar pulley models with pulleys of different radius. 97
5.6 Points, dimensions, and directions of interest when modelling muscle geometry. 98
5.7 Muscle moment arms. 100

5.8 The optimized musculoskeletal geometry. 103
5.9 The routine to determine a sit-to-stand for the musculoskeletal model. . . . 108
5.10 Evenly spaced snapshots of predicted sit-to-stand. 109
5.11 Optimal sit-to-stand from a 46 cm chair. 110
5.12 Joint torques for optimal sit-to-stand from a 46 cm chair. 111
5.13 Normalized predicted muscle forces compared to normalized EMG. 113
5.14 Predicted sit-to-stand joint angles profiles. 115
5.15 Predicted sit-to-stand event timing. 116

A.1 Experimental data flow. 151

B.1 Force-deformation behaviour of three hyperelastic springs. 157
B.2 Changes in force-deformation behaviour from changes in parameters. . . . 158

C.1 Musculoskeletal geometry initially and after grouping equivalent muscle units. 161
C.2 Iliopsoas moment arm from experiment and simulation. 165
C.3 Rectus femoris moment arm at the hip from simulation with a straight knee. 167
C.4 Rectus femoris moment arm at the knee from experiment and simulation. . 167
C.5 Vasti moment arm from experiment and simulation. 169
C.6 Hamstrings moment arm at the hip from experiment and simulation. . . . 170
C.7 Hamstrings moment arm at the knee from experiment and simulation. . . . 170
C.8 Gluteus maximus moment arm from experiment and simulation. 171
C.9 Tibialis anterior moment arm from experiments and simulation. 172
C.10 Gastrocnemius moment arm at the knee from experiment and simulation. . 174
C.11 Gastrocnemius moment arm at the ankle from experiments and simulation. 174
C.12 Flexor digitorum longus moment arm from experiments and simulation. . . 175

C.13 Tibialis posterior moment arm from experiments and simulation. 176

C.14 The optimized musculoskeletal geometry. 177

D.1 The minimum length path around a cylinder. 179

D.2 Points, dimensions, and directions of interest when wrapping a cylinder. . . 180

D.3 The geometry at a point of contact with the cylinder. 181

D.4 Relating the two- and three-dimensional wrap through similar triangles. . . 183

E.1 The routine to determine a sit-to-stand for the musculoskeletal model. . . . 185

List of Tables

2.1 Clinically relevant phases of sit-to-stand. 15

2.2 Joint ranges of motion. 22

2.3 Biomechanical characteristics of five sit-to-stand models. 35

2.4 Motion prediction characteristics of five sit-to-stand models. 36

4.1 Parameters of the four candidate spring models. 76

4.2 Comparison of event timings from two sit-to-stand experiments. 86

5.1 Musculoskeletal geometry. 101

5.2 Musculoskeletal geometry. Continued. 102

5.3 Musculoskeletal geometry. Concluded. 103

A.1 Summary of participant information. 150

C.1 Evidence or prior modelling of anatomical obstacles. 162

C.2 Iliopsoas geometry optimized 165

C.3 Rectus femoris geometry optimized 166

C.4 Vasti geometry optimized 168

C.5 Hamstrings geometry optimized 169

C.6 Gluteus maximus geometry optimized 171

C.7 Tibialis anterior geometry optimized 172
C.8 Gastrocnemius geometry optimized 173
C.9 Flexor digitorum longus geometry optimized 175
C.10 Tibialis posterior geometry optimized 176

1

Introduction

The goal of this thesis is to predict healthy sit-to-stand. Sit-to-stand (STS) is the everyday motion used to change from a seated position to a standing one. It is so prevalent in daily life that community-dwelling adults perform in excess of 40 STSs, on average, per day [1].

STS has a direct impact on quality of life and, as an aspect of functional mobility [2], is required to perform actions of daily living [3]. However, it may not be until STS becomes physically or cognitively challenging that the significance of this motion is recognized. Regardless of the reason for reduced ability, perhaps due to the effects of injury, illness, or aging, difficulty performing STS is common, especially in an aged population. It was reported in the Rotterdam Study that 30% of men and 45% of women aged 55 years and older experience moderate to severe disability in rising [4]. This is particularly concerning because difficulty performing STS negatively impacts health and well-being and is associated with decreased mobility, decreased balance, increased fall-risk, increased immobility-related disease, and increased institutionalization [5–7].

STS is an important skill to be able to perform. It is worthwhile to be proactive about maintaining STS for as long as possible and to work to develop or re-establish this skill if it is absent. In terms of promoting STS, physical therapy, assistive devices, and/or arthroplasty may be indicated. While it is possible to perform clinical studies to

examine how these interventions affect STS, it may prove more economical and, in a patient population, compassionate to perform preliminary testing in simulation. This motivation speaks to a long-established goal of simulation in biomechanics: to be implemented as a tool fundamental to the design of implants, surgeries, and rehabilitation programs [8–10].

Accurately anticipating how a patient will respond to physical therapy, surgery, an assistive device or other changes to their environment remains a "holy grail" of biomechanical simulation [11,12]. When a natural phenomenon such as motion adaptation to an intervention can be predicted through modelling and simulation, it is conceivable to test and tune interventions "in silico". However, before predicting motion with an intervention it is prudent to first predict the motion without. In a similar vein, before predicting pathological motion it is sensible to predict the motion without pathology. Thus, the goal of predicting healthy STS became the first and central focus of this thesis.

1.1 The problem, the challenge, and the approach

The future of medical intervention design and planning lies in the gap between simulation and experimentation. A big-picture goal of predictive biomechanical simulation is to augment the subjective implicit models used by design and medical professionals with objective models based in physics and physiology. Together, the information from these models should give the professional a more complete understanding of design and/or treatment options and position them to make decisions for better patient outcomes. The most significant barrier to this goal, at this time, is the lack of validation of model-based results [11]. This is the gap that needs to be filled: the unknown disparity between simulation results and potential human results. In a simulation aiming to predict the effect of intervention on pathological STS, it should be foundational to validate that healthy STS is predicted when models of pathology and intervention are removed. However, as will be elaborated in Chapter 2, there are not validated models of healthy STS prediction. The lack of validated

predictions of healthy STS is impeding progress toward predicting pathological STS and the goal of predicting outcomes of interventions.

Predicting healthy STS and validating the results requires the development of new perspectives and new descriptions of human motions and human models and their integration with existing research. Each of these areas — validation, motion prediction, and biomechanical modelling — bear key challenges in STS prediction research. One of the challenges is that result validation is practically impossible because the STS motion does not enjoy a commonly-accepted normative description (i.e. a description establishing the norm of this motion). In gait research, for example, it is the seminal works of Murray [13] and Winter [14] that are cited as the normative biomechanics against which observed gaits are measured. In contrast, the definition of STS in a given study depends greatly on the aim of the study [7], and often differs substantially from one study to the next. In fact, as of 2016, the published biomechanics literature contains at least 9 ways of defining each the beginning and end of STS [15]. The absence of a universal standard impedes communication of ideas and sharing of STS information within the biomechanics community and makes it difficult to objectively discuss what is and what is not healthy STS. This thesis addresses this challenge in two ways: first, by collecting STS data and updating an existing normative description of STS, and second, by comparing STS predictions to descriptions of STS from the literature.

The next challenge is that motor skill acquisition, including STS learning and adaptation, remains a mysterious phenomenon. Although there are theories of motor learning, the most popular being Adams' *closed-loop theory* and Schmidt's *schema theory*, they rely on the foundation of a pre-existing movement pattern [16]. The process by which novel skills are naturally learned (i.e. how the pre-existing movement pattern has come to be) is not explained in its entirety [16,17] and therefore it is a consequential challenge to describe such a mechanism *in silico*. Because optimal control can be used for hypothesis testing, it is a valuable tool in motion prediction where so much is unknown. A last challenge is

that the mechanical component of this research is based in the complex and dynamic human system. The overarching goal of biomechanical modelling and simulation is to create more accurate representations of the human body applicable for analysis of the variables of interest. This means simplifying the human system to abstractions of its nature. It includes measuring behaviours and parameters of interest when reasonable, and inferring what remains. Modelling for STS is particularly challenging because it is a demanding task characterized by large ranges of motions and large tissue deformations. It is because of the challenges of this project that the research in this thesis is motivated by physiology and medicine, propelled by optimization, and centred in modelling and simulation of multibody biomechanical systems.

With the goal of predicting healthy STS, this thesis focuses on the opportunities at the intersection of biomechanical modelling and predictive simulation. Specifically, the foci are: building validated models for STS prediction, developing STS prediction routines, and comparing resulting motions to normative STS. The biomechanical modelling work completed as part of this thesis spans multiple disciplines. First, a set of Bézier curves, which seem well suited to predictive biomechanical simulations, were used to geometrically model human motions. Next, a rigid, three-link sagittal plane model was constructed for representing the skeletal system, as is seen elsewhere in STS prediction research. Then, a constitutive force-deformation relationship, determined from experiment, was developed for modelling the buttocks-chair contact. Last, optimization was used to refine the geometry of the musculoskeletal system for consistency with previous studies of human anatomy and physiology. This thesis also includes modelling in the optimal control problem for predicting STS. The STS prediction routine designed in this thesis is based on iteration and optimality, and is purely predictive. With the assumption that healthy people naturally prioritize mechanical efficiency, disinclination to a motion is described as a cost function of joint torques, muscle stresses, and physical infeasibility including slipping and falling. Comparing results from these models in the optimal control routines to healthy

STS throughout this thesis makes the differences between simulation and experimentation known. Analysis and synthesis of data from clinical, kinematic, and kinetic studies formed the basis of understanding of healthy STS. Further insights were gained from experiment and used to update the definitions of normative STS. This research in modelling, predictive simulation, and validation endeavours for harmony with the nature of human movement and, as such, the models and predictions made within this thesis are powerful for application to healthy STS and scalable for future research.

1.2 Contributions

The primary aim of this thesis is to synthesize a healthy STS motion pattern. In achieving this goal, significant contributions to the fields of biomechanical modelling and predictive simulation of STS are made in four main areas: validating STS predictions, modelling the biomechanics of STS, geometric modelling of the musculoskeletal system, and proposing a dynamic optimization routine for STS prediction. Gains are made in STS prediction validation, first in the exercise of comparing predicted motions to normative STS data in the literature for the first time, thereby establishing a benchmark for future work in STS prediction, and second in updating definitions and timing of STS events for the purpose of describing healthy STS. Advancements are also made in biomechanical modelling for STS; these are elaborated next. First, this thesis describes the most comprehensive planar model of a female human in STS prediction. For the first time, the buttocks model used in this STS prediction work was characterized by measured STS force-deformation buttocks behaviour. Also, the implications of fixing the feet to the ground in STS prediction was acknowledged by describing disinclination to a motion as a cost function of physical infeasibility including slipping and falling, for the first time. Contributions are also made to musculoskeletal modelling: first in the extension of the patellar pulley model proposed by Brand et al. [18] to greater ranges of motion and greater dimensionality, and second in the creation of a

validated model of musculoskeletal geometry for the deLeva [19] female anthropometric data set. The final contribution is in proposing a dynamic optimization routine for STS prediction. Implementation of the new models and new optimal control strategy together in this thesis produces gross motion patterns characteristic of healthy STS when compared with normative data from the literature.

1.3 Applications

Portions of research accomplished in this thesis are directly applicable in many fields. For example, the updated description of STS, presented in Chapter 4, is immediately relevant to clinicians or researchers interested in the STS motion. Also, the validation results of the STS predictions in this thesis should be used when discussing work in STS prediction. Outside of validation, the biomechanical models built as part of this thesis are a benefit to researchers interested in modelling a female subject, modelling the primary flexors and extensors of the lower extremities, and/or modelling buttocks vertical force-deformation behaviour, for example.

As a whole, the research accomplished in this thesis is intimately applicable to further studies in healthy STS prediction. Given a hypothetical scenario, for example, selecting the seat height of a replacement chair, a biomechanist (or physiotherapist, or patient, etc.) may want to know, "Will the chosen seat height affect chair rise strategy?" This question could be explored through motion prediction, as in Chapter 3. There are many parameters of the human and chair models constructed in this thesis that may be modified to investigate their influence on predicted STS. Hypotheses do not necessarily need to be in regards to motion outcomes, either. Theories of why people choose (consciously or not) given motion patterns can also be explored through motion prediction [20] and this thesis has established an amenable infrastructure for this flavour of research.

A natural progression of this thesis work will be in adjusting the models to alter the health of the subject and predict the effects of these changes on STS. As mentioned previously in this Chapter, the ability to perform STS can be compromised for many reasons. Commonly cited pathologies are: arthritis [1,21–24], low-back pain [25], obesity [26], paralysis [27, 28], Parkinson's disease [29–32], and stroke [7, 33–39]. An aspect of arthritis, for example, may be incorporated in the model by increasing joint stiffness so that the STS predicted may be more representative of that of a patient. Alternatively, or possibly concurrently, the model of preference may be adjusted, for an arthritic population, to prioritize motions that reduce joint loading.Should the model of motion prediction be generally applicable to motion adaptation, which is hypothesized, it will be possible to use these models when investigating the progression of or pathology.

Once progression of pathology may be predicted, it should also be possible to predict how motion patterns may adapt in response to a therapeutic intervention. Available and anticipated interventions supporting STS take a variety of forms from general strength training [24, 36] to targeted physical therapy [10, 32, 38, 39], from grab bars [40] to non-powered orthoses [41] to joint replacements [42,43], functional electrical stimulation [28,44–47] mechanical lifts [48,49], or powered orthoses [50–52]. STS prediction will be influential in the design and planning of these interventions both for general clinical populations and for patient specific cases. As opposed to the previous example of chair selection, consider instead an orthopaedic surgeon considering a new surgical technique for a patient with a unique presentation. Motion prediction could provide the surgeon with information about how different prospective treatment plans will affect the patient's mobility outcomes in the short and long term, prior to intervention. This is the future of this thesis work, accurately anticipating how a patient will respond to physical therapy, surgery, an assistive device or changes to their environment.

1.4 Thesis Structure

This thesis includes six body chapters, described in this Section. The first chapter is this Introduction. Next is Chapter 2, a Literature Review. These are followed by Chapters 3, 4, and 5 which focus on the design of the biomechanical model and STS optimal control problem. The last chapter, Chapter 6, is the Conclusion.

Chapter 2 has a strong focus on synthesis. First, clinical, kinematic, and kinetic descriptions of STS are investigated, forming an aggregate description of STS that is referred to throughout the remainder of this thesis. Next, context is provided for the few bodies of work focusing on predicting healthy STS. Then, the key areas of research of this thesis, biomechanical modelling, predictive simulation, and validation, are identified.

In Chapter 3, a motion pattern imitating STS is synthesized and compared to normative descriptions of healthy STS. First, the human is represented as three rigid links in the sagittal plane. Second, candidate STS trajectories are described geometrically by a set of Bézier curves. Third, disinclination to a motion is described as a cost function of joint torques, with the assumption that healthy people naturally prioritize mechanical efficiency. Using these torque-driven models and optimal control strategy together produces gross motion patterns characteristic of healthy STS.

In Chapter 4, a constitutive model of the buttocks is defined from experimentally collected data. This visco-hyperelastic buttocks model is included in the biomechanical model and replaces the simple linear spring-damper model used in Chapter 3. Beyond supporting construction of the buttocks model, results of the experiment indicate that healthy young adults complete STS significantly faster than has been reported in the literature and, consequently, modifications to the normative description of STS are proposed.

In Chapter 5, a model of musculoskeletal geometry is constructed for the primary STS muscles in the deLeva [19] female anthropometric data set. These muscles are added to the biomechanical model of Chapter 4, although muscle dynamics are not included.

Maintaining the assumption that healthy people naturally prioritize mechanical efficiency, disinclination to a motion is described as a cost function of joint torques *and* muscle stresses. Using these new models and the new optimal control strategy together produces gross motion patterns *and* normative events characteristic of healthy STS.

Chapter 6 concludes this thesis. It summarizes the research achieved and recommends prospective research supported and motivated by this work.

2

Literature Review

This Chapter is a review of the existing literature in experimental biomechanics, modelling, and predictive simulation relevant to sit-to-stand (STS). Biomechanical systems modelling is an active research area. There were, for example, more than 20 presenters at the 2017 Symposium on Computer Simulation in Biomechanics [53]. Some biomechanists work in the area of predictive simulation, however works specific to STS are few and works focusing on understanding healthy STS are rare. Therefore, many of the ideas discussed in this Chapter are being presented in the context of STS for the first time as it was necessary to make connections to more developed areas of research to provide sufficient context to this thesis. And, as biomechanical modelling and simulation is a diverse field, research from a variety of disciplines including physical therapy, orthopaedics, rheology, nonlinear dynamics, and control theory are examined.

The two main goals of this Literature Review are: (1) to provide detail on the theories and existing research that have inspired the work in the remainder of this thesis, and (2) to provide context for the motivation of this thesis in terms of filling gaps in the literature and advancing knowledge in these areas. Specifically, the gaps that will be addressed are the lack of female models in the STS prediction research (when it is females who report the most difficulty in STS), the lack of validation in STS prediction research, the lack of

suitable buttocks models for STS prediction, and deficiencies of existing musculoskeletal models for this application.

There are five sections to this Literature Review. Section 2.1 describes the STS motion through three lenses: clinical, kinematic, and kinetic. The definition of STS developed in this Section is referenced as the standard of healthy STS motion throughout this thesis. Section 2.2 provides a brief review of biomechanical modelling. In this Section, the major challenges in adapting biomechanical models popular in gait analysis, for example, to STS are discussed as well as models and modelling strategies that will be used to build the rigid-link model of Chapter 3, the buttocks model of Chapter 4, and the musculoskeletal model of Chapter 5. Section 2.3 reviews motion prediction work in biomechanics, and identifies preferred control strategies and popular performance criteria. It motivates the descriptions of the optimal control problems in Chapter 3 and Chapter 5. Section 2.4 is a detailed review of the state-of-science of STS prediction. In Section 2.5, the findings of this Literature Review are synthesized and key areas of research, in modelling and validation, to advance STS prediction are identified.

2.1 Biomechanical descriptions of sit-to-stand

The nature of biomechanical analyses of STS can be classified as either descriptive or normative. Descriptive analyses present observed phenomena: body kinematics, reaction forces, or electromyography (EMG) of STS. There are studies comparing the STS motions or EMG activity between young subjects and elderly subjects [54], between subjects with different chairs [55], and when altering STS strategies including foot placement [55, 56] and hip flexion [57]. Alternatively, normative studies present data defining STS. These normative studies are the important minority in the literature that make it possible to objectively discuss what is and what is not STS. There is not one published resource that

portrays all aspects of STS together, but the works presented in this section provide a comprehensive understanding of normative STS.

Typically, when researchers speak of STS they are referring to a chair rise using a momentum-transfer strategy. In the momentum-transfer strategy, there is a period of instability when the buttocks leave the chair during which the centre of mass is not over the base of support. Therefore, this strategy requires sufficient momentum to transfer the centre of mass over the feet. There are, however, other legitimate strategies of STS including the stabilization strategy and the combined strategy [6]. In the stabilization strategy, a person repositions their centre of mass over their feet before standing. This repositioning may be by means of moving their buttocks forward and/or their feet backward and/or bending at the hips. In the combined strategy, a person repositions the body to shorten, but not eliminate, the distance between the centre of mass and feet. An individual at a given stage of life typically has a preferred strategy, and will adapt their STS technique to account for physical, neurological, or environmental changes [6]. The studies describing normative STS focus on the momentum-transfer strategy.

Physical therapists have studied STS kinematics to develop standard movement patterns. The work of Nuzik, et al. is particularly useful as it provides mean and standard deviations of 7 identifying angles at 5% intervals of STS [58], as in Figures 2.1 and 2.2. In a clinical setting, these kinematic patterns may be compared with an individuals STS to determine if the motion is typical or pathological and to set goals for treatment.

Researchers have also divided STS into phases. These divisions have been made both for therapeutic [10] and for scientific [27] purposes. Event markers divide the phases of STS. The clinically relevant events of STS as described by Schenkman et al. are given in Table 2.1, while the events of STS as described by Kralj et al. are given in Equations 2.1 through 2.6, where F_X is the force in the anterior and posterior directions, F_Y is the vertical force, and M_Z is the moment about an axis perpendicular to the sagittal plane measured from one force plate, as in Figure 2.3. These events have also been presented in

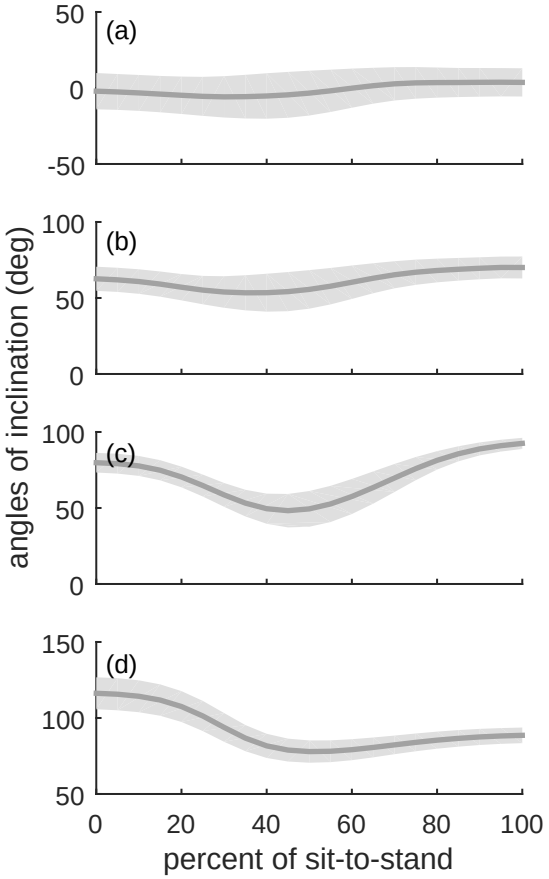

Figure 2.1: Sit-to-stand angles of inclination of the: (a) Frankfort plane, (b) neck, (c) trunk, and (d) pelvis, measured in the experiments of Nuzik et al. [58].

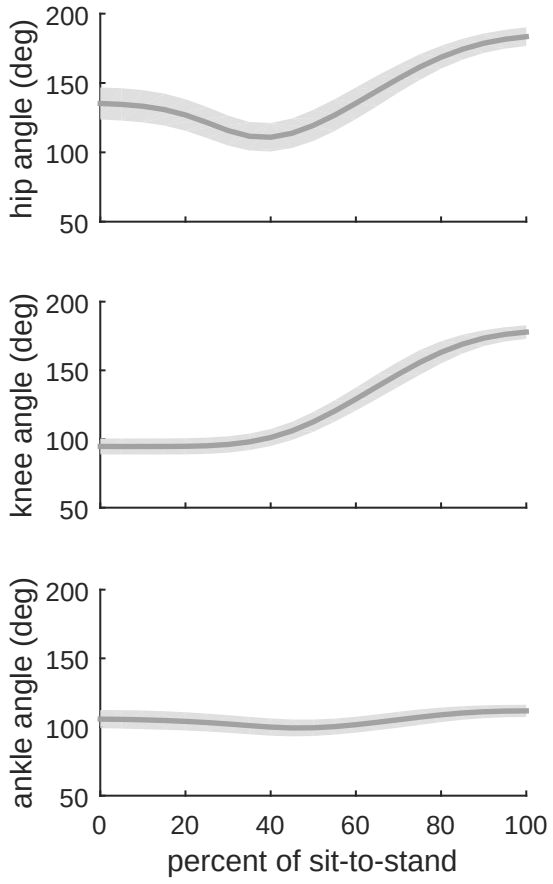

Figure 2.2: Sit-to-stand angles between body segments, measured in the experiments of Nuzik et al. [58].

time, as in Figure 2.4. While there is harmony between the descriptions of the phases and events of STS between authors, their definitions are not one-to-one. The greatest similarity between descriptions is in the flexion momentum phase described by Schenkman, which Kralj has divided into two phases: initiation (event_0 to event_1) and seat unloading (event_1 to event_2). The Schenkman and Kralj descriptions of the phases of STS, with one being based in kinematics and the other predominantly based in kinetics, makes it possible to be quite objective when evaluating STS from motion capture and force platform data.

Table 2.1: Clinically relevant phases of sit-to-stand, reported by Schenkman et al. [10].

Phase	Name	Starting event	Description
I	Flexion momentum	End of quiet sitting	Forward momentum is generated in the upper body while the lower body remains relatively stationary.
II	Momentum transfer	Seat-off	The momentum of the upper body is transferred to the whole body, which moves anteriorly and upward.
III	Extension	Maximum ankle dorsiflexion	The joints extend and the whole body moves upward.
IV	Stabilization	End of hip extension	Movements of rising end and quiet standing is achieved.

initiation, event_0 :

$$\left|\frac{dF_X}{dt}\right| \geq 2.5\% \left(\frac{dF_X}{dt}\right)_{peak-to-peak} \quad or \quad \left|\frac{dM_Z}{dt}\right| \geq 2.5\% \left(\frac{dM_Z}{dt}\right)_{peak-to-peak} \tag{2.1}$$

event_1 :

$$\left|\frac{dF_Y}{dt}\right| \geq 10\% \left(\frac{dF_Y}{dt}\right)_{peak-to-peak} \tag{2.2}$$

seat-off, event_2 :

$$F_X = maximum \tag{2.3}$$

event_3 :

$$\frac{dF_Y}{dt} = minimum \tag{2.4}$$

event_4 :

$$\theta_{knee} = \theta_{knee\,standing} + 2^\circ \tag{2.5}$$

standing on, event_5 :

$$F_Y = (100\% \pm 1\%)\, bodyweight \tag{2.6}$$

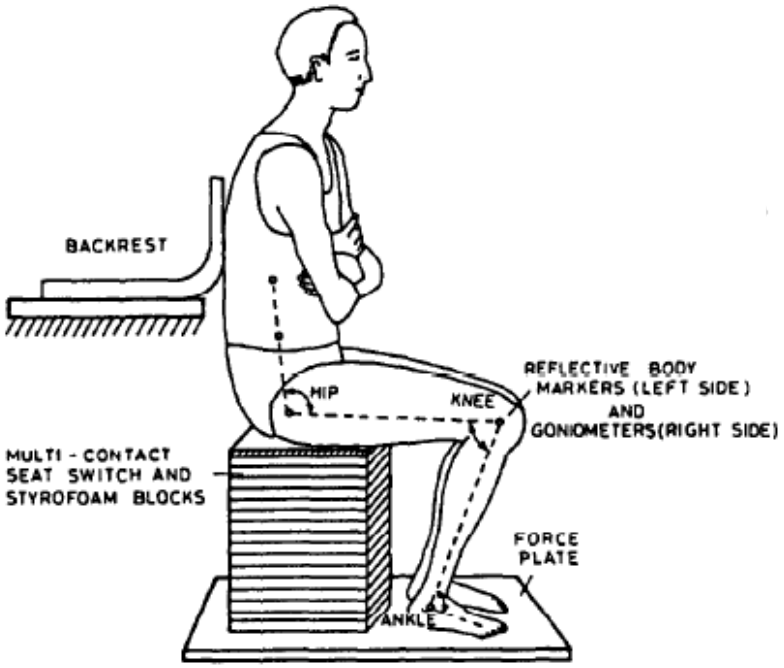

Figure 2.3: Schematic of experimental set-up by Kralj et al. [27].

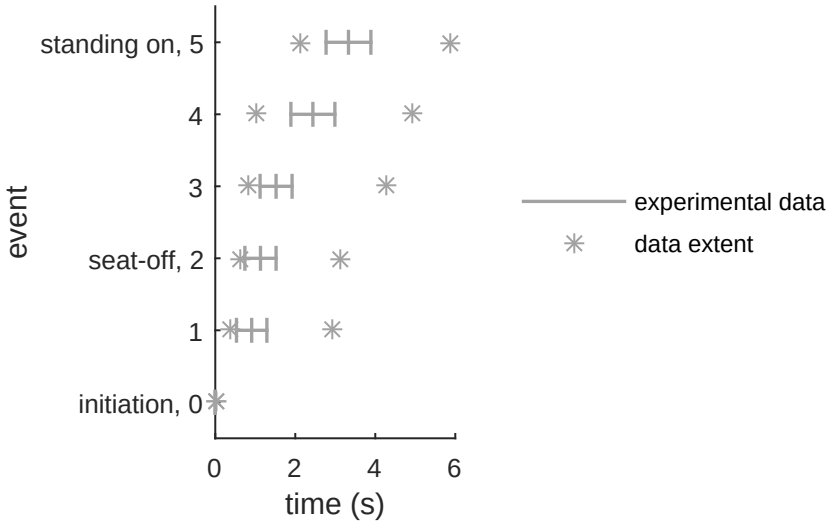

Figure 2.4: Sit-to-stand event timings, showing means, standard deviations, and extents, measured in the experiments of Kralj et al. [27].

In conclusion, healthy STS is a specific motion pattern with defined kinematic and kinetic events in time. The works presented in this section, when combined, provide a comprehensive understanding of what is and what is not STS.

2.2 Biomechanical modelling for sit-to-stand

Biomechanical modelling, in the sense of this work, is a simplification of the body to a mathematical model in an attempt to represent biomechanical phenomena. There exists a wide variety of biomechanical models in the literature constructed using a range of modelling approaches. Determining which of these models are appropriate and useful in modelling STS is vital to this thesis, as the validity of any assessment based on the model is only as good as the model itself.

The simplest STS models are linked segment models. Linked segment modelling is the well-established science of reducing the human body to mechanically described segments and joints. A schematic of a linked segment model may look like Figure 2.5. In this representation, segments are assumed rigid and each segment is represented as a rigid body with centre of mass and moment of inertia about a known point [59]. Anthropometrics of a linked segment model may be derived from established datasets, [19, 60–62] or by means of direct measurement. In all, the length, mass, centre of mass location and mass moment of inertia ought to be determined for each segment for a kinetic analysis.

One such analysis, commonly performed, is an inverse dynamic analysis of experimentally observed motion. In an inverse dynamics analysis of STS, kinematics and external forces were input to the linked-segment model to calculate net joint reaction forces and moments [29], as in Figure 2.6. Analyses of experimental STS have gone an additional step to estimate muscle forces [63]. Further analysis could include estimation of bone on bone forces or muscle activation, muscle excitation and/or neural commands. However, these

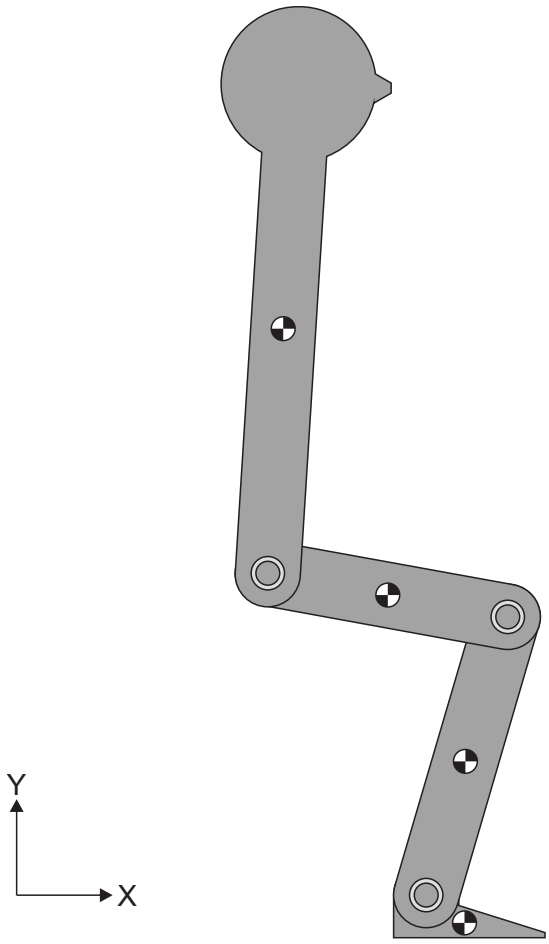

Figure 2.5: A planar link-segment model of a human body with HAT (head-arms-torso), thigh, leg, and foot segments.

further analyses require advanced biomechanical modelling for a more thorough description of the phenomenon.

There is not a single "complete" biomechanical model of the human capable of describing all human motions. When the answers to multi-faceted biomechanical questions are sought, it is the nature of this field, including this thesis, that multiple models (and parameters from different populations) are combined to develop "Frankenstein models" [65]. However, when models are combined to answer a novel question, it is important to consider

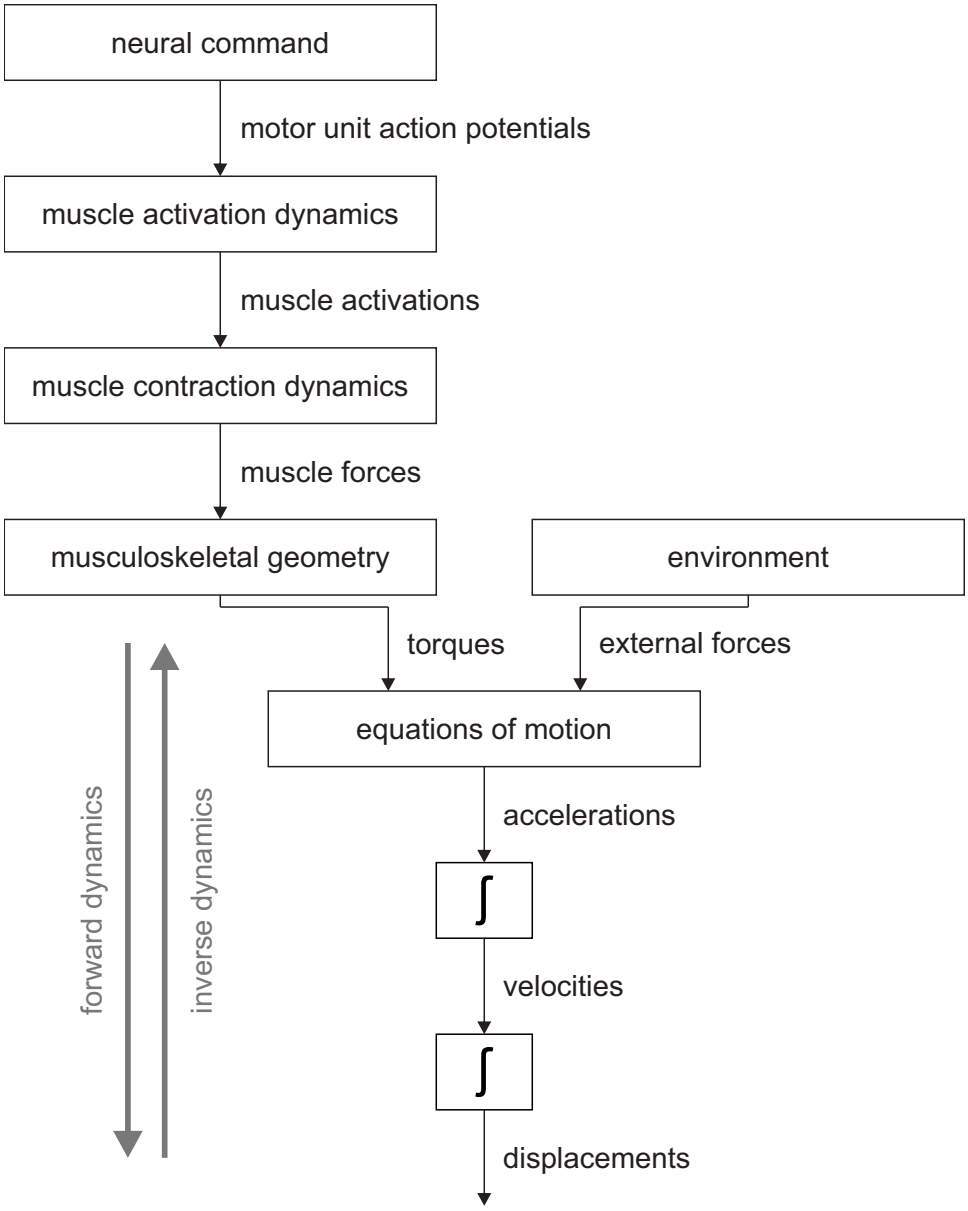

Figure 2.6: The dynamics of human motion, adapted from Buchanan et al. [64].

the usefulness and validity not only of the component models, but also of their inclusion in the Frankenstein model, and if these carry over to the new context of the research.

Measurement and modelling of humans for biomechanical analyses has been an important aspect of biomechanics since its founding. With respect to context, a majority of

biomechanical models were developed based on measurements from men for the purpose of gait analysis. There are three glaring differences, in terms of biomechanical modelling, between a walking male and a female standing from seated. These differences and their consequences will be explored in the remainder of this Section. The first difference is that males and females have different physical geometry. The second difference is the presence of contact between the buttocks and environment during STS, which does not occur when walking. The third difference is in the range of motions made in these activities, where the range of STS joint angles is much greater than those produced during walking.

With respect to differences in physical geometry between men and women, the majority of influential and well-recognized biomechanical datasets are based on data from males without consideration of a female counterpart. There are exceptions to this [19, 62, 66, 67] and from these we can be sure that the geometry of males and females are different. Still, we are in a position where there aren't "complete" models of men and there are fewer "partially complete" models of women.

Contact modelling is an active research area within and beyond the biomechanics community. Some biomechanical contacts can be considered rigid in terms of healthy gross motions, but for others it is important that the forces causing or caused by deformations at the continuum level not be ignored [68]. Researchers interested in human gait have made considerable efforts in the creation of foot-ground contact models [69, 70]. The STS equivalent of foot-ground contact would be buttocks-chair contact; however, there are very few biomechanical contact models of buttocks. Magnetic Resonance Imaging (MRI) studies have shown finite strains, with deformations on the order of centimeters, in the buttock in quiet sitting [71]. However, existing buttocks models were built for design and analysis of chairs, either in vehicles [72, 73] or for patient support systems (e.g. wheelchairs) [71]. Both of these applications are interested in buttocks contact with minimal changes in deformation. The alternate to these models is to look to constitutive models of excised, porcine,

fat [74] and muscle [75] tissues, which may behave similarly to human tissues, and which were built with larger ranges of deformation considered.

Another important difference in the geometry of STS from walking is the range of motion (RoM) of the joints of the lower extremity. Table 2.2 shows that the RoM of the joints in gait represent only a small portion of their healthy RoM. With a majority of research focused on gait, it is no surprise that a majority of experiments have investigated muscle properties only within the gait RoM and that muscle models, built for gait, were designed for this smaller RoM.

Table 2.2: Joint ranges of motion.

Joint	Natural [76]	Walking [77, 78]
Hip	120° flexion to 30° extension	32° flexion to 12° extension
Knee	135° flexion to 10° extension	73° flexion to 0° extension
Ankle	20° dorsiflexion to 50° plantarflexion	10° dorsiflexion to 20° plantarflexion

These differences in geometry become very important when muscles are included in a biomechanical model to describe a musculoskeletal system. In a musculoskeletal model there must be, at the very least, knowledge of muscle moment arms across the joints to determine the moments and motion produced for a given muscle force. To relate muscle activations (a) and forces produced (F^{mt}), the lengths of musculotendenous units (l^{mt}) must be known over time, as in Equation 2.7 [64],

$$F^{mt} = f(a, l^{mt}, \dot{l^{mt}}, F^m_O, l^m_O, l^t_S, \alpha_0) \tag{2.7}$$

where F^m_O is the maximum isometric muscle force, l^m_O is the optimal muscle length, l^t_S is the tendon slack length, and α_0 is the pennation angle at optimal length. If bone on bone forces are desired, the lines of action of muscle forces are necessary. These aspects of muscle geometry are most often determined experimentally and described using a musculoskeletal model.

Models of musculoskeletal geometry most commonly describe a muscle path using a set of coordinate points specifying proximal and distal attachment points to the skeleton and possibly intermediate via-points or wrap points, allowing musculoskeletal geometry to be calculated analytically. In this discussion, a via point is a point a muscle is always constrained to pass through while a wrap point is a point the muscle is constrained to pass through when the joint(s) the muscle spans are within a specified range [79]. One such dataset specifying these points is from White et al. [80]. This model is designed for use in gait analysis. It includes one fixed via point for each of the iliopsoas, gastrocnemii, tibialis anterior, and tibialis posterior while recommending alternate path modelling for the quadriceps. A second data set from Carhart [81] is designed for use over larger ranges of joint angles and includes more via and wrap points to capture the geometry of anatomical constraints in the muscle path.

With the advantages of musculoskeletal geometry datasets, there are also shortcomings. The first concern is that both the White and Carhart models generate non-physiological (negative) moment arms for some muscles within a healthy range of joint angles [82]. This moment arm inaccuracy happens for two reasons, first because a muscle's path may cross to the other side of the joint, and second because a modelled muscle will sometimes bend back over itself across a joint. The second concern is that when describing muscles using fixed points including wrap points, there are physiologically unrealistic changes in lengths when the wrap point goes from active to inactive [82]. Both scenarios can lead to inaccuracies in muscle force or muscle activation calculations which may confound ideas of the effort of a motion or comparison with experimental EMG.

The biomechanical system supporting motion is complex, but the model of this system for use in predicting STS should be only as complex as necessary. While the question of which human systems to model and to what granularity has been explored extensively in gait, the same cannot be said for STS research. It will be a necessary challenge of this

thesis to build an appropriate biomechanical model for STS prediction, with awareness that any phenomena predicted using this model can be only as good as the model itself.

2.3 Motion prediction in biomechanics

A human motion prediction problem is an optimal control problem in the sense that optimal control theory is the study of how dynamic systems may be controlled to optimize performance. While optimal control was founded in the 1950s, the first applications of optimal control in biomechanics were published around 20 years later with the works of Chow and Jacobson [83], Ghosh and Boykin [84], and Hatze [85], who controlled the dynamics of their respective two- or three-link human models to predict gait, a "kip" on a gymnastics bar, and a kick. Since this time, optimal control has been used by a small subset of biomechanists to predict human motion.

In any hypothetical scenario, motion prediction requires a biomechanical model, controls to influence the behaviour of the model, and a performance criterion to optimize. Biomechanical modelling was the focus of the previous section; therefore, the remainder of this section will focus on controls and performance criteria.

2.3.1 Controls

The controls of a motion prediction problem describe the behaviour of the control variables, and therefore the human model. Figure 2.6 relates the nervous, muscular, and skeletal systems and shows the congruency between internal and external forces and human motion. The dynamic equations of motion relate forces to the corresponding motions. Because of these interrelationships, any of the variables along an arrow in Figure 2.6 is a candidate for a control. Popular choices for musculoskeletal simulation controls are joint torques, muscle forces, and muscle excitations [86] (related to muscle activations).

The choice of controls also has bearing on the form of the optimal control problem. Historically, most researchers in biomechanics have chosen to express controls as an explicit function of time, such that the optimal control problem is framed using a dynamic optimization method (in biomechanics terms) or as a control parameterization method [87] (in control theory terms). Expressing the controls as an explicit function of time makes the control open-loop. The alternative to expressing the controls in terms of time is to express them as functions of model variables, in which case the control is closed-loop. Both optimal control approaches, as well as hybrid combinations of the two, are widely accepted in the field of biomechanics. Open-loop control is generally a simpler formulation; however, closed-loop control is able to respond to real-time perturbations of the model or environment.

Once the controls formulation is chosen, the choice of solution method influences how those controls are described in the optimal control problem. There are three main classes of numerical methods for solving optimal control problems: dynamic programming, direct methods, and indirect methods [88]. For the first 20 years of human motion prediction, researchers almost exclusively used dynamic programming approaches. In dynamic programming the period of motion is divided into intervals, discretizing controls and states so that the problem is solved in stages [89, 90]. In the 1990s, direct solution methods, starting with direct single shooting, became the popular approach. In direct single shooting, control variables are parameterized, and may be included as constraints, to convert the optimal control problem to an optimization problem [91, 92] and solved approximately using traditional optimization techniques. In the 2000s, direct collocation approaches gained popularity in the biomechanics community [93–95]. In direct collocation, states are also parameterized, and/or included as constraints, in a large-scale nonlinear programming problem. And in the last decade, multiple shooting methods, where the interval of interest is divided into sub-intervals and then solved approximately, have appeared in the research [96]. Most recently, there has been an emergence of indirect solution methods in

biomechanical motion prediction, used to investigate the role of continual neural control in execution of motions [97, 98].

2.3.2 Performance criteria

The performance criteria (or cost function) of a motion prediction problem describe the preferences of the human model. There are times when the primary performance criterion of a motion is self-evident, for example, when studying how to jump as high as possible, how to run as fast as possible, or how to lift a full cup of hot coffee as smoothly as possible. However, appropriate performance criteria are elusive for many activities of daily living and determining these criteria remains an open challenge of biomechanics [86]. For these motions, a performance criterion should be based on the foundational theory that people move in ways that are optimal. For example, Crowninshield and Brand hypothesized that natural motions minimize some unknown function (U) of muscle (M), ligament (L), and articular surface contact (C) forces over all time,

$$U = A^M \sum_{i=1}^{m} \left(k_i^M F_i^M\right)^{n^M} + A^L \sum_{i=1}^{l} \left(k_i^L F_i^L\right)^{n^L} + A^C \sum_{i=1}^{c} \left(k_i^C F_i^C\right)^{n^C} \tag{2.8}$$

where k are constants, n are exponents, and A are weighting factors [99].

Performance criteria that have been successfully implemented, however, are typically less complex than Equation 2.8 and most often consider that every-day motions are performed in ways that are most energy-efficient [99, 100]. Looking to Figure 2.6, energy-efficiency or its inverse, effort (E), can be estimated at different levels of the model. At the joint torque level, effort may look like

$$E_{torque} = \sum_{i=1}^{j} c_i M_i^2 \tag{2.9}$$

where j are the joints, M are the moments, and c are weighting factors [101]. At the muscle level it may be represented as

$$E_{force} = \sum_{i=1}^{m} F_i^2 \tag{2.10}$$

where F are the forces produced by the muscles [102]. Or,

$$E_{stress} = \sum_{i=1}^{m} \left(\frac{F_i}{PCSA_i} \right)^2 \tag{2.11}$$

where $PCSA$ are the physiological cross-sectional areas of the muscles [102]. Or, looking to the neural level,

$$E_{activation} = \sum_{i=1}^{m} \left(\frac{F_i}{F_{MAXi}} \right)^2 \tag{2.12}$$

where F_{MAX} is the maximum isometric muscle force [103] and the term $\frac{F}{F_{MAX}}$ is closely related to the muscle activation, a, in Equation 2.7.

As has been a theme of this Section, the choice of performance criteria is largely dependent on the form of the model and hypotheses of how motions originate naturally. It is reasonable, although not necessary, that a performance criterion is naturally motivated. It is both reasonable and necessary that any prediction is considered in the context of assumptions made when specifying performance criteria.

2.4 Previous work in sit-to-stand prediction

Researchers have been studying STS prediction for over 25 years. Initially, time histories of excitation-type signals to lower extremity muscles were optimized. These signals were modelled by linearly interpolated nodes in time, and motions were determined by minimization of functions of muscle stresses and peak forces [104] or movement time [105]. The effects of varying muscle strength [105] and seat height [24] were sought. The interest in predictive STS was later control-oriented, and triple inverted pendulum [106] and trajectory tracking [51,107,108] problems were investigated. Most recently, research motivations in this area have swung back toward a biomechanical focus. In one vein of research, motions were again predicted using dynamic optimization, but bilateral joint angle profiles [109] were modelled as controls. In another vein, STS was predicted in the presence of external assistance [110].

STS prediction studies can also be divided by research focus. In the control-oriented work, the focus is most often the validity of a specific controller to what is typically cast as an idealized inverted triple pendulum problem [106, 108] with little or no attention to biological constraints or motivations. Some of these studies focus on intervention and are motivated to describe the human body as a simple plant to include in the controller of an intelligent exoskeleton [51] or functional electrical stimulation (FES) therapy system [107]. The remaining works aim to answer foundational questions of human nature: why and how humans move the way we do. This Section provides a comprehensive overview of these remaining works, the first four of which happen to be theses, in chronological order.

2.4.1 Garner, 1992

The first (Master of Science in Engineering) thesis on the topic of predictive simulation of STS was written by Brian A. Garner [104]. A significant portion of the thesis work is published as a research article in the Journal of Biomechanical Engineering [92]. The thesis is entitled "A dynamic musculoskeletal computer model for rising from a squatting or sitting position." As can be deduced from the title, both squat-to-stand and sit-to-stand motions are investigated in this work. One of Garner's key conclusions is "how" these motions are executed are inherently different and the presence of the chair is the source of this difference. Focusing on STS, Garner's objectives were to determine a biomechanical model and performance criteria appropriate for predicting this motion in silico.

Garner's biomechanical model, seen in Figure 2.7, is comprised of three rigid-link segments, three ideal revolute joints, and eight Hill-type muscles including tendon, moving exclusively in the sagittal plane. The seat-chair interface is modelled as a point-on-point exponential spring and linear damper with a simple friction model.

Neutral excitations to each muscle over the duration of motion were modelled using linearly interpolated nodes, evenly distributed as a proportion of motion, whose value

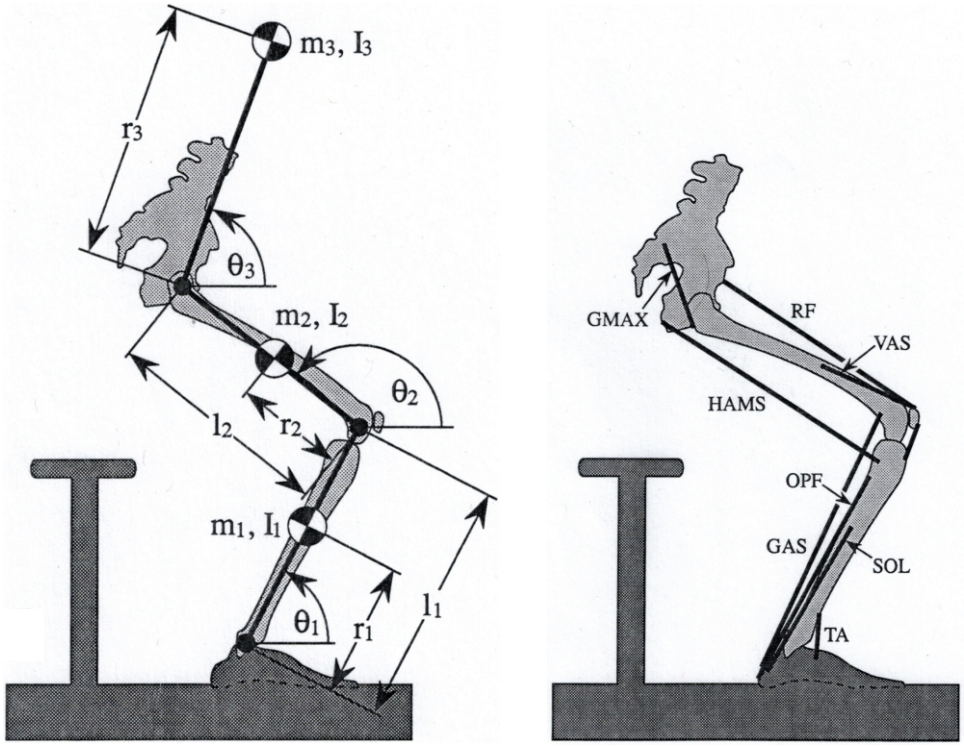

Figure 2.7: Garner's planar, three-segment, eight musculotendinous unit human model [104].

represents the proportion of the maximum allowable force of the muscle. These nodes as well as the duration of the STS task are the model controls.

Through comparison of experimental EMG and patterns of muscle force resulting from four different performance criteria, Garner concludes that greatest similarity between model and experiment is achieved when muscle stresses are minimized while sitting, and peak force rates developed by the muscles are minimized after seat-off as in Equation 2.13, where s are seconds to maintain dimension.

$$U = \frac{5}{3s} \int_{t_0}^{t_{seat-off}} \sum_{i=1}^{8} \left(\frac{F_i}{F_{MAXi}} \right)^2 \mathrm{d}t + \frac{1s}{3} \int_{t_{seat-off}}^{t_f} \sum_{i=1}^{8} \left(\frac{\dot{F}_i}{F_{MAXi}} \right)^2 \mathrm{d}t \tag{2.13}$$

This two-part performance criterion predicted what was considered sufficient agreement with experimental kinematics.

2.4.2 Daigle, 1994

Kristen E. Daigle, Garner's colleague at the University of Texas at Austin, wrote the (Master of Arts) thesis, "The effect of muscle strength on the coordination of rising from a chair in minimum time: predictions of an optimal control model" [105]. Daigle focused on understanding the effects of muscle strength on STS. This work is particularly relevant to understanding the difficulties in performing STS encountered by patients whose muscle strength is compromised.

The biomechanical model used in this work is built on the model from Garner. It has a total of eighteen musculotendinous units. There is an added foot segment (so that the toes instead are hinged to the floor), and further compliance is included in the model of the seat-chair interface. Rather than the two-part performance criterion specified by Garner, whose resulting sagittal plane motion Daigle considers dissimilar to experimental kinematics, Daigle used the unambiguous minimum motion time as the objective. Muscle force over the duration of motion is modelled using nodes, as in Garner, and altered strength simulations are run with muscles varying between 50 and 200% of the accepted strength value.

Through simulation, it was determined that uniarticular muscles are the primary power producers in STS. In fact, the only biarticular muscle classified as a major contributor was the biarticular hamstrings. The two muscle groups found to be most influential in successful execution of STS are the uniarticular hip extensors and the vasti, with weaker models even more reliant on the vasti.

2.4.3 Domire, 2004

Ten years later, the (PhD in Kinesiology) thesis, "A biomechanical analysis of maximum vertical jumps and sit-to-stand" was written by Zachary J. Domire [24]. A portion of this work was also presented at the International Society of Biomechanics 20th Congress [111]. This thesis is an anthology containing four papers building to a final paper investigating the effects of strength training on STS. Domire, like Daigle, recognized the importance of muscular strength in achieving STS and saw strength training as a means of maintaining or regaining this skill. As evaluating a strength training program experimentally is both time-consuming and expensive, the overarching goal of this work was to develop a model and simulation protocol to be used as a precursor to experimental testing.

An intermediary goal of this thesis was to evaluate the influence of chair height on STS performance. For this purpose, Domire built a sagittal plane biomechanical model with three segments, three ideal revolute joints, and eight muscles with rigid series elastic elements and rigid tendons. The chair model and performance criterion used are those designed by Garner. The controls are node values defining the time histories of neural excitations to each Hill-type muscle model and the movement duration, constrained to be less than or equal to two seconds. It was demonstrated that as chair height is reduced, muscles take on configurations with reduced moment arms and/or unfavourable lengths, and STS becomes increasingly difficult.

Next, the effect of strength training on STS was investigated. A minimum time performance criterion was used for these simulations. STS was predicted with all muscles (1) having the accepted maximum isometric force, (2) with this force increased by 25% for all muscles, and (3) with the increase applied to specific groups of muscles only. The best performing model was the one where maximum isometric force was increased for all muscles. Domire suggests that this model not only stood up faster, but changes in maximum joint velocities and maximum horizontal momentum indicate that the motion was easiest

to control. Domire compared his results with experiments and noted general agreement in vertical reaction forces. In conclusion, Domire recommended a balanced strength-training program to improve STS.

2.4.4 Ozsoy, 2014

The most recent (PhD in Engineering) thesis on the topic of STS prediction was written by Burak Ozsoy [109]. It is entitled, "Three dimensional sit-to-stand motion prediction." A significant portion of the thesis work is published in the proceedings of the American Society of Mechanical Engineers 2014 International Design Engineering Technical Conferences & Computers and Information in Engineering Conference [52]. It is the only one of these theses with a three-dimensional biomechanical model. The intention of this work is to describe a generic STS simulation method. The scenarios explored include STS for healthy young adults, and healthy elderly.

The models used by Ozsoy are modifications of the digital human model [112]. The STS motion is broken into five phases and for each, the joint angles are modelled as a quartic B-spline whose knots parametrize the controls. That is, this is an inverse dynamics model without muscles. Ozsoy implements a multi-objective cost function, minimizing both joint torques squared and differences in reaction forces between sides of the body to determine knot locations. A number of constraints, including joint range of motion and maximum joint torques, are enforced in simulations. Many of these appear exactly or in an equivalent form from previous theses. Elderly models were made by decreasing both joint range of motion and maximum allowable joint torques significantly.

A comparison was made between STS predicted for a healthy model and that seen in experiment. Peak angular velocities, peak angles, and peak chair reaction forces were determined to be similar to those measured experimentally. The order of magnitude and the temporal order of peak joint torques matched the literature. It was noted that the horizontal centre of mass excursion was significantly greater than was seen in experiment,

and Ozsoy notes that this is reasonable as the model has no perception of fall-risk. By this comparison, the model and simulation method were considered validated for a healthy population.

2.4.5 Mombaur and Ho Hoang, 2017

The final work discussed in this Section is that of Mombaur and Ho Hoang. In their article "How to best support sit to stand transfers of geriatric patients," Mombaur and Ho Hoang explore an exciting frontier of predictive STS research, where assisted STS (i.e. STS in the presence of an assistive device) is predicted [110]. This work does not address the question of why people perform STS the way they do so much as apply criteria found from studies of other movements to STS. In its endeavour to discover how changing a person's environment influences STS, it is relevant to the long-term goal of this PhD research of using predictive simulation of STS in assistive device design.

Relative to previously mentioned researchers, Mombaur and Ho Hoang constructed the most complex rigid link model, with eight links actuating in the sagittal plane. Targeting a patient population, they had the forethought to consider both male and female models and (like Ozsoy) to use anthropometrics representative of geriatric (elderly) people. Other aspects of their biomechanical model are more simple than previous studies, however. For example, Mombaur and Ho Hoang excluded muscles in this model and described seat-chair contact simply as a unilateral contact constraint. Instead, they paid attention to modelling three styles of robotic mobility aids as external forces applied to the patient.

Like Garner, Mombaur and Ho Hoang cast the STS prediction problem as a two-phase optimal control problem. In this formulation, the joint torques of the model and supporting forces of the assistive device are both optimized from sitting to standing to minimize a multi-objective cost function of joint torques, mechanical work, angular velocity of the head, and smoothness of external force profiles. The STS motion resulting from this prediction describes how a patient might interact with an assistive device of the given

form. By comparing the forces predicted between the device and patient to the physical capacities of a patient, this work may be used to objectively inform the design and selection of mobility aids.

This research would be more in line with the topic of this thesis if the aids were constrained such that they could contribute no force, because then we would see how the modelled geriatric patient responds in absence of an assistive device. However, as was stated by Mombaur and Ho Hoang, there was not experimental data available from a compatible patient population to use for validation, so perhaps the results of a prediction without aids would be less meaningful. Nevertheless, the work of this article is a glimpse at what should be the next steps when a pathological motion can be predicted — to predict that motion with an intervention in order to inform intervention design and selection. For the advancements made in predictive simulation of STS with an intervention, this paper is inspirational and a motivator of this thesis work.

2.4.6 Summary

In the five main works of predictive STS presented, there exist themes in why and how predictive simulation of STS is performed. The "why" is often two-fold: first, to better understand when and how humans move the way we do and, subsequently to apply this knowledge to better preserve or restore STS for those facing a loss of mobility. The specific "how" varies according to the research decisions made by each researcher. Table 2.3 and Table 2.4 summarize the key differences between the principal works in STS prediction.

It is interesting to observe the similarities and differences in research choices made when designing the biomechanical models. For example, all models in the five main works of STS prediction move in the sagittal plane exclusively except for Ozsoy's model, which may make it superior for studying pathological STS. Also, all models include HAT, thigh, and leg segments. The Daigle model also includes a foot, while the Ozsoy model emphasizes the pelvis as being separate from the HAT, and the Mombaur and Ho Hoang model divides

Table 2.3: Biomechanical characteristics of five sit-to-stand models.

Work	Garner	Daigle	Domire	Ozsoy	Mombaur
Dimensions	2	2	2	3	2
Anthro-pometrics	Male	Male	Male	Male	Male and female
Segments	HAT Thigh Leg	HAT Thigh Leg Foot	HAT Thigh Leg	HAT Pelvis Thighs Legs	Head Upper trunk Lower trunk Pelvis Upper arm Forearm Thigh Leg
Muscles	8	18	8	0	0
Tendons	Flexible	Flexible	Rigid	N/A	N/A
Seat-chair contact model	Exponential spring Linear damper	Exponential spring Linear damper	Exponential spring Linear damper	Kinematic constraint	Unilateral contact constraint

Table 2.4: Motion prediction characteristics of five sit-to-stand models.

Work	Garner	Daigle	Domire	Ozsoy	Mombaur
Solution method	Dynamic optimization	Dynamic optimization	Dynamic optimization	Dynamic optimization	Direct multiple shooting
Controls	Muscle excitations	Muscle forces	Muscle excitations	Joint angles	Joint torques External forces
Performance measure	Muscle stresses Peak muscle force rates	Time	Time	Joint torques Left-right symmetry	Joint torques Work Head velocity
Constraints	Muscle limits	Muscle limits	Muscle limits STS duration	Joint angles Joint torques	Joint angles, velocities, forces, torques External forces

the HAT into six segments. In these cases it is practically impossible to comment on the effects of these modelling choices because they are generally presented without reference to previous predictive STS research and no work makes an objective comparison of their results to a standard description of STS.

One area where this limitation is highlighted is in the choice of muscles in the model. Garner included 8 muscles, modelled for gait [18], in his biomechanical model and recommended the inclusion of additional uniarticular muscles [104]. Daigle included 10 more muscles [105] but did not address the effects of this change, and Domire resorted to the original model presented by Garner [24]. Later, Ozsoy and Mombaur and Ho Hoang excluded muscles from their models, but Ozsoy made their inclusion a primary recommendation for future work. After 25 years of research, the literature lacks an established set of muscles to include in biomechanical models for STS prediction.

Another area to comment on is the description of seat-chair contact. The simplest buttocks model omitted contact entirely [106, 108]. The location of the centre of mass in this set up is well behind the base of support in the seated position, and the only natural response is for the model to fall down, which is not the goal of this work. At the other extreme, rigid contact models, for example considering the hip to be hinged to the chair while the upper body flexes and disengages at maximum flexion [109], restricted the motion of the lower extremities in ways that are incongruous with experimentally observed STS. The one compliant buttocks model used in a model for STS prediction employs an exponential spring and linear damper [104]. The equilibrium position of this spring was not stated, and for the STS motion observed in experiment there is a trade-off between having a chair that is practically ineffective and one that is implausibly sticky, and all equilibrium positions produce physically unachievable net ankle moments [113] during sitting, making STS impossible. None of these models are appropriate for STS prediction.

By choosing different models and controls, applying different constraints, and specifying different performance criteria, the five studies explored in this Section are unique. However, it is very difficult, if not impossible, to discuss which research decisions hold most merit as validation attempts have been oversimplified in all of these works. Plans to address this limitation and more are presented next.

2.5 Conclusion

This Chapter has explored STS through three lenses: experimental biomechanics, biomechanical modelling, and biomechanical motion prediction. All of these will be discussed in this Section.

In terms of experimental biomechanics, many researchers have collected experimental STS data and, although there is not one all-encompasing description of normative STS, this motion is well described from a clinical perspective in the work of Schenkman et al. [10] and defined in terms of kinematics and kinetics when the studies of Nuzik et al. [58] and Kralj et al. [27] are considered together.

The foundational concepts of biomechanical modelling are well-established in the literature. Nevertheless, there is an absence of validated models for biomechanically describing STS. This thesis endeavours to continue the strong tradition of biomechanical modelling to advance knowledge of the STS motion. The model developed in Chapter 3 of this thesis is a female Frankenstein model built from models used previously in STS research, with models from gait studies, and models developed in other areas of the biomechanics literature. There are model components however, including the buttocks and muscle geometry, that required major deviations to overcome deficiencies in previous models.

Like biomechanical modelling, the foundational concepts of motion prediction are also well-established. However, biomechanical motion prediction is a niche field of study. There is not an established "best" problem formulation or solution method for biomechanical motion prediction. Still, dynamic optimization has long been an influential strategy and was used in four of the five major works in STS prediction, as seen in Table 2.4. Previous researchers have affirmed that dynamic optimization provided "good" STS prediction results, motivating the use of dynamic optimization in this thesis. In all Chapters, the STS motion is described geometrically by a set of Bézier curves with parametrized control points. Assuming that people prefer to move in ways that are efficient, disinclination to a

motion is described as a cost function of joint torques (as in Equation 2.9) in Chapter 3 and Chapter 4 and as a cost function of muscle stress (as in Equation 2.11) in Chapter 5.

Each main work in STS prediction touches on the previous themes to an extent. Table 2.3 and Table 2.4 show that, in these five works, there are large variations in biomechanical modelling choices, motion controls, and performance criteria. However, the influence of these works are limited by the fact that their results are generally presented without reference to previous research and without comparison to a STS standard.

In this thesis, there is unprecedented comparison of both predicted kinematic and predicted kinetic results to healthy STS in a meaningful way, by discussing the physical feasibility of the resulting motion and comparing it with normative data in the literature. This means that, for the first time, the fundamental need and responsibility as a researcher to assess the choices made in modelling and predicting any motion is being met in this thesis. From this comparison, the validity of the modelling choices made in all chapters are discussed with context and the results establish a benchmark for future work in STS prediction.

It was mentioned previously in this Section that the buttocks model, designed in Chapter 4 of this thesis, is substantially different from previous buttocks models. Assessment of existing buttocks models has determined that those that are physiologically realizable are either too time-consuming to use in a dynamic optimization routine for STS prediction, or inaccurate over the expected range of tissue deformation in STS [71]. In Chapter 3, the buttock is modelled as a one-dimensional Kelvin-Voigt element, intended for use with off-road-vehicle operators [73]. However, extending the results of Chapter 3, Chapter 4 details the design of a lumped parameter, force-deformation, Kelvin-Voigt model of buttocks-chair interaction motivated by constitutive models of soft biological tissues found elsewhere in the literature.

The other modelling area requiring substantial re-design is modelling of musculoskeletal geometry. The model of musculoskeletal geometry used by Garner has been superseded by

the White and Carhart models, introduced in Section 2.2, which have proven insufficient for describing musculoskeletal geometry for motions with large ranges in joint angles [82], such as STS. In Chapter 5, a musculoskeletal model is built that is motivated by existing musculoskeletal models [80,81] with attention to reported muscle lengths [114] and experimentally measured moment arms from across the biomechanics literature. This model strategically incorporates muscle path modelling strategies, such as muscle wrapping [115–117], used more commonly in the upper extremity, in a model of the lower extremity. This model takes account of the recommendations of Garner to include more uniarticular muscles in a musculoskeletal model for STS and Ozsoy's hypothesis that muscles are integral to STS prediction.

These improvements in biomechanical modelling and validation of STS predictions will overcome the greatest gaps in past STS prediction research. The models built will serve as a starting point for future work in STS prediction and will be useful in applications across the field of modelling and simulation of human movement. The care taken in validation in this thesis should serve as a model to future work in STS prediction and will promote collaborative communication within this research community.

3

Predictive Sit-to-Stand of a Three-Link Torque-Driven Model[1]

The aim of this work is to model how a healthy individual rises from a seated position. This is a first initiative in understanding pathological sit-to-stand (STS), the reality of an increasing proportion of the population struggling with this motion. Researchers have been studying STS prediction for over 25 years. The key works in this area, examined in the Literature Review, have been focused on actuating a triple inverted pendulum, typically with male anthropometrics, from a seated pose to a standing pose. The models and optimal control strategies used by past researchers are, however, limited to applications with idealized plants and motions. This Chapter builds on the tradition of modelling and predictive simulation of STS by construction of a three-link-model and use of dynamic optimization to solve for a STS motion requiring minimal effort. Also, this Chapter provides, for the first time, an objective assessment of the predicted STS with respect to established descriptions of healthy STS.

[1]This research is published as "Constrained dynamic optimization of sit-to-stand motion driven by Bézier curves," in The Journal of Biomechanical Engineering [118].

This Chapter has three major components. The first component is a discussion of the structure of the biomechanical model. With a future goal of predicting pathological STS, the model created describes a female, as women have proportionally more difficulty performing STS according to self-reporting studies [7]. The second component is a description of the optimal control framework used. The control strategy invoked is unique in that it considers physical limitations of humans in STS and that it is purely predictive. The last component is a comparison of the predicted STS to healthy STS in a meaningful way, by discussing the physical feasibility of the resulting motion and comparing it with normative data in the literature. This Chapter, thereby, establishes a benchmark for future work in STS prediction.

3.1 Biomechanical model construction

The human is represented as three rigid links in the sagittal plane. This model captures aspects of joint, foot, and buttocks physiology, which makes it the most comprehensive planar model for predicting STS to date.

3.1.1 Model components and parameters

A schematic of the human model, created in MapleSim [119], is seen in Figure 3.1. Its skeleton consists of two legs moving in parallel, each with a foot fixed to the ground, leg, and thigh, and a head arms torso (HAT). The arms of the model are crossed in front of the chest as is required of patients performing a clinical STS test [21]; such that the model reflects the clinical test. For simplicity, a three link model was chosen in this work. It is possible to include more links in the biomechanical model and, for example, the inclusion of eight links is a feature of the model made by Mombaur and Ho Hoang [110]. Opportunities to free additional body segments from this model are discussed in Chapter 6. Body segment parameters [19], foot [62], and pelvis [67] dimension of a healthy female human are from

the literature. Joint damping [120] and passive elastic moments [121] are included in the model. Knees are constrained from extending beyond straight to avoid bifurcation.

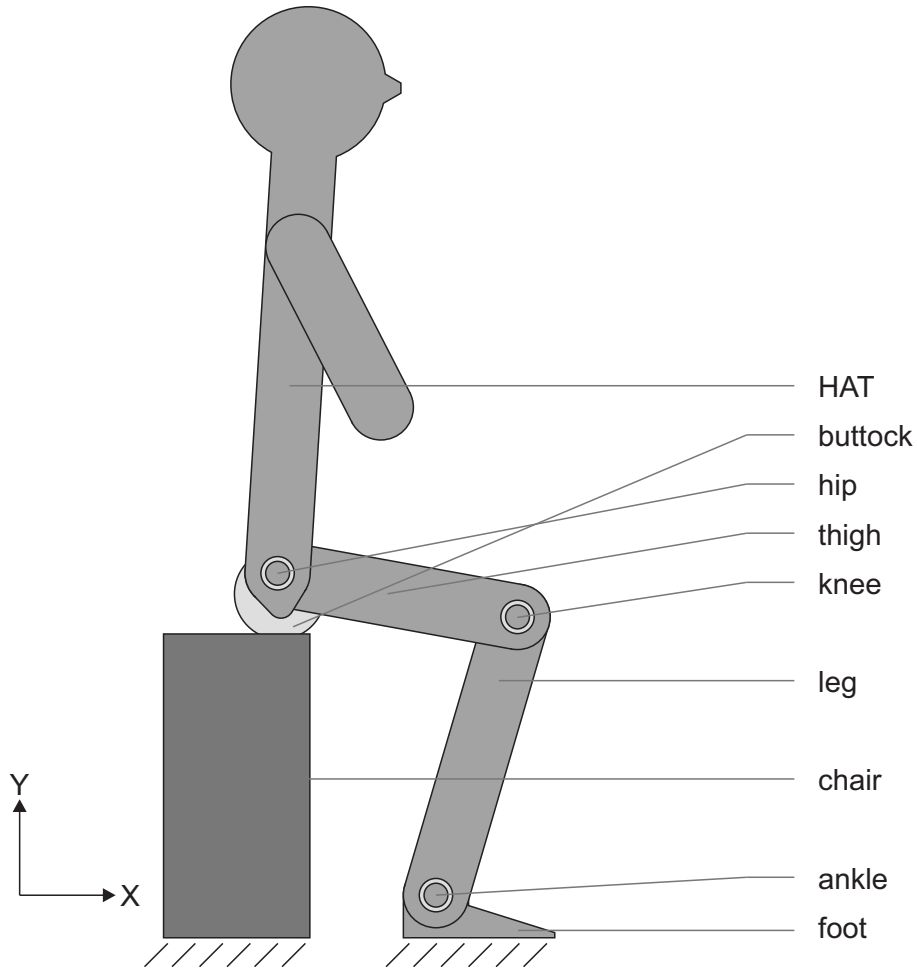

Figure 3.1: A schematic of the three-link sagittal plane model while seated.

Buttocks model details are included in the next chapter. Suffice it to say for now, that buttocks are added to the HAT as one-dimensional Kelvin-Voigt elements [72, 73] of representative female dimension [71] with a gap [122]. This Modelica model ensures continuity in the force profile and disallows pulling between the buttocks and chair [123].

The chair is assumed to be of steel construction, rigid, backless, armless, and of standard adjustable height [124]. A hyperbolic tangent regularized friction model, previously used

for feet [69], is included between the buttocks and chair with coefficient of friction of canvas on steel [125].

3.1.2 Fixed foot implications

The position of the foot is predetermined and fixed. Foot location has major influence on the ability to perform STS [7] and people will move their feet to a favourable position prior to initiating STS, when convenient. This stabilization strategy is not always accessible because of the immediate environment or physiotherapists instructions [126] and therefore the decision is to disallow it in this simulation.

Fixing the foot introduces the possibility for the model to respond unnaturally in situations where a foot ought to lift from or slip relative to the ground. These cases are determined considering the foot as in the free body diagram in Figure 3.2. The foot of the model is of known dimension (d) and weight (W). The coefficient of static friction (μ) between skin and metal is assumed between the foot and ground. For forces, A_Y, A_X, and moment A_M, the system is determined and it is possible to solve the static equilibrium equations for r_N, F_f, and N to establish if the conditions for static equilibrium are in violation. The modelled system is in error when conditions are incongruent with static equilibrium of the foot. Equations 3.1 through 3.3 quantify these errors. First, when the modelled foot, were it not fixed to the ground, ought to tip,

$$error_t = \begin{cases} r_N - d_{toe} & r_N > d_{toe} \\ r_N + d_{heel} & r_N < -d_{heel} \\ 0 & otherwise \end{cases} \tag{3.1}$$

when it should lift,

$$error_l = \begin{cases} |N| & N < 0 \\ 0 & otherwise \end{cases} \tag{3.2}$$

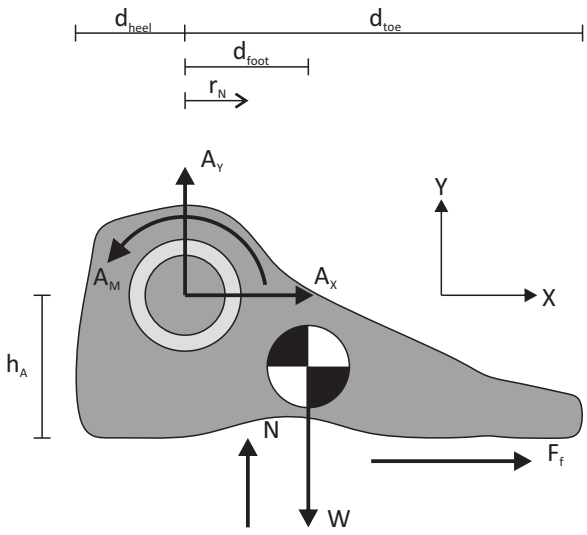

Figure 3.2: Free body diagram of the foot.

and when it should slip,

$$error_s = \begin{cases} |F_f| - \mu N & |F_f| > \mu N \\ 0 & otherwise \end{cases} \tag{3.3}$$

A last implication of fixing the feet is defining the model's workspace. The chosen controls, described in the following section, may specify an (X,Y) hip location outside of its workspace, so Equation 3.4 is added

$$error_h = \begin{cases} \sqrt{X^2+Y^2} - (l_{thigh} + l_{leg}) & \sqrt{X^2+Y^2} > l_{thigh} + l_{leg} \\ 0 & otherwise \end{cases} \tag{3.4}$$

where l_{thigh} and l_{leg} are the length of the thigh and leg, respectively.

From Equations 3.1 through 3.4, $error_h$, $error_t$, $error_l$, and $error_s$ are excursions of the specified hip location beyond the model's workspace, excursions of the centre of pressure beyond the base of support, pulling forces at the ankle, and lateral forces at the ankle exceeding stiction, respectively. In a successful STS transfer, there is zero cost associated with these errors.

3.2 Optimal control framework

For this three-degree of freedom model, the location of the hip joint centre and inclination of the upper body are chosen as controls to fully control this system. Based on previous work in predictive STS, explored in Chapter 2, the optimal control problem is framed as a parameter optimization problem.

The locations of the controls in time are modelled using composite Bézier curves so that a control point has global rather than local influence on curve shape [127], and not only is it unnecessary to bound them in value when optimizing, but the solution space is smoother. The choice of kinematics as controls is advantageous in directly describing quiet sitting and standing poses. Moreover, the ability to define and redefine the hip position is useful in exploring effects of seat height and relative anterior-posterior (AP) foot position, known to influence natural STS [7], on the predicted motion.

Defining a cost function for the optimizer is an attempt at modelling preferences in motion. The cost function created here penalizes mechanical effort with respect to the foundational theory that people move in ways that are energy-efficient [99, 100] and, for the first time, motions contrary to standing, (i.e. slipping and falling), which an individual would avoid when getting up from a chair.

The optimal control strategy, dynamic optimization of time histories of the generalized coordinates, allows increasing motion complexity through an iterative technique. It is in harmony with the foundational belief that natural, practiced motions are optimal and learned. The complexity of the optimization problem is increased by performing degree elevation, but by seeding the solver with the solution of the problem with fewer control points, it remains manageable.

3.2.1 The controls

The global (X,Y) position of the hip relative to ankle location and angle of inclination of the HAT are represented as three composite Bézier curves, or paths, in the time domain. Bézier curves are smooth parametric curves with points defined, in [127], by a function of the form

$$\mathbf{p}(u) = \sum_{i=0}^{n} \mathbf{p}_i \binom{n}{i} u^i (1-u)^{n-i} \qquad u \in [0,1] \tag{3.5}$$

where the term $\binom{n}{i}$ is the binomial coefficients. In matrix form this is,

$$\mathbf{p}(u) = \mathbf{U}\mathbf{M_B}\mathbf{P} \tag{3.6}$$

where $\mathbf{U}$ is a 1 x n+1 row matrix of the powers of the parametric coordinate u,

$$\mathbf{U} = \begin{bmatrix} u^n & u^{n-1} & \dots & u^1 & 1 \end{bmatrix} \tag{3.7}$$

$\mathbf{M_B}$ is the n+1 x n+1 Bézier basis transformation matrix, and $\mathbf{P}$ is the n+1 x 1 column matrix of two-dimensional control points, $\mathbf{p}$. To transform between u and time, u is multiplied by the final time.

The initial paths are shown in Figure 3.3. The sitting component is the first part of each path and describes the coordinate in quiet sitting as two sitting control points of equal value, as seen in the Figure. For example, the control points, (X_{sit},0) and (X_{sit},1) define the Bézier curve representing the AP position of the hip, X, during quiet sitting. As such, the AP position of the hip is described for the entirety of quiet sitting as

$$X(u) = \begin{bmatrix} u & 1 \end{bmatrix} \begin{bmatrix} -1 & 1 \\ 1 & 0 \end{bmatrix} \begin{bmatrix} (X_{sit}, 0) \\ (X_{sit}, 1) \end{bmatrix} \tag{3.8}$$

Multiplying this out,

$$X(u) = (X_{sit}, u) \tag{3.9}$$

That is, the hip is at the location X_{sit} at all times during quiet sitting. As mentioned in Equation 3.5, u assumes values between 0 and 1 inclusively. It is analogous to a percentage

of motion and is scalable to suit the motion of interest. In the case of quiet sitting, multiplying u by 0.5 seconds gives the desired (static) motion seen in the first half second of the following figure.

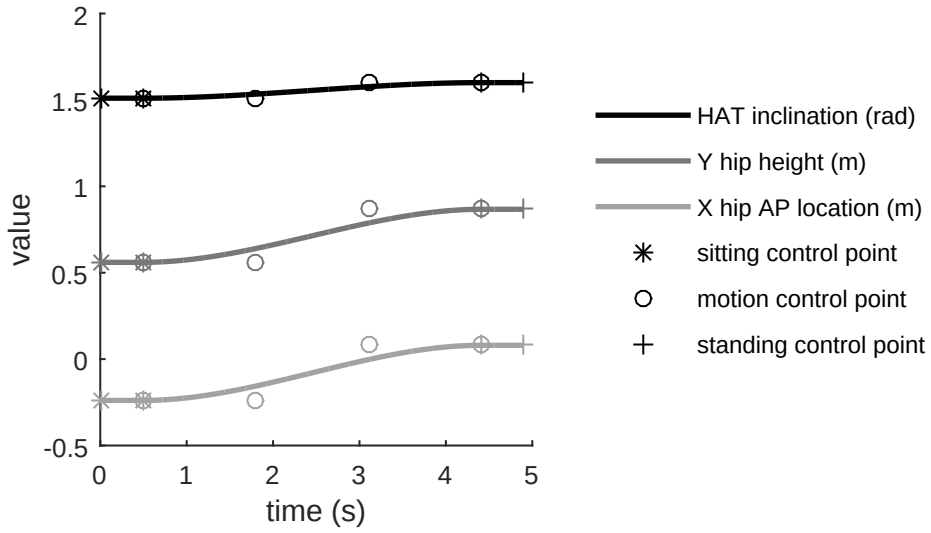

Figure 3.3: Three Bézier curves describing the initial motion paths with sitting, motion, and standing components.

The motion component is the middle part of each path and begins and ends with two control points of sitting and standing values, respectively, to enforce first derivative continuity. The standing component of is the final part of each path and again has two control points to parameterize quiet standing. Coordinate values for sitting and standing are determined from the literature [58] with freedom given to the sitting hip height and standing hip AP position because simulation results are very sensitive to the initial buttocks deformation and because of natural patterns of balance in quiet stance [128]. In this parameterization of a human motion, there are bounds that must be observed. Hip height is bounded to enforce contact with the chair during sitting, and all points must maintain their sequence in time to prevent the model from being directed to two places at once.

That is,

$$\mathbf{p}_{i,1} > \mathbf{p}_{i-1,1} \qquad i = 1, \ldots, n+1 \tag{3.10}$$

Beyond this, only the number and value of control points restricts possible motions. A five-second window is prescribed for the path; including a half second each for each of the sitting and standing components, to be able to represent STS motions slightly longer than the average plus one standard deviation [27].

The paths, and therefore the candidate STS motions, are determined by the locations of the control points. Initially, the possible shapes of these curves are limited as only the two intermediate points of each path may move in time and only points parametrizing the hip height while sitting, and hip AP position while standing may change in value. For greater freedom, two control points, free to move in time and value, are added to the motion component of each path while preserving the shape of the path by the process of degree elevation.

By degree elevation, the number of control points is increased while the shape of the curve is maintained. Because both the previous ($\mathbf{p}$) and new ($\mathbf{p}'$) set of control points must generate the same curve, it is true that

$$\mathbf{p}'(u) = \mathbf{p}(u) \tag{3.11}$$

For one degree elevation, this is

$$\sum_{i=0}^{n+1} \mathbf{p}'_i \binom{n+1}{i} u^i (1-u)^{n+1-i} = \sum_{i=0}^{n} \mathbf{p}_i \binom{n}{i} u^i (1-u)^{n-i} \tag{3.12}$$

which is true when

$$\mathbf{p}'_i = \left(\frac{i}{n+1}\right) \mathbf{p}_{i-1} + \left(1 - \frac{i}{n+1}\right) \mathbf{p}_i \tag{3.13}$$

In short, a Bézier curve described by a set of control points may be described by a larger set of control points determined from the original set. This work leverages this attractive characteristic of Bézier curves.

3.2.2 Objective function construction

Candidate motions are evaluated for optimality including feasibility. Impossible configurations ($error_h$), motions that ought to result in tipping ($error_t$), lifting ($error_l$) or slipping ($error_s$) of the foot are penalized as follows,

$$cost_{error} = w_h \int_0^5 error_h^2 \mathrm{d}t + w_t \int_0^5 error_t^2 \mathrm{d}t + w_l \int_0^5 error_l^2 \mathrm{d}t + w_s \int_0^5 error_s^2 \mathrm{d}t \quad (3.14)$$

where $w_h = 1$ N^2, $w_t = 10^3$ N^2, $w_l = 1$ m^2, and $w_s = 1$ m^2, are weighting factors and $error_h$, $error_t$, $error_l$, and $error_s$ are calculated from Equations 3.1 through 3.4. It is important to the optimal control identification process, described in the next sub-section, that these errors are weighted because, from observation, it is detrimental to either focus on or disregard them entirely.

Beyond feasibility, optimality is determined in accordance with the theory that the healthy population performs everyday motions in ways demanding minimal exertion, which in this model is considered as the time history of active joint torques [52, 101, 110] determined by inverse dynamics. Therefore, the effort of a candidate STS motion is evaluated as the sum of required joint torques, squared, as in Equation 3.15

$$cost_{torque} = \int_0^5 A_M^2 \mathrm{d}t + \int_0^5 K_M^2 \mathrm{d}t + \int_0^5 H_M^2 \mathrm{d}t \quad (3.15)$$

where A_M, K_M, and H_M are the net ankle, knee, and hip joint moments, respectively.

The overall cost of a candidate STS motion is

$$cost = cost_{torque} + cost_{error} \quad (3.16)$$

3.2.3 Computation of optimal controls

An initial optimization problem is solved to establish a feasible STS starting-point. The initial motion is passed to the model, and errors in feasibility are calculated. Control point

locations are adjusted by *fmincon* in MATLAB [129] to decrease errors (Equation 3.14). The routine exits with the first solution with zero associated error. This STS motion is used to seed the solver in the iterative dynamic optimization routine.

The iterative dynamic optimization routine is shown in Figure 3.4. The initial motion is passed to the model, and errors in feasibility and the joint torques required to complete the STS are calculated. Control point locations are adjusted by *fmincon* to decrease cost (Equation 3.16). This choice of a gradient-based solver likely influences the importance of weighting errors, as mentioned, aiming for a value large enough to influence the cost of the solution, but not dictate it. The optimal control points are those that minimize cost with zero associated error. The cost of this candidate motion is recorded when the routine terminates. This process is repeated after elevating the degree of each path by one, giving increased freedom to possible solutions. This process is iterated until successive solutions demonstrate convergence.

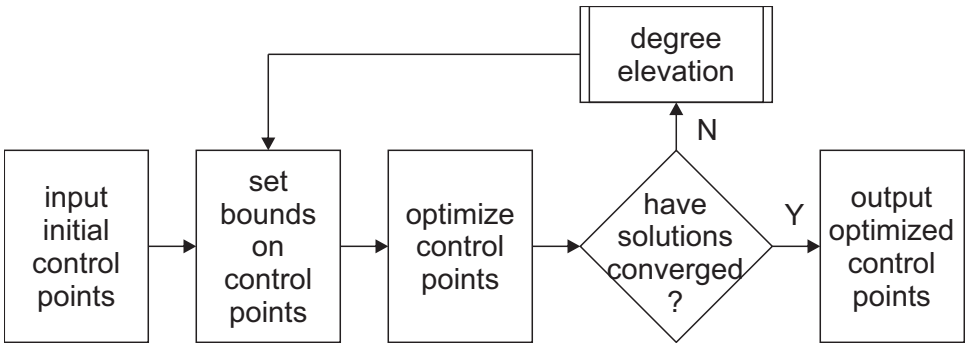

Figure 3.4: The iterative routine to determine an optimal sit-to-stand.

The range of required joint torques is evaluated against normative joint torque strengths of old females [113], as in Figure 3.5, as a final, manual, check of feasibility and a prediction acceptance criterion. The solution at the end of this process is purely predictive STS.

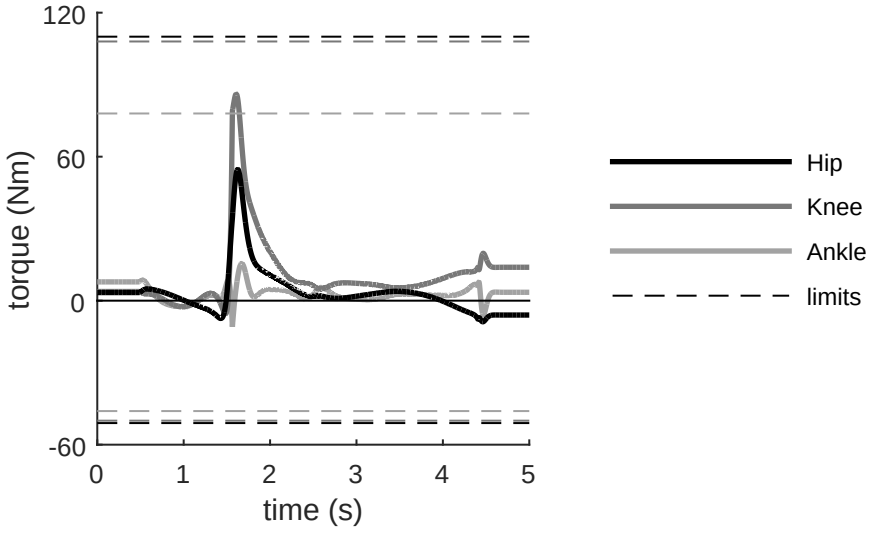

Figure 3.5: Joint torques for optimal sit-to-stand from a 46 cm chair compared to joint torque strengths (horizontal limit lines), reported in Schultz et al. [113].

3.3 Resulting motion

STS predictions are fully parameterized by the locations of the control points. The iterative process described in the previous section adds control points necessary in defining coordinate paths that converge to a solution. While there is limited freedom in the initial set of control points, the final paths demonstrate the versatility of a higher-order Bézier curve. The optimal coordinate paths of STS from a 46 cm chair are shown in Figure 3.6.

Paths of optimal control points were input to the model and ground reaction forces were determined through inverse dynamics to define the start and end of the predicted STS as in Equations 2.1 and 2.6. The resulting motion is shown as a series of snapshots in Figure 3.7. It is a point of curiosity that the model chooses a standing pose with legs straighter and HAT more forward than observed in experiment. Looking to Figure 3.7, above, the predicted standing posture does resemble standing and from Figure 3.5 it is clear that the predicted standing posture is more cost effective (Equation 3.16) than the pre-

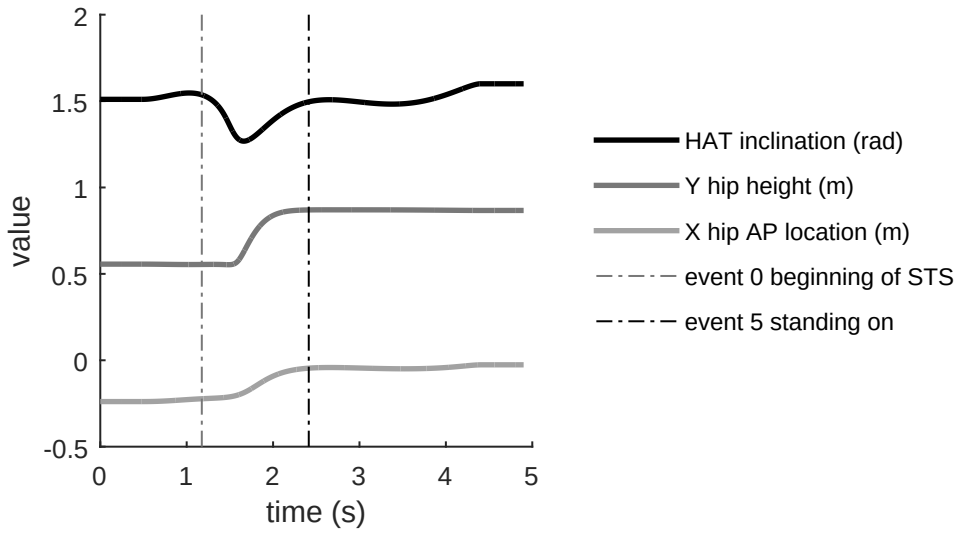

Figure 3.6: Optimal sit-to-stand from a 46 cm chair.

scribed standing posture. This predicted end-posture describes statically stable standing and deemed acceptable for this exercise.

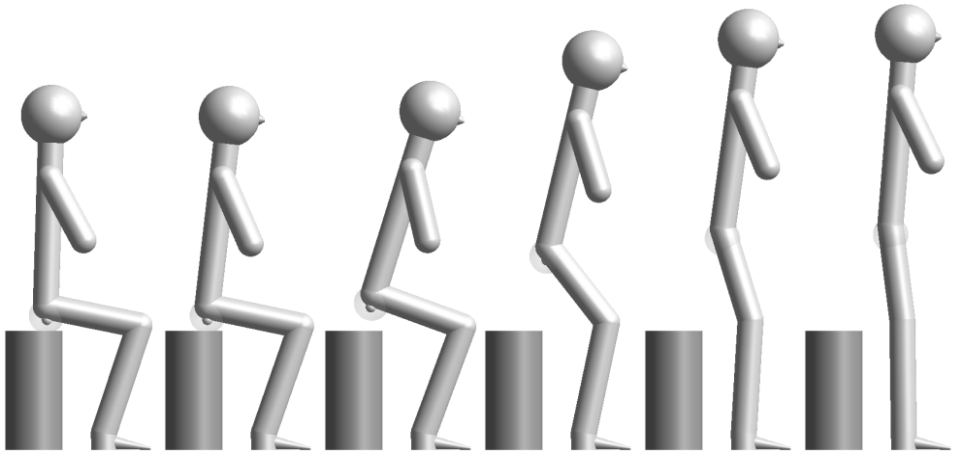

Figure 3.7: Evenly spaced snapshots of predicted sit-to-stand.

The prediction looks reasonable, as has been said of past work. From sitting, the model flexes the HAT, the buttocks lift from the chair, and the ankles dorsiflex and then return

to a neutral posture while the knees and hips extend to standing. To examine how valid is this optimal STS, it is compared to normative data from the literature.

3.4 Comparison with healthy sit-to-stand

A predicted STS is evaluated against two sets of normative data introduced in Chapter 2: one, from a paper by Nuzik et al., describing angular positions at evenly-spaced intervals [58] and the other, from a paper by Kralj et al., defining the timing of kinematic and kinetic events [27] of STS in a healthy population. As has been mentioned, STS is strongly influenced by seat height and AP foot location. It is impossible to replicate definitively the sitting pose in either paper with the limited information given for the stature of our biomechanical model, so the results of three conditions are examined. The first considers a chair height of 51 cm, the maximum height of a standard adjustable chair [124], which provides best agreement to sitting joint angles from Nuzik et al. The second considers a chair lowered to 46 cm, the only height common between papers, with foot location kept constant. The third results are for a chair furthered lowered to 42 cm, a height within range of the chairs used by Kralj et al., and the minimum height of a standard adjustable chair. All chair conditions are for the same subject, as if the same person sat in three different chairs.

The kinematics and kinetics calculated, for the optimal paths predicted, are next compared to the normative occurrence of events separating the phases of STS: quiet sitting, initiation, seat unloading, ascending with vertical acceleration, deceleration, stabilization, and quiet standing [27].

Figure 3.8 shows the differences between predicted results and normative joint angle data. The plot of the hip angle does not include a standard deviation for comparison with this lumped HAT model because the mean is calculated as a function of the pelvis and trunk angles reported by Nuzik et al. shown in Figures 2.1 and 2.2. The predicted

joint angles closely follow the normative trends during STS and, from the 51 cm chair, are often within 1 standard deviation of healthy variation. Because of the model's stature, initial angles are deviated for the lower chairs. The prediction with 46 cm chair faithfully represents the range of ankle dorsiflexion from Nuzik et al. from a chair of equal height. Two trends noticed will be discussed further in the Discussion Section. First, a trend of increasing peak hip flexion with decreasing chair height was observed in the hip angle curve of Figure 3.8. Second, there is a decrease in peak flexion angular velocity of the hip as the chair height increased from 42 cm and 46 cm to 51 cm as seen in Figure 3.9.

As can be observed from Figure 3.6, the prediction reshapes the paths of the generalized coordinates and shortens the duration of STS from 3.96 s to 1.24 s. From all seat heights, the final event of STS, standing on, was predicted to occur within 1.5 s, quicker than even the minimum of what was observed in experiments from the literature. It follows that when event times are compared to their normative occurrence during STS, as in Figure 3.10, few are predicted within range of what is expected from a healthy population.

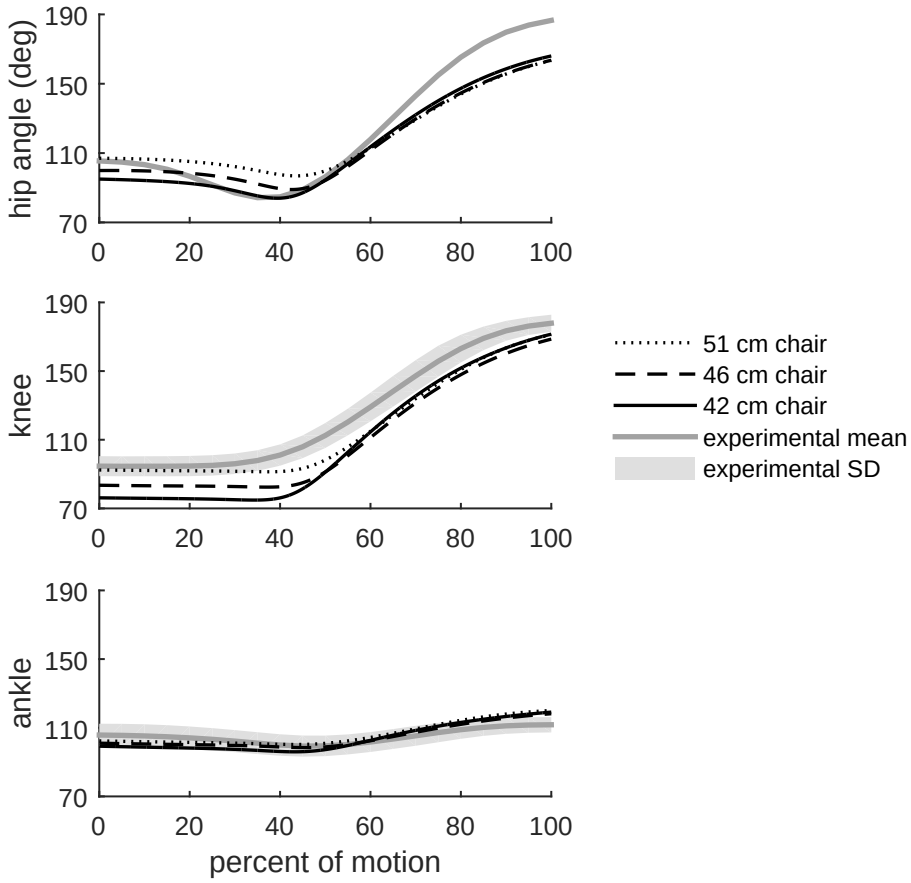

Figure 3.8: Sit-to-stand joint angle profiles as predicted from three chairs compared to experimental sit-to-stand from a 46 cm chair, measured by Nuzik et al. [58]. Seat-off of all predictions is aligned to 47 percent motion. The root mean square errors are 14.3 deg, 9.7 deg, and 4.2 deg at the hip, knee, and ankle, respectively for the 51 cm chair. Similarly, the root mean square errors are 12.9 deg, 15.0 deg, and 3.5 deg, for the 46 cm chair, and 11.6 deg, 17.2 deg, and 4.9 deg, for the 42 cm chair.

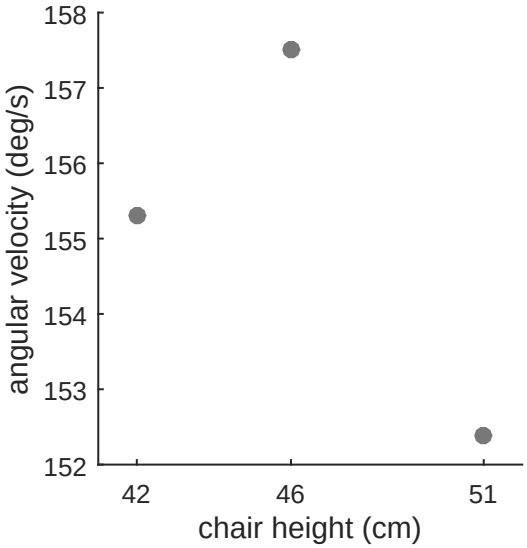

Figure 3.9: Maximum flexion angular velocity of the hip.

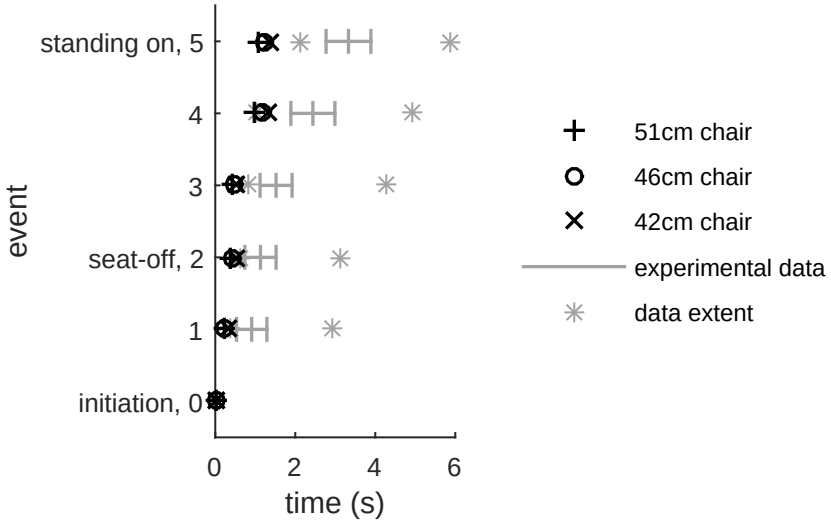

Figure 3.10: Predicted sit-to-stand event timing from three chairs compared to experimental means, standard deviations, and ranges, measured by Kralj et al. [27].

3.5 Discussion

This work has described how healthy females stand from a seated position using a three-link biomechanical model. The proposed model is the most comprehensive planar model used for predicting STS to date and is capable of producing the following gross motions of healthy STS when the chosen controls are driven: HAT flexion, seat off, ankle dorsi- and plantar flexion, knee and hip extension.

Minimizing exertion and using a function of joint torques (Equation 3.15) as intermediary when evaluating candidate motions is not new, however minimizing infeasibilities (Equation 3.14) in the motion is. These performance criteria appear to contain some truth in how healthy people stand from seated and as a result, it predicts STS with generally good agreement to that found in the literature [10, 27, 58].

This is the first use of Bézier curves in dynamic optimization of STS, an application for which they have proven advantageous. As is characteristic of Bézier curves, control points have global rather than local influence on curve shape and so not only is it unnecessary to bound them in value when optimizing, the solution space is smoother. Their shape-conserving properties in degree elevation allow the solution space to start with a small number of control points, or variables, to optimize. The iterative optimization routine maintains a relatively smooth solution space and facilitates use of a computationally inexpensive, gradient-based solver. By exploiting the possibility of degree elevation for Bézier curves, there is no need to predetermine the number of control points defining the final curve, avoiding either prematurely restricting the solution space to exclude the natural solution or over-doing it and having a large and potentially unwieldy optimization problem from the beginning. Also, this method is in harmony with the fundamental belief that natural, practiced motions are optimal.

It was noticed that predictions of STS from decreasing chair height produce increasing angular displacements. This is a phenomenon observed in a healthy population [7] and

the first serendipitous result of this work. A second is the accurately predicted trend of increased hip flexion angular velocity with decreased chair height, from approximately 100% knee height to approximately 80% knee height [7,130], at STS initiation. Finally, the observation that the demand of predicted STS, defined in terms of cost (Equation 3.16), increases with decreasing chair height as expected [7].

The consistencies between prediction and experiment speak to the quality of this model and the motion optimization approach. Predicting over-all motion patterns, characteristic events, and subtle changes in motions caused by changes in chair height is unprecedented in predictive STS research. These results, for a healthy model, give confidence that the model and STS prediction strategy are a credible starting point to predicting pathological STS.

However, there are some places where the prediction fell short. The model did not faithfully predict the standing posture reported in the literature and assumes an end posture with the ankles less flexed and the HAT more inclined than expected. This difference is indicative that people prioritize more than mechanical efficiency when standing, such as spatial awareness and the ability to reject an environmental disturbance are of personal importance, and this model does not address these. Regardless, this alternate end-posture describes statically stable standing and deemed acceptable for this exercise for the time being.

Caution is another human tendency the model does not observe and a possible reason the STS predicted is relatively too quickly. There are, again, further reasons for this. Pure torque producers actuate the model and while the torques are within physiologically plausible ranges there are no checks, at this time, that they can be physically produced by the muscles spanning these joints, which have activation and deactivation time requirements. This point will be addressed in Chapter 5 of this thesis. A last possibly is that the experiments captured anticipatory or terminating motions that are not necessarily mechanically productive to STS and therefore not produced by this model, but there is no intention of

exploring this idea at this time. The discrepancies in event timing are further discussed in Section 4.4.

Requiring immediate exploration, the model predicts the hip and therefore ischial tuberosity locations well above the chair in quiet sitting and the buttocks deformation is substantially less than what is expected. The linear spring-damper and corresponding constants used in this model have created particularly stiff buttocks. Not only does this choice influence kinematics, but also kinetics at a defining level of STS. Chapter 4 addresses the challenge of buttocks modelling for predictive STS.

It is difficult to put these results into context in the greater research community because of the minimal comparison of existing studies to other studies or experimental findings. It is possible to say that this model is superior to others in that it is physically plausible where others are not, in terms of attention to torque limits, for example. It is more versatile than existing models that use, at best, a pre-set numbers of nodes, evenly spaced in time. Possibly the greatest boon of this purely predictive work to another researcher is the unprecedented comparison of both kinematic and kinetic results to normative data that should serve as a benchmark for future work in STS prediction.

4

Better Buttocks for Sit-to-Stand Simulation

The buttocks are reported to transmit between 18 and 77 percent of body weight during quiet sitting [131] and to remain in contact with the chair for the first third of healthy sit-to-stand (STS) [27]. It is important to the work of predicting STS to have a buttocks model capable of characterizing this relatively large force acting while the model sits. The purpose of this work is to model the dynamic response of the soft human buttocks for STS prediction.

When building the biomechanical model, as in Chapter 3, the potential to use buttocks models from past researchers in STS prediction [51, 52, 104–106] was investigated. As discussed in the Chapter 2, their models proved underwhelming in terms of physical meaning and validation. Elsewhere in the literature, constitutive models of component tissues of the buttocks, for example adipose (fat) or muscle, for large ranges of deformations exist [74, 75, 132]. There are models for groups of tissues in small range of deformation, for example seated buttocks [72, 73]. There are also finite element models of individual tissues that have been grouped, for example transverse muscle over adipose tissue, applicable for larger deformations [71]. However, the literature lacks a validated model of buttocks tis-

sues, as a whole, for large changes in deformation, which is necessary for this work. Thus emerged the requirement of describing a buttocks model for application in STS prediction.

First, force-deformation behaviour of the buttocks was collected from 15 healthy participants in a STS experiment to characterize the model. Inspired by the observed behaviour, candidate spring models were specified and, substituting these in a Kelvin-Voigt element, candidate models of buttocks were made. Next, each model was driven by the experimental kinematics and model parameters were tuned to best match the forces measured. Then errors were calculated for each model for each participant to determine which model best represented the participant population.

The model whose response best matched experimental results replaced the simple buttocks model in the biomechanical model from Chapter 3 and that STS prediction routine was run again. The predicted motion was compared to that from Chapter 3 and to normative STS to determine if this buttocks model is viable for use in STS prediction, and to what extent changes in this physical aspect of the model changed the predicted motion.

4.1 Mechanical behaviour of the buttocks

The buttocks are comprised of three tissue layers. The deepest layer is transverse gluteus muscle, superficial to the muscles is adipose tissue, and superficial to both is a layer of skin. In terms of mechanical behaviour, there is an expectation that the buttocks behave as a visco-hyperelastic material [131]. In terms of mechanical properties, the literature lacks information [133] required for mathematical modelling. This section addresses a portion of this need by providing measurements of the force-displacement behaviour of the buttocks in STS. This behaviour is important to developing the mechanical model of the buttocks for STS prediction because, at minimum, a reasonable model ought to produce physiological ranges and profiles of force for a typical STS motion.

4.1.1 Experimental procedure

Fifteen healthy participants, 7 female (23.4 years (3.9), 1.63 m (0.06), 58.1 kg (7.5)) and 8 male (26.1 years (3.2), 1.82 m (0.04), 79.1 kg (8.1)), performed a STS experiment detailed in Appendix A. Participants sat comfortably, toward the front edge of a chair of standard (46 cm) height [124]. This forward sitting posture, an example of which may be seen in Figure 4.1, isolates the majority of interaction between the seat and participant through the buttocks, the response of which is of interest in this experiment. Sitting, the participants were asked to place their feet in a comfortable location where they would not need to move them to stand up. For two minutes, participants remained seated. On cue, they crossed their arms on their chest and sat quietly. On a second cue, three seconds later, they stood up. Participants stood still for five seconds while the collection was completed. On a third cue, the participant walked on the spot for one minute at a self-selected pace to encourage buttocks tissues to return to a neutral state. On a final cue, the participant sat again. This STS task was completed a minimum of eight and a maximum of ten times.

4.1.2 Experiment set-up

Throughout the experiment, participants wore a system of active optical markers. This system consisted of clusters (i.e. markers that are rigidly connected) attached to the right thigh, the right leg, the right foot and the pelvis, as shown in Figure 4.1. Palpation and digitization of bony landmarks created virtual markers on these locations, which were tracked assuming the respective segment as a rigid link. Placements of virtual markers include the right greater trochanter, each of the right medial and lateral femoral epicondyles, right medial malleolus, anterior superior iliac spines and posterior superior iliac spines.

The movement of the markers and, by extension, the kinematics of the subject were captured by a system of six banks of Optotrak Certus cameras at a rate of 100 Hz while, simultaneously, kinetics were collected at 2048 Hz from a pair of Advanced Mechanical

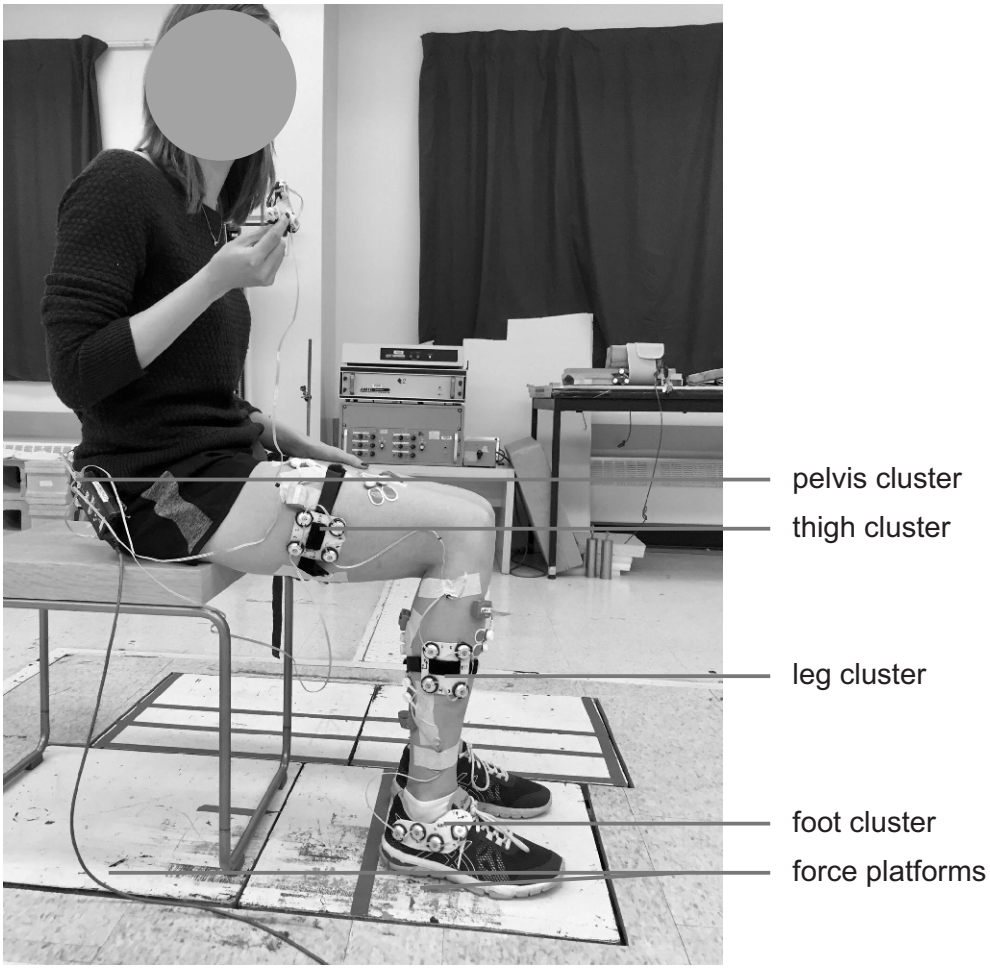

Figure 4.1: One participant, wearing the motion-capture clusters, is sitting on one force platform with feet on another.

Technology Inc. (AMTI) OR6-7 force platforms as seen in Figure 4.1. Studying these kinematics and kinetics together provide insight into the role of the buttocks in STS.

4.1.3 Data processing

Prior to analysis, the data was filtered using a dual-pass Butterworth filter with 6 Hz cut-off frequency. The data was next analyzed for event markers of normative STS, as in Equations 2.1 through 2.6. This analysis required summation of the vertical and fore-aft

force plate data, their first derivatives, and knee kinematics. By calculating knee angles from the relative sagittal-plane geometry of the markers on the greater trochanter, femoral epicondyles, and medial malleolus, consistency with event definitions in the literature [27] was maintained.

Few of the 147 collected trials exhibited normative STS as defined by Kralj et al. [27]. Some trials failed to meet this standard because there was too much movement while sitting or standing to discern STS initiation and termination (i.e. event_0 and event_5). For the remainder of the trials, the difference was overwhelmingly because participants in this study completed STS more quickly than even the fastest subject in Kralj et al. It is assumed this discrepancy is because of differences in the populations and/or environments of the experiments, as discussed in Section 4.4. Because the participants in this study were performing their natural STS, and because of the differences between this study and the study performed by Kralj et al. the focus on timing of all normative events was relaxed. Trials were accepted on the criteria that all events of STS were demonstrated in the defined order. Still, 9 trials were discarded. The remaining 138 trials were analysed for modelling.

Typically, people sit on their ischial tuberosities (ITs). The locations of the ITs, shown in Figure 4.2, are not easily measured directly by external palpation. In this study, the locations of the ITs were instead approximated from the locations of the superior iliac spines, which are easily palpated. The anterior superior iliac spines (ASISs) and posterior superior iliac spines (PSISs) were marked and tracked in the experiment. Approximating the locations of the ITs from the superior iliac spines requires use of a standardized pelvis geometry dataset, pelvis scaling guidelines, and an assumption of left-right pelvis symmetry. The specific method of approximating the locations of these ITs is next.

To approximate the locations of the ITs, first, each subject's pelvis type is categorized according to the dataset of human pelvises from Reynolds et al. [67]. A pelvis is categorized as a female, a smaller male, or a larger male pelvis based on the subject's sex, height, and mass, as in Equation 4.1. For each pelvis type, the Reynolds dataset provides reference

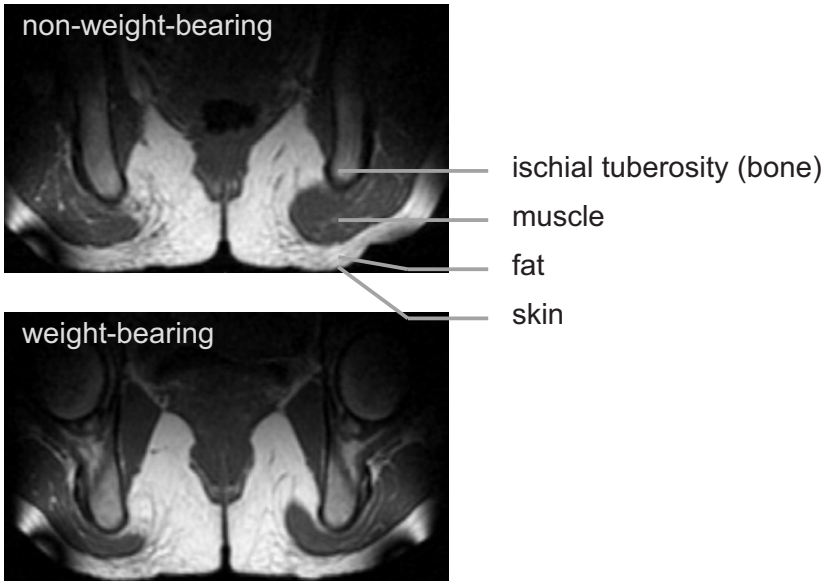

Figure 4.2: Magnetic resonance image of buttocks while lying down (non-weight-bearing) and sitting (weight bearing). Adapted from Linder-Ganz et al. [71] and used with permission.

pelvis geometry with the expected locations of bony landmarks including the anterior superior iliac spines, the left posterior superior iliac spine, and the left IT.

$$pelvis\,type = \begin{cases} female & sex = female \\ larger\,male & height > \dfrac{1657kg - mass}{883\frac{kg}{m}} \\ smaller\,male & otherwise \end{cases} \tag{4.1}$$

The next steps to approximating the locations of the ITs are illustrated in Figure 4.3. After determining which reference (Reynolds') pelvis represents the participant best, locations of the bony landmarks, available only for the left side of the reference pelvis, are reflected across the sagittal plane allowing consideration of the right side of the pelvis as well. Then, the reference pelvis model is scaled anterior-posteriorly and mediolaterally, according the guidelines of White et al. [80], to the geometry of the participant, calculated from the virtual markers placed on the superior iliac spines during the experiment. By

rotating and translating the reference pelvis model, the model tracks the superior iliac spines of the participant for the captured STS motion, identifying expected locations of the ITs for each participant for each trial.

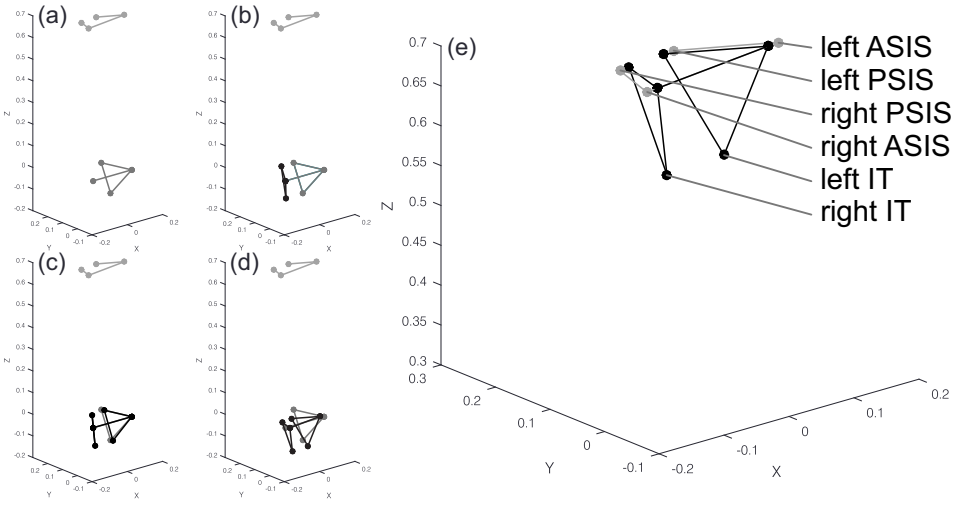

Figure 4.3: Illustrated procedure of approximating the locations of a participant's ischial tuberosities (ITs) from their anterior superior iliac spine (ASIS) and posterior superior iliac spine (PSIS) locations (light gray), a reference pelvis geometry from Reynolds et al. [67] (dark gray), and the scaling guidelines of White et al. [80]. In the top, left-hand corner, plot (a) represents the geometries as they are initially. Plots (b)-(e) represent the reference geometry; (b) reflected sagitally, (c) scaled to the participant, (d) aligned to the participant, (e) superimposed on the participant to estimate IT locations.

There is an element of uncertainty in the estimated location of the ITs because they are not measured directly. Reynolds et al. [67] made measurements on 28 female skeletons, 26 larger male skeletons, and 33 smaller male skeletons, and found standard deviations of 11 mm, 9 mm, and 8 mm, respectively, in the caudal-cranial direction. It is anticipated that discrepancies of similar scale exist in the location of the participants' ITs calculated using the method described in this Section. Nevertheless, now that the locations of the ITs have been estimated, it is possible to analyze the STS forces in light of IT motion.

4.1.4 Experimental results

Experimental data from STS initiation to seat-off is of interest when building a one-dimensional, lumped-parameter buttocks model. After removing the weight of the chair from the data, the vertical component of force on the force plate under the chair starts steady with a small, gradual bump, signifying an increase and then decrease in force, before a rapid descent to zero as seen in Figure 4.4. Female participants in this study sat with approximately 78% of their body weight, on average, on their buttocks. Similarly, male participants sat with approximately 79% of their body weight on their buttocks. These values are just beyond the top of the 18% to 77% range of normalized forces reported in the literature [131].

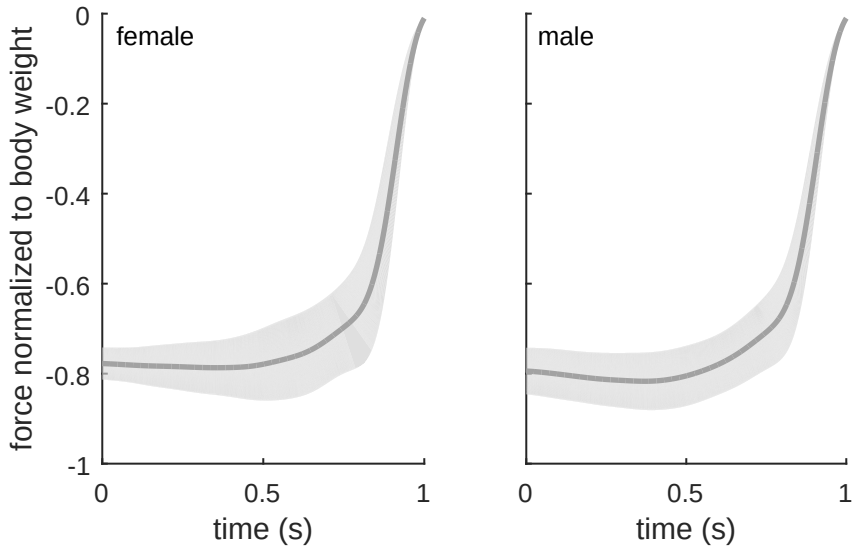

Figure 4.4: Average force profiles at the chair in the second leading to seat-off.

The motions of the ITs, and therefore buttocks deformations, show a similar pattern to that of the forces. Deformation (ΔL) is considered as the change in the thickness of tissue under the ITs from the undeformed thickness, that is

$$\Delta L = l - L \tag{4.2}$$

where l is the tissue thickness and L is the reference tissue thickness, as described in Figure 4.5. Buttocks in the experiment are deformed to a maximum of 3.9 cm on average in both females and males, with an average undeformed dimension of 8.6 cm in females and 7.3 cm in males. This -45% average deformation in females and -53% average deformation in males is within the -27% and -54% range reported in Linder-Ganz et al. [71], measured in six participants. The buttocks are under relatively constant strain until there is a gradual downward shift before a rapid descent to zero. In some cases, but not all, there is a bump, more easily observed in the female deformation rate data in Figure 4.6, between approximately 0.3 and 0.7 seconds before seat-off. This bump signifies that the ITs are driving downward and therefore buttocks tissues are deforming further before standing. Observed deformation rates reach a maximum of less than 0.4 m/s at or very near seat-off.

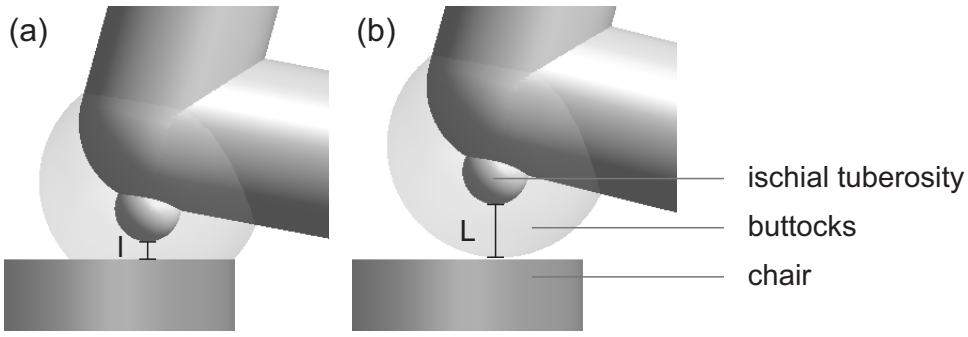

Figure 4.5: The buttocks (a) deformed and (b) undeformed.

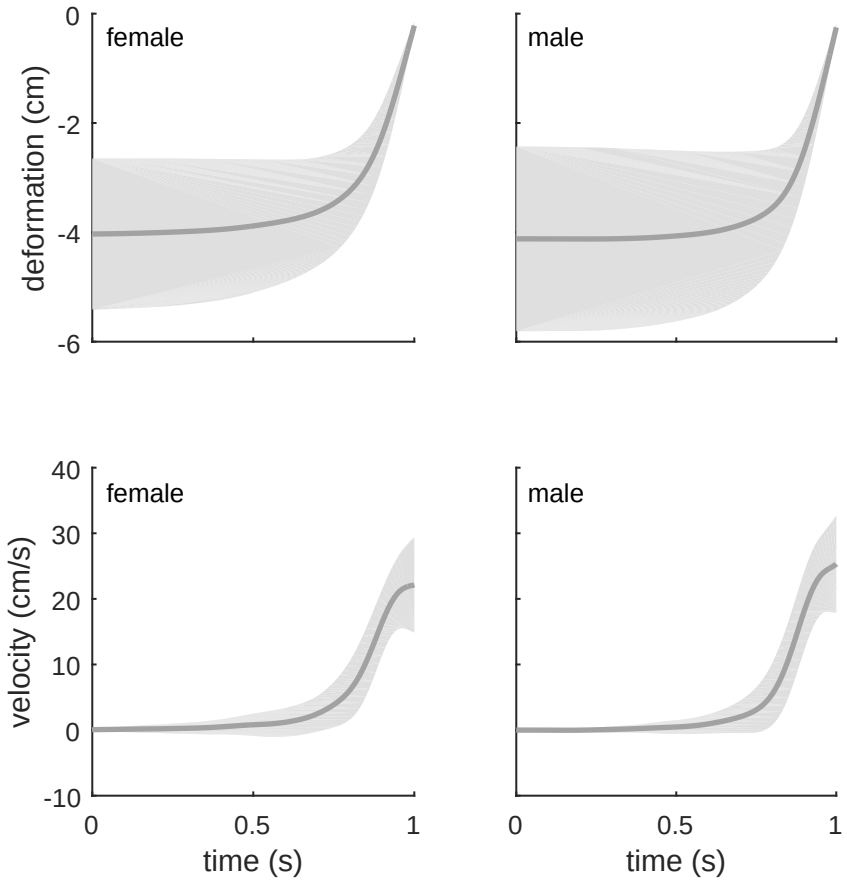

Figure 4.6: Average deformation of the buttocks and vertical velocity of the ischial tuberosities in the second leading to seat-off.

These forces and deformations are considered together to gain insights into the material behaviour of the buttocks. Figure 4.7 shows force-deformation curves of the buttocks during STS. In both females and males, the relationship between force and deformation are non-linear and demonstrate signs of viscoelasticity (portion of hysteresis loop) where deformations are relatively large. In all, buttocks deformations during STS are non linear and finite (i.e. large).

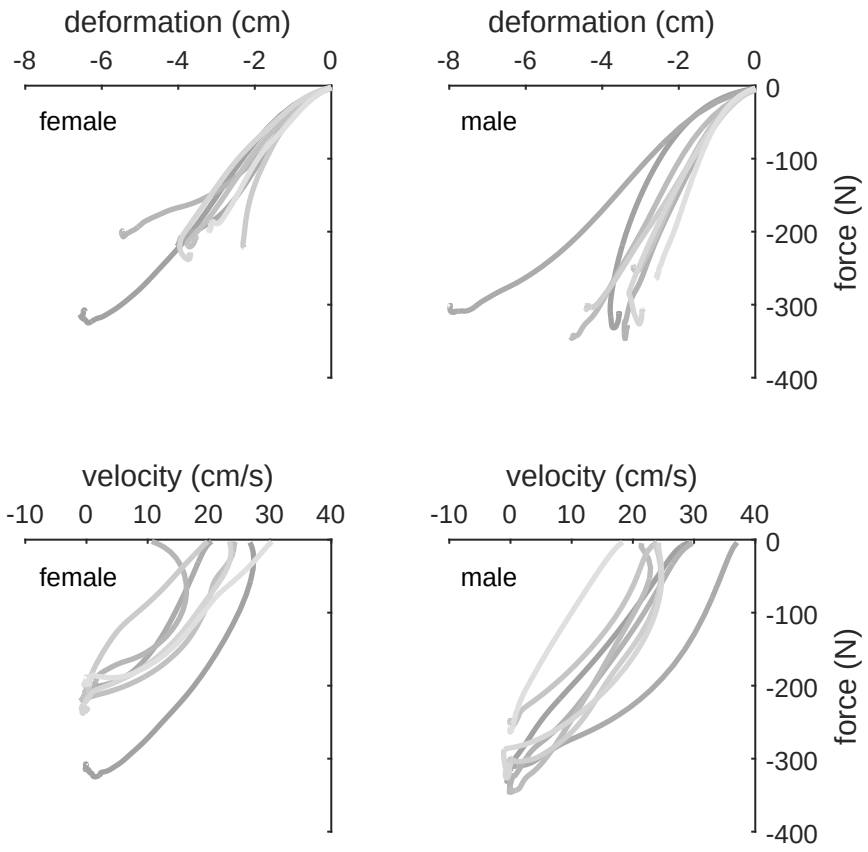

Figure 4.7: Average force-deformation and force-velocity behaviour of each participant's buttock, measured in the sit-to-stand experiment.

4.2 Characterizing the buttocks

The relationship between the forces going through the buttocks and buttocks deformation informs the choice of mechanical buttocks model for implementation. This relationship appears comparable between females and males from the experimental data described in the previous section, and so, for purposes of modelling, the data is lumped together for a larger sample size.

The force-deformation curves in Figure 4.7 are non-linear. The Figures exhibit large deformations and evidence of viscoelasticity. These observations motivate a visco-hyperelastic material model of the buttocks. This section addresses this need by using the experimental data collected and material modelling to construct a lumped parameter force-displacement model of the buttocks.

4.2.1 Constructing the model

From the literature and the presented experiments, it is clear that the dominant response of the buttocks during STS is characteristic of a visco-hyperelastic solid. This motivates a Kelvin-Voigt material model with a non-linear spring element. Inspired by models of soft tissues in this and other applications, three hyperelastic spring models are derived in Appendix B, characterized by neo-Hookean, Mooney-Rivlin, and Ogden strain energy density functions, respectively. A linear spring model, used in Chapter 3, is considered as a baseline of performance.

The equation of a linear spring is well known,

$$F_{linear} = kx \tag{4.3}$$

where k is the spring stiffness and x is the lengthening (or shortening) of the spring from it's equilibrium state, as in Figure 4.8. With regards to the buttocks model, the displacement x is the deformation, ΔL, from Equation 4.2.

Neo-Hookean and Mooney-Rivlin models are, in fact, Ogden-type models of first and second order, respectively. A third order "Ogden" model was also derived, and the equivalent spring equations of these hyperelastic models are

$$F_{nH} = \mu_{nH}\left(\lambda - \lambda^{-2}\right) \tag{4.4}$$

$$F_{MR} = \mu_{MR1}\left(\lambda - \lambda^{-2}\right) + \mu_{MR2}\left(\lambda^{-3} - 1\right) \tag{4.5}$$

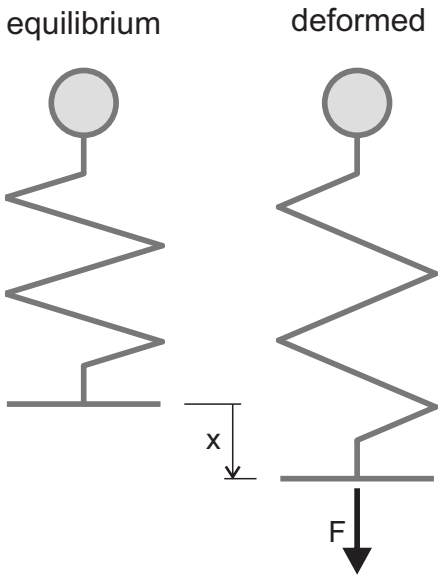

Figure 4.8: Deformation of a spring.

$$F_O = \mu_{O1}\left(\lambda - \lambda^{-2}\right) + \mu_{O2}\left(\lambda^{-3} - 1\right) + \mu_{O3}\left(\lambda^{\alpha-1} - \lambda^{-\frac{\alpha}{2}-1}\right) \tag{4.6}$$

where λ is the principal stretch ratio,

$$\lambda = \frac{l}{L} \tag{4.7}$$

from the lengths defined in Equation 4.2.

These hyperelastic spring equations are used to describe the force developed in the spring of the Kelvin-Voigt element under deformation.

A damper is used to describe the viscous property of the buttocks as,

$$F_d = c\frac{dx}{dt} \tag{4.8}$$

where c is the damping coefficient.

Adding an elastogap [123] to the Kelvin-Voigt element alleviates the trouble of sticking identified in previous work and enforces continuity in contact forces in STS. It accomplishes

this by bounding the force developed in the damper as in Equation 4.9 and Figure 4.9. For a negative spring force

$$F_{damper} = \begin{cases} F_{spring} & F_d < F_{spring} \\ -F_{spring} & F_d > -F_{spring} \\ F_d & otherwise \end{cases} \tag{4.9}$$

the contact force of the Kelvin-Voigt element is

$$F = F_{spring} + F_{damper} \tag{4.10}$$

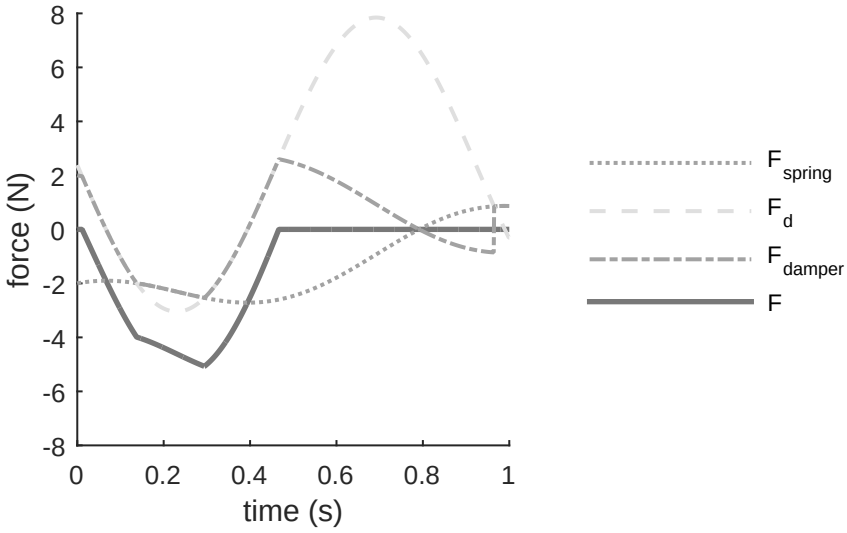

Figure 4.9: Example effects of the elastogap model.

There are now four forms of candidate buttock models, all with parameters to be determined, and it remains unknown which is the best for use in STS prediction.

4.2.2 Parameter identification

The behaviours of the constitutive models depend heavily on their parameters. These parameters, shown in Table 4.1, are physical in nature and assumed to be consistent for

each participant over the trials performed. Natural variability, which may motivate a desire to define subject-specific parameters, is neglected and parameter values are sought that best represent the buttocks across the participant population for use in the biomechanical model.

An optimization scheme was used to identify best parameters for each model across the population of participants based on the experimental data collected. The experimental kinematics of each subject is used to drive their pelvis model for all trials they completed. This biomechanical model is augmented with each buttocks model. The corresponding, simulated, kinetics are calculated by the candidate buttocks model and compared to experimentally collected kinetics. Errors in the simulated kinetics are evaluated in a least squares sense as

$$sum\,of\,squared\,errors = \sum_{i=1}^{n} \left(F_i - \widehat{F}_i\right)^2 \tag{4.11}$$

where n is the number of frames, F_i is the vertical buttocks force measured at the ith frame and $\widehat{F}_i$ is the force produced by the model from the geometry of the ith frame. The best parameters for each model come closest to reproducing the experimental force when driven with experimental kinematics.

Parameters were unbounded with the exception of the damping coefficient. Because the rate of deformations recorded in experiments, shown in Figure 4.6, were particularly low, it is possible that this parameter was not adequately excited for identification and a lower limit of 371 Ns/m [72, 134] was set in the parameter optimization routine.

The identified parameters are provided in Table 4.1. That the identified values of the damping parameters are the minimum possible value, in three of four models, reaffirms the assumption that there is a lack of data for determining the damping coefficient. The simulated force profiles from the experimental kinematics are shown in Figure 4.10.

When simulated with experimental kinematics, all of the spring models had a mean response similar to the experimental mean. The Mooney-Rivlin model tracks the mean best. The linear model and neo-Hookean model are underestimating the force for a majority

Table 4.1: Parameters of the four candidate spring models.

Model	Parameter	Identified value	
Linear	k	12700	N/m
	c_l	371	Ns/m
neo-Hookean	μ_{nH}	53	N
	c_{nH}	371	Ns/m
Mooney-Rivlin	μ_{MR1}	213	N
	μ_{MR2}	34	N
	c_{MR}	371	Ns/m
Ogden	μ_{O1}	2090	N
	μ_{O2}	94	N
	μ_{O3}	7650	N
	α	-0.7	-
	c_O	815	Ns/m

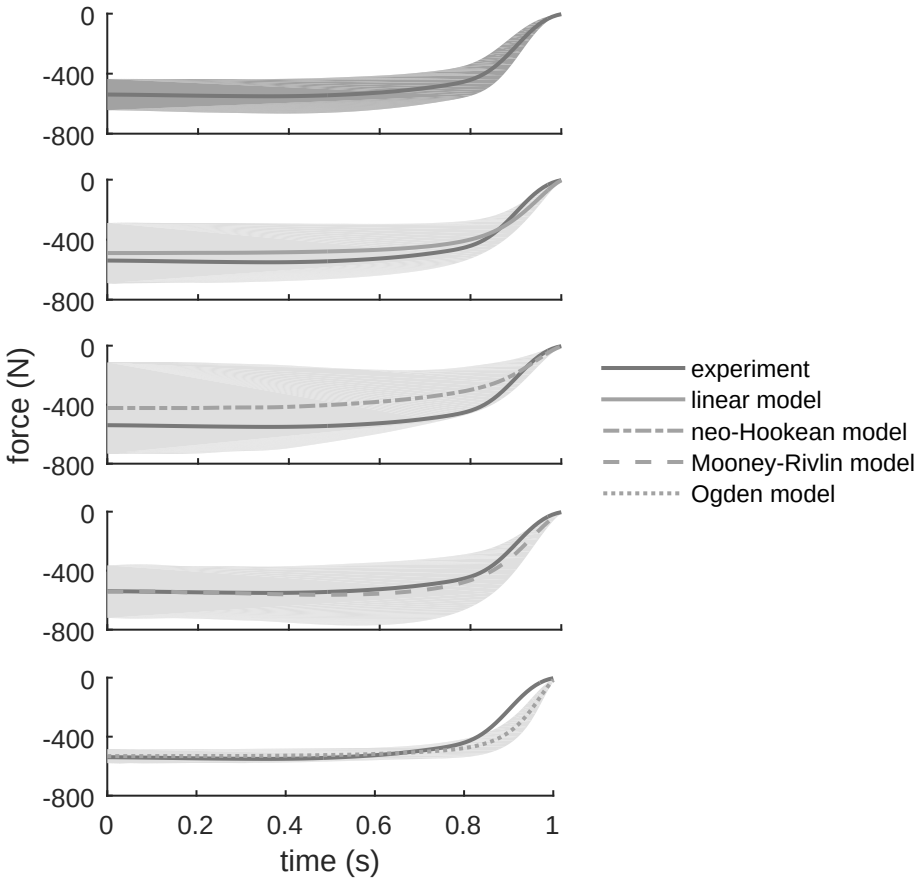

Figure 4.10: Experimental forces leading to seat-off versus simulated forces from the candidate buttocks models.

of sitting. All models over-estimate force close to seat-off (approximately 0.9 to 1.0 s in Figure 4.10) although the neo-Hookeam model makes the closest approximation. There are differences in variance of forces also. All models other than the Ogden model have greater variability than was seen in experiment, with the neo-Hookean having the greatest standard deviation. From this evidence, it is assumed that one model will prove best for representing general buttocks. A statistical analysis is performed to identify this model.

4.2.3 Statistical analysis

The goal of this exercise is to determine the buttocks model to be implemented in the biomechanical model, introduced in Chapter 3. The biomechanical model may be described as a Frankenstein model, with sub-models and parameter values from across the literature gathered together. It is not representative of an individual; similarly, its buttocks is not expected to be representative of one individual, but it is important that it have buttocks that could reasonably belong to a person. For this reason, the preferred buttocks model is one that best represents the participant population.

In this case, "best" was decided as the model whose kinetic response to experimental kinematics best matched experimental kinetics. The sum of squared errors was calculated as in Equation 4.11 for the four optimized models for each simulated trial and normalized to the number of frames per trial. Errors within each participant were averaged so that each participant-model pair has an associated error. The errors of the models are right skewed, as seen in Figure 4.11. As the distributions of errors are non-normal, the Kruskal-Wallis test (*kruskalwallis* in MATLAB) rather than the classical analysis of variance (ANOVA), was used to compare them.

The Kruskal-Wallis test rejected the null hypothesis that each models errors come from the same distribution. From this result, a multiple comparison test was performed, using the MATLAB function *multcompare*, to determine which of the models have statistically different errors. This test concludes that the mean rank of the third-order Ogden model is statistically different from the mean ranks of the linear ($p<0.04$) and neo-Hookean ($p<0.01$) models. Although the test did not show statistical difference between the Mooney-Rivlin model and linear ($p<0.47$) model, both the linear and neo-Hookean models were removed from consideration on the bases that they are statistically inferior to the third-order Ogden model and that their mean errors are greater than the mean error of the Mooney-Rivlin model.

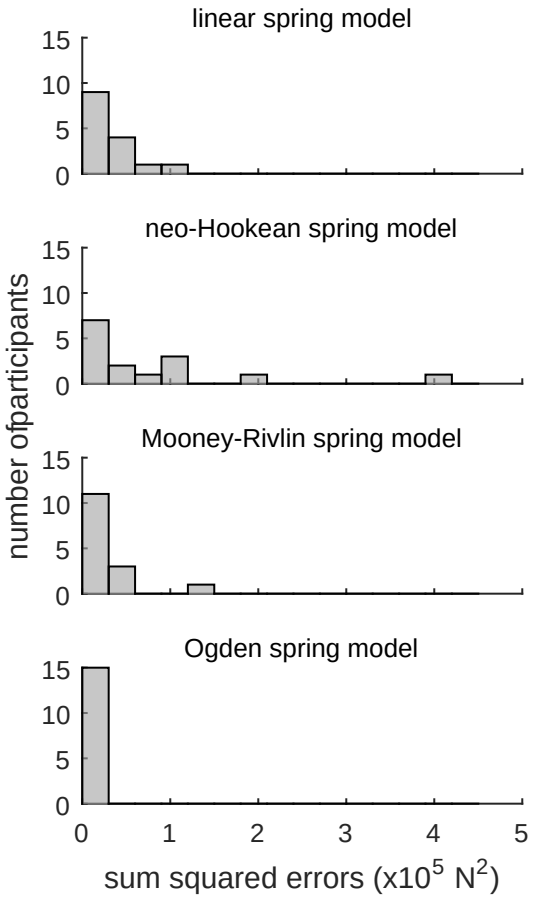

Figure 4.11: Errors of the candidate buttocks models.

Next, the responses of the two remaining spring models to deformation were compared. The range of stretch (Equation 4.7) found in experiment was applied, with results plotted in Figure 4.12. It is important to keep in mind that elastic and viscous effects are lumped together in the experimental results and the lines of the modelled force are for the candidate springs alone. It is also useful to remember that the dampers modelled in the Kelvin-Voigt elements of the buttocks are able to contribute damping forces up to the magnitude of the spring force. With this in mind, both models follow the trend of experimental data between stretches of 0.7 and 0.4 reasonably well. Between stretches of 1 and 0.7, the Ogden model is

specifies quite a large contact force (with a curve under the experimental data) reflective of the separation of the experimental force curve and the Ogden model's force curve in the 0.2s before seat-off in Figure 4.10, while the Mooney-Rivlin model performs markedly better. Between stretches of 0.4 and 0.2, the Ogden model dictates the material phenomenon of yielding followed by strain hardening to a level that is not seen in the experimental data, while the Mooney-Rivlin model dictates particularly large forces but no such anomalous behaviour. Over all, the force-deformation(stretch) behaviour of the Mooney-Rivlin spring more closely represents the force-deformation behaviour of the buttocks seen in experiment, and is the preferred model.

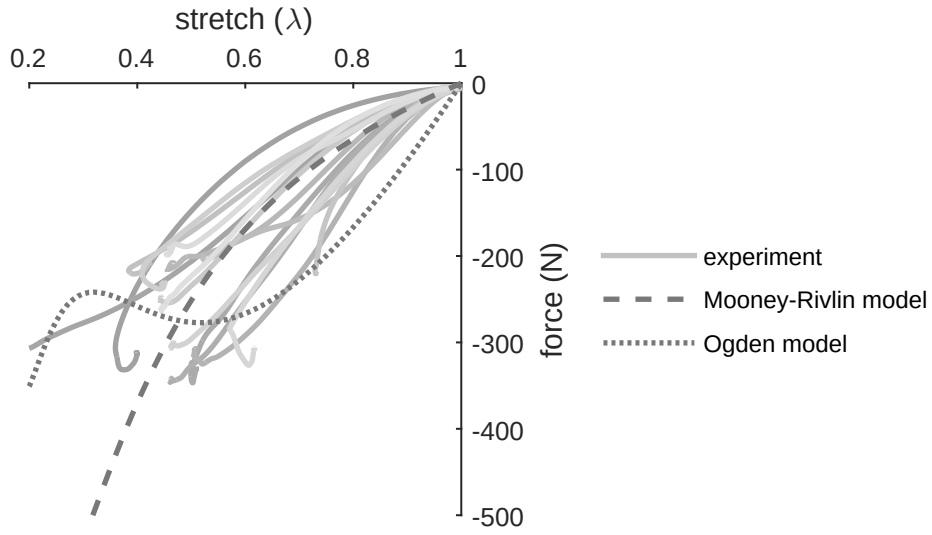

Figure 4.12: Force-deformation behaviour of the participants' buttocks and the candidate spring models.

4.3 Sit-to-stand prediction with better buttocks

The purpose of developing this buttocks model is to use it in a biomechanical model for STS prediction. The "old" linear buttocks model [73] used in Chapter 3 was removed

from the biomechanical model and the "new" Mooney-Rivlin buttocks model determined in Section 4.2 replaced it. The weighting factor w_t in Equation 3.14 was increased from 10^3 N^2 to 1.3×10^3 N^2 so that the magnitude of the errors produced using the new buttocks model were similar to those using the old buttocks model for the initial motion paths. The STS prediction routine outlined in Chapter 3 was run again for the updated biomechanical model for a 46 cm chair. This produced the STS motion in Figure 4.13. As before, the gross motions predicted are consistent with healthy STS.

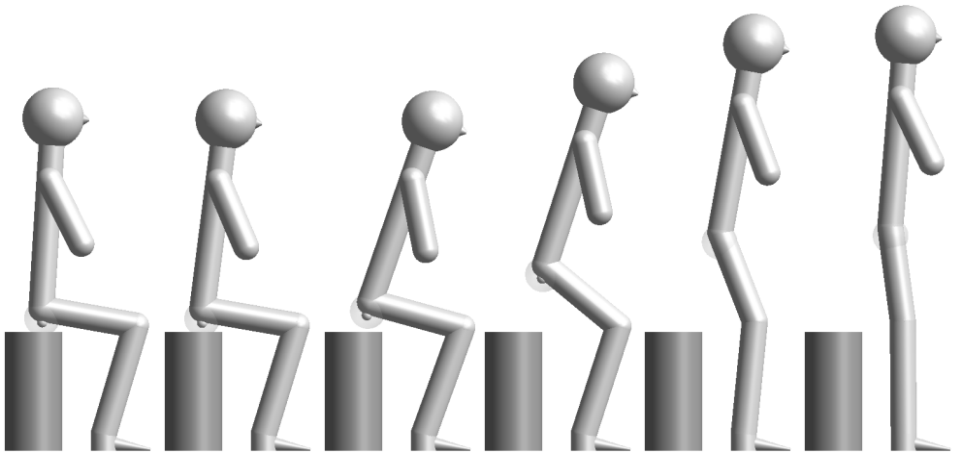

Figure 4.13: Evenly spaced snapshots of predicted sit-to-stand.

4.3.1 Comparison with the prediction using the Chapter 3 model

The optimal coordinate paths of STS from a 46 cm chair are shown in Figure 4.14 for models with each the old and new buttocks. The STS motions predicted using each model are comparable with a major difference being STS duration and three minor differences in kinematics. As can be observed, the prediction reshapes the paths of the generalized coordinates and lengthens the duration of STS to 1.55 s with the new model, compared to 1.24 s with the old model. Even so, 1.55 s is much faster than STS durations reported in the literature. The first minor difference is that the new buttocks model lends itself to a STS with less anterior-posterior translation of the hip prior to STS. The second minor

difference is that the hip of the model with the new buttocks doesn't extend prior to flexion. And the last minor difference is that the is that the hip of the model with the new buttocks flexes more deeply. These kinematic differences are reflected the first two snapshots of both Figures 4.13 and 3.7 in that the model with the new buttocks "digs into" the chair before seat-off, while the previous model does not.

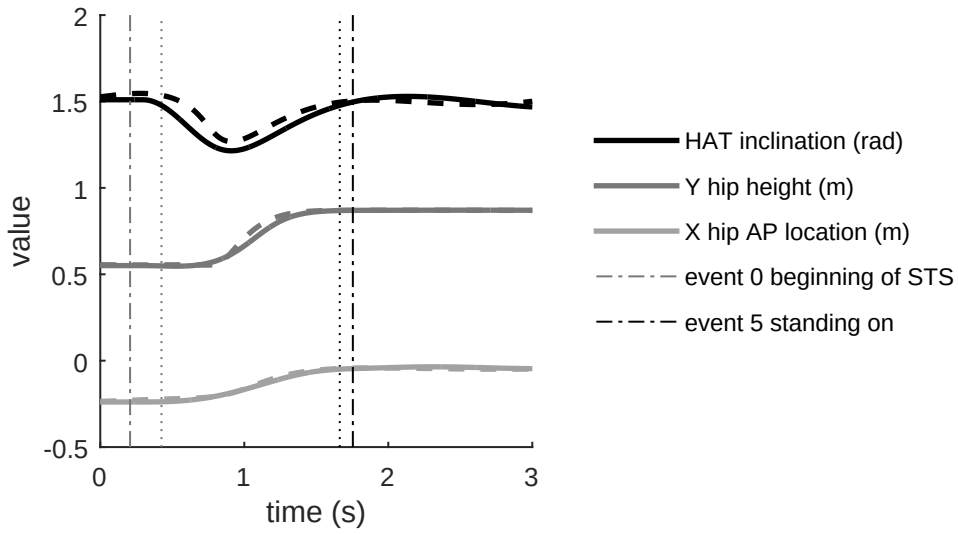

Figure 4.14: Optimal sit-to-stand from a 46 cm chair with the new buttocks model, compared to the results of Chapter 3 (dashed curves and dotted vertical lines).

Although the STS motions may be similar, there are large differences in the joint torques associated with the optimal STS of each model, as seen in Figure 4.15. The over-all trends of joint torques are similar but the peak torques required are lower with the new buttocks model, although they are be sustained longer.

According to Equation 3.15, the optimal STS of the model with the new buttocks is more costly, and requires greater exertion, than the old model. In this sense, it can be thought of as being more difficult, which is true in the sense that it is more difficult to get up from a chair with a softer cushion than a firmer one [135]. Perhaps it is also true

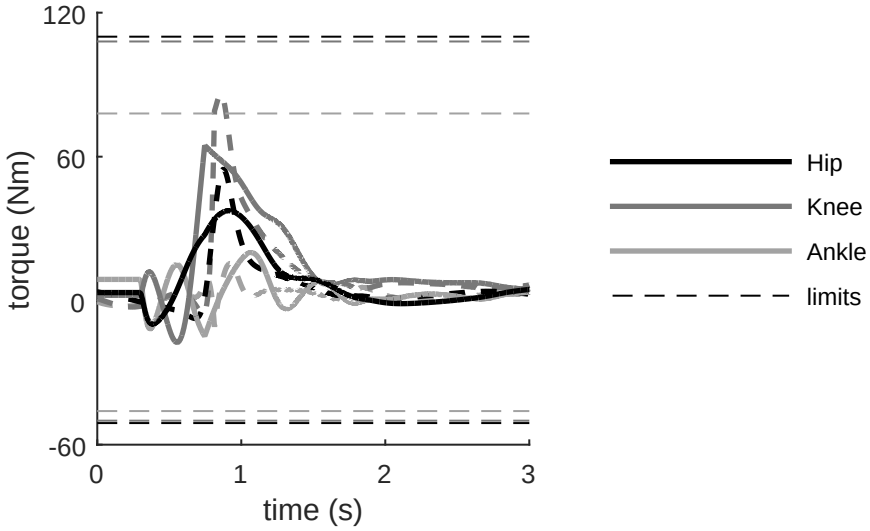

Figure 4.15: Joint torques for optimal sit-to-stand from a 46 cm chair with the new buttocks model (solid curves), compared to the results of Chapter 3 (dashed curves), compared to joint torque strengths, reported in Schultz et al. [113].

that a softer chair should be preferred by a person reluctant to produce large joint torques, preferring to sustain moderate joint torques for a longer duration of STS.

4.3.2 Comparison with healthy sit-to-stand

To examine the validity of the STS prediction, it is compared to normative data from the literature in Figures 4.16 and 4.17. The predicted angles closely follow the normative trends during STS, although the hip appears particularly flexed in sitting and standing and the knee is particularly flexed in sitting. Although STS is predicted to take longer with the new buttock, only three of the six events of STS are predicted within the range of times reported in the literature.

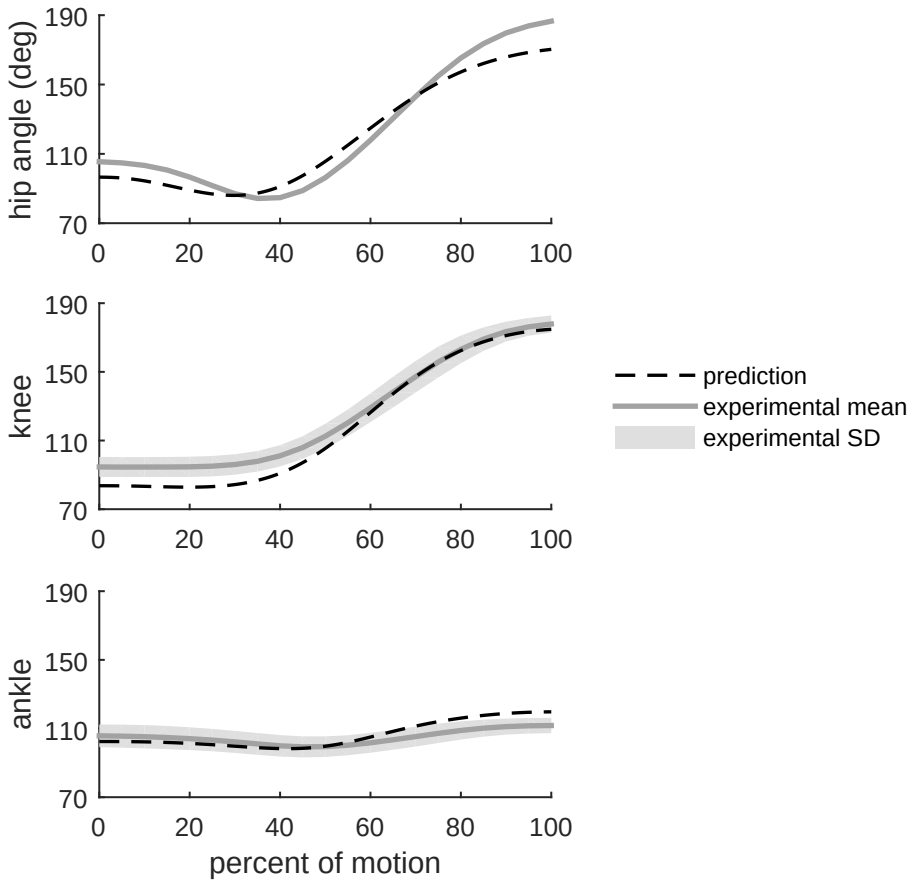

Figure 4.16: Predicted sit-to-stand joint angles profiles compared to experimental sit-to-stand, measured by Nuzik et al. [58]. Seat-off of the prediction is aligned to 47 percent motion. The root mean square errors are 8.9 deg, 8.0 deg, and 4.8 deg at the hip, knee, and ankle, respectively.

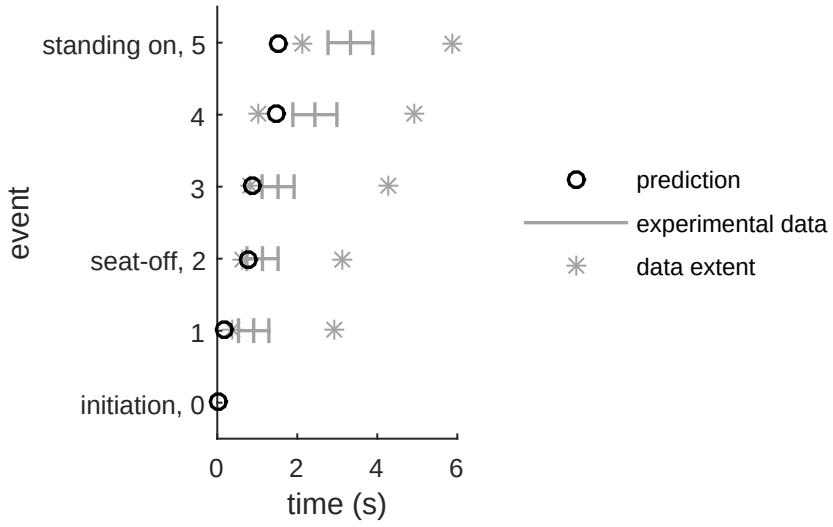

Figure 4.17: Predicted sit-to-stand event timing compared to experimental means, standard deviations, and ranges, measured by Kralj et al. [27].

4.4 Updating the description of sit-to-stand

In both Chapters 3 and 4, what appears to be a relatively fast STS has been predicted. The predicted STS motions had durations of 1.24 s and 1.55 s respectively, while Kralj et al. suggests the duration should be 3.33 s on average [27] and gives a range from 2.12 s to 5.86 s, as seen in Table 4.2.

As mentioned in Section 4.1, many of the participants in the STS experiment completed STS more quickly than even the fastest subject in the study by Kralj et al. did. For purpose of comparison, the trails collected in the STS experiment with clear STS initiation (event_0) and termination (event_5) were processed according to the methods of Kralj et al. These 138 trials were analysed for similarity to Kralj et al. in terms of kinematic and kinetic trace patterns, existence of STS events, and duration of STS phases: initiation (event_0 to event_1), seat unloading (event_1 to event_2), ascending (event_2 to event_4), and stabilization

Table 4.2: Comparison of event timings (s) from two sit-to-stand experiments.

study	measure	initiation $event_0$	$event_1$	seat-off $event_2$	$event_3$	$event_4$	standing on $event_5$
Kralj et al.	average	0.00	0.91	1.13	1.52	2.44	3.33
	standard deviation	0.00	0.38	0.39	0.40	0.55	0.56
	maximum	0.00	2.94	3.12	4.28	4.92	5.86
	minimum	0.00	0.40	0.62	0.82	1.02	2.12
This study	average	0.00	0.88	1.51	1.84	2.58	2.76
	standard deviation	0.00	0.62	0.62	0.65	0.70	0.75
	maximum	0.00	3.19	3.50	3.57	4.28	5.29
	minimum	0.00	0.00	0.62	0.78	1.33	1.64

($event_4$ to $event_5$) and overall STS duration with comparison to timing reported in Kralj et al.

Comparison of $event_0$ criteria indicate that they occur at times that are statistically significantly different, and one does not always precede the other. The same is true of $event_5$ criteria. To promote consistency of event definitions across trials and participants, $event_0$ and $event_5$ definitions from Kralj et al. were modified from their presentation, as Equations 2.1 and 2.6 respectively, such that

$$\text{event}_0: \quad \left|\frac{dM_Z}{dt}\right| \geq 2.5\% \left(\frac{dM_Z}{dt}\right)_{peak-to-peak} \tag{4.12}$$

$$\text{event}_5: \quad F_Y = 99\% bodyweight \tag{4.13}$$

Trials were synchronized to the beginning of standing (event0), and event times are presented in Table 4.2 where they are compared with the findings of Kralj et al. The par-

ticipants in the experiments performed STS an average of 0.57 s faster than the participants of the previous study.

It is hypothesized that the participants in this study stand up quicker than the participants in the study by Kralj et al. because of differences in study environments and populations. Timing differences remained after controlling for the environmental factor of seat height. In terms of populations, no sex differences were observed, but the participants in Kralj et al. are both significantly taller at the hip and significantly older than in this study. It is established that younger adults typically perform STS more quickly than relatively older adults [6, 113], which may explain why participants in this study (24.9 years (3.6)) found a quiet standing posture 0.57 s more quickly than was reported for the older population (32.6 years (6.7)).

In light of these findings, it is proposed that the results of this study are more representative of normative STS for a healthy, young adult population between 1.54 and 1.91 m tall, and should be used for this population when seat-height is within standard range of 42 to 51 cm [124].

4.5 Discussion

In this Chapter, the force-deformation behaviour of buttocks during STS was measured and modelled. From the tissue models considered, the Kelvin-Voigt element with Mooney-Rivlin spring faithfully represented the data collected in the STS experiment. It is a visco-hyperelastic model, characteristic of the tissues of the buttocks. It is computationally inexpensive and produces plausible forces over the measured range of STS tissue deformations. And, when implemented in the biomechanical model and STS prediction routine, this buttocks model allowed for prediction of STS closer to what has been reported in the literature than the model from Chapter 3.

STS is a challenging and interesting motion to study in part because of the large ranges of motion the body goes through. In this Chapter, it was observed that buttocks experience large deformations, on the order of centimetres, and transfer proportionally large forces, with maximums in the vicinity of 3/4 body weight, during STS. The buttocks models that exist in the literature are either not valid for these large ranges of deformation or are too complex for a dynamic optimization problem. The modelling work in this Chapter has addressed these shortcomings by building candidate buttocks models without discontinuities in force at lift-off and without sticking, and by tuning these models to experimentally collected STS data. After statistical analysis, two of the four models remained in contention. The Mooney-Rivlin model was chosen because it best represented the force-deformation behaviour measured.

The buttocks model proposed will, however, fail for models that are exceptionally more massive than the participants in the experiment. As is seen in Figure 4.10, the Mooney-Rivlin spring described by the parameters in Table 4.1 has a maximum compressive strength of approximately 1200 N (600 N $\times 2$) and should not be expected to represent the buttocks force-deformation behaviour of models of similar or greater weight. The heaviest subject in the experiments weighed approximately 916 N and, if a considerably heavier subject is of interest, it may be worth-while to collect subject-specific data on this person and re-parameterize the model or to use the buttocks model with a linear spring from Chapter 3.

The Kelvin-Voigt buttocks model with Mooney-Rivlin spring has proven useful for applications of STS simulation and prediction. When implemented in a STS prediction routine it has produced a STS motion with over-all patterns and the events characteristic of healthy STS. These results, for a healthy model, again give confidence in the validity of the proposed buttocks model.

The temporal STS data collected in the experiment provide evidence that healthy young adults, such as the participants in the study, complete STS more quickly than what has been reported in Kralj et al, as shown in Table 4.2. This discovery is especially relevant to

this Chapter as the timing of STS events predicted with this better buttocks are all within the range of event times observed in the experiment. From the results of this Chapter, the agreement of the kinematic trends and accurate timing of the predicted STS compared to experimental STS, there is strong evidence that the models built are predicting a STS motion characteristic of healthy young adults.

5

Contributions of Muscles to Sit-to-Stand

Voluntary motion is the result of coordinated contraction of skeletal muscle. The muscles produce moments about joints dependent on muscle force and musculoskeletal geometry. Introduced in Chapter 2, Garner's 8-muscle musculoskeletal model is the best-known for sit-to-stand (STS) prediction [104] and, inspired by his recommendations to include more uniarticulate muscles, the model in this Chapter includes 10 muscle units representing the major flexors and extensors of the lower extremity [120]. These muscles are iliopsoas, rectus femoris, vasti, gluteus maximus, hamstrings, tibialis anterior, gastrocnemius, soleus, flexor digitorum longus, and tibialis posterior as seen in Figure 5.1.

Section 5.1 of this Chapter details the construction of a musculoskeletal model built upon the rigid link model of the previous Chapters. This model is built with attention to the modelling work of previous biomechanists and is strongly motivated by studies of human anatomy and physiology. After incorporating the model of musculoskeletal geometry into the three-link-model, Section 5.2 describes how information from the muscles is incorporated into the STS prediction routine of Chapter 3, and the remaining sections discuss the implications of considering muscular effort in STS prediction.

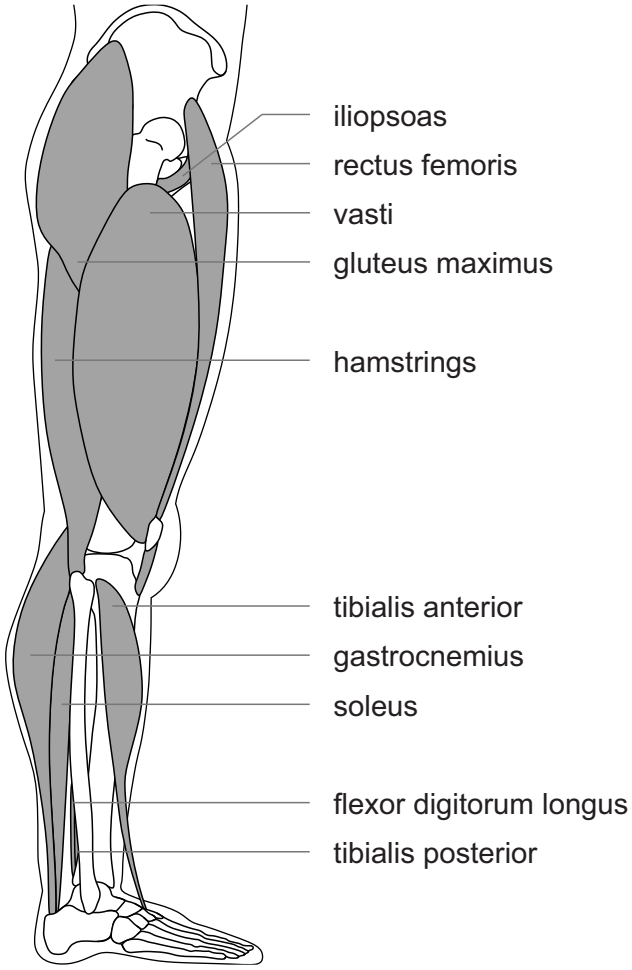

Figure 5.1: Major flexors and extensors of the lower extremity.

5.1 Modelling musculoskeletal geometry

Details of musculoskeletal geometry are required to include muscles in the biomechanical model formed in the previous Chapters. Depending on the application, this geometry may include moment arms, lengths, effective attachment points, and lines of action of the musculotendinous units, which will be referred to as muscles for brevity. In this Chapter, knowledge of moment arms calculated from effective attachment points will be sufficient

for analysis. It is a non-trivial task to integrate experimental geometry data from the necessary variety of sources for a system of muscles.

Muscle path modelling is a common way of describing this geometric information. In lower extremity muscle path modelling, the path of a muscle is (in theory) determined experimentally and often described using a set of attachment points, via points (points the muscle is constrained to pass through), and wrap points (points the muscle is conditionally constrained to pass through). Wrapping surfaces (geometric constraints on the muscle path) have also been in muscle path modelling, most commonly in the upper extremity [115]. These muscle path models are typically built for a biomechanical model of specific stature for a specific motion, and challenges arise when the model of interest is of a different stature or a different motion is of interest. The dataset of White et al. [80] is a model of muscle paths, designed for gait, specifying attachment points, one via point for each of the iliopsoas, gastrocnemius, tibialis anterior, flexor digitorum longus, and tibialis posterior muscles, and recommending an alternate path modelling strategy from Brand et al. [18] for the quadriceps. A second data set, from Carhart [81], was designed for use over slightly larger ranges of joint angles and includes many more via points and wrap points. The musculoskeletal geometry in this work is based on the model developed by White et al. referred to as the White model, with influence from the data set provided by Carhart, referred to as the Carhart model. The musculoskeletal model developed in this Chapter meets the challenge of extending these models for the biomechanical model from Chapter 3 and Chapter 4 and modelling musculoskeletal geometry over the entire ranges of healthy joint angles presented in Table 2.2.

A key advantage of this strategy of modelling musculoskeletal geometry is that muscle origins, insertions, as well as effective origins and insertions, lines of action, moment arms, lengths, and velocities are all available and consistent within the model.

5.1.1 Musculoskeletal model mapping

While neither the White model nor the Carhart model is appropriate for this work, because, for example, both generate negative muscle moment arms during a healthy STS motion, there are insights gained from each. The White model is unique in providing locations of muscle origins and insertions in relation to joint centres as well as guidelines for subject-specific scaling [80], while the Carhart model provides further detail about muscle geometry at larger ranges of motion [81] and is a foundational component of the OpenSim Gait models [136].

A first step in representing the musculoskeletal geometry for the model in this Chapter was scaling the White model to the three-link model and augmenting it with the Carhart model. This augmentation was accomplished by mapping each segment of the Carhart model to the same segment in the White model in a least squares sense using all points in common between the segments of each model. It was necessary to allow rotation (and translation) of the Carhart model because anatomical axis definitions (and joint centre locations) were not provided by Carhart. The points from the White model were then discarded, leaving the musculoskeletal geometry in Figure 5.2. These points describe the initial musculoskeletal geometry of the model and will be modified and/or tuned before their use in a motion prediction routine.

5.1.2 Geometric constraints and muscle wrapping

In the classic case of gait analysis, it may be true that via and wrap point models are sufficient when modeling the musculoskeletal geometry of the lower extremity because the range of joint angles is relatively small, as was seen in Table 2.2. However, when motions such as STS are of interest, a model of musculoskeletal geometry valid for a much larger range of joint angles is required. The potential for errors due to simplifications in muscle path modelling magnifies as the joint's range of motion increases, reducing the accuracy

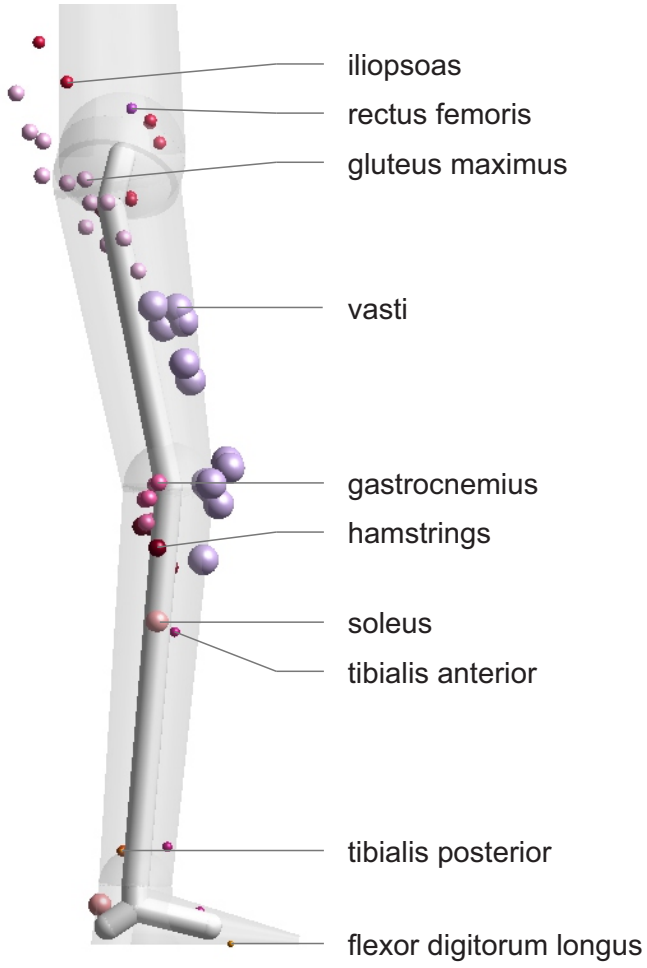

Figure 5.2: Attachment, via, and wrap points describing musculoskeletal geometry initially.

of the estimated muscle forces. Models such as the patellar pulley model, recommended in the White model, aim to address the need for accurate musculoskeletal modelling of anatomical constraints.

The patellar pulley model is a strategy of representing the effect of patellofemoral articulation on the moment arms of the quadriceps muscles about the knee [18]. In the patellar pulley model, the patella is idealized as an infinitely long and infinitely thin frictionless rod. The rod runs in the medial-lateral direction and its location is determined by the angle of the knee joint and from the effective radius of the femoral condyles (R_f) and patellar

thickness (T_p), as in Equations 5.1 and 5.2 where positive θ is knee flexion, positive X is anterior, and positive Y is proximal in the femoral reference frame as described by Brand et al. [18] and shown in Figure 5.3. Please notice that when $\theta = 0$, $X_B > R_f$ and so, the singularity in Equation 5.2 is not encountered. The location of the patellar pulley (X_B, Y_B) is plotted as a function of knee angle in Figure 5.4. This patellar pulley model is only valid for smaller ranges of knee joint angle, because when the knee goes into deep flexion (> 80 degrees in Figure 5.4) it specifies that the patella run up the thigh (which is unrealistic - try flexing your knee.)

$$X_B = \begin{cases} (R_f + T_p)\ \cos\theta & X_B > R_f \\ R_f & otherwise \end{cases} \tag{5.1}$$

$$Y_B = \begin{cases} -(R_f + T_p)\ \sin\theta & X_B > R_f \\ -(R_f + T_p)\ \sin\theta - \dfrac{R_f - (R_f + T_p)\cos\theta}{\tan\theta} & otherwise \end{cases} \tag{5.2}$$

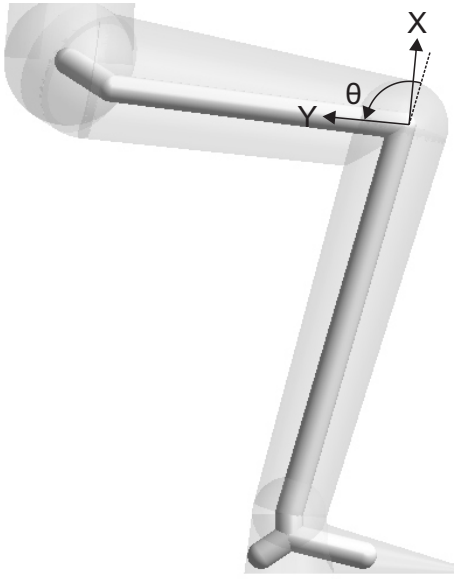

Figure 5.3: Femoral reference frame for patellar pulley model.

The patellar pulley model was modified in two ways before implementation in this biomechanical model. First, the Y value was adjusted such that the minimum value is

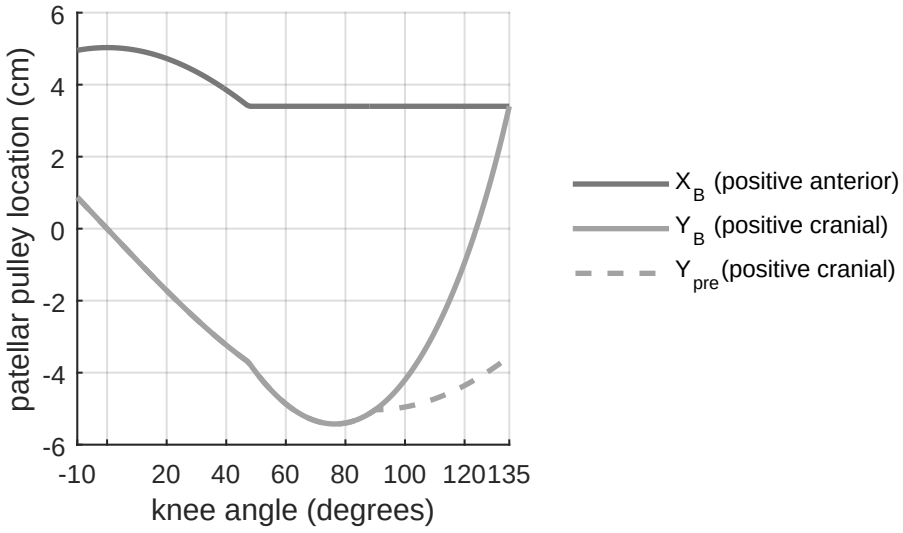

Figure 5.4: Patellar pulley location assuming typical female skeletal geometry [120, 137]. Y_{pre} is defined in Equation 5.5.

chosen when the knee is in flexion, as in Equation 5.5 and shown as the dashed line in Figure 5.4.

$$Y_{B1} = -\left(R_f + T_p\right)\ \sin\theta \tag{5.3}$$

$$Y_{B2} = -\left(R_f + T_p\right)\ \sin\theta - \frac{R_f - \left(R_f + T_p\right)\cos\theta}{\tan\theta} \tag{5.4}$$

$$Y_{pre} = \begin{cases} Y_{B2} & X_B \leq R_f \ and \ Y_{B2} < Y_{B1} \\ Y_{B1} & otherwise \end{cases} \tag{5.5}$$

Second, the axis of the patella defined in the patellar pulley model is given three-dimensional geometry. That is, the pulley was given a radius. This was accomplished by bringing the point (X_B, Y_{pre}) at distance

$$length_{pre} = \sqrt{X_B^2 + Y_{pre}^2} \tag{5.6}$$

from the origin, toward the knee joint centre by one patellar thickness, as in Figure 5.5 such that the location (X, Y), as in Equations 5.7 and 5.8, is representative of a point on the articulating surface of the patella.

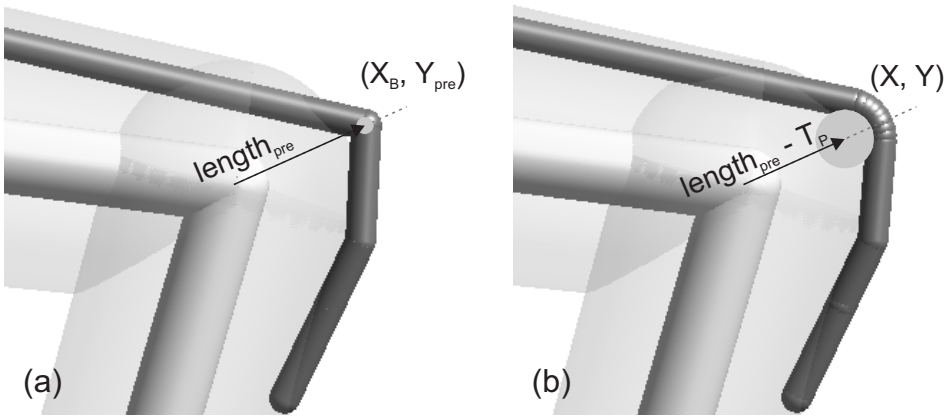

Figure 5.5: Patellar pulley models with pulleys of radius (a) 0 (please note, a small radius is shown for visualization purposes), and (b) patellar thickness.

$$X = X_B \frac{length_{pre} - T_P}{length_{pre}} \tag{5.7}$$

$$Y = Y_{pre} \frac{length_{pre} - T_P}{length_{pre}} \tag{5.8}$$

With reference to the convention shown in Figure 5.6, the patellar pulley is now specified in the thigh reference frame with centre at point (X,Y) with a medial-laterally running long axis (0, 0, 1) and radius of patella thickness, as in Appendix C. By including proximal and distal attachment points of the vasti and rectus femoris, this patellar pulley becomes a reasonable three-dimensional model of a patellar obstacle for modelling quadriceps geometry.

This cylindrical wrapping geometry has certain benefits; it does not have anatomically unnatural edges or vertices where a muscle may contact it, it is relatively simple to de-

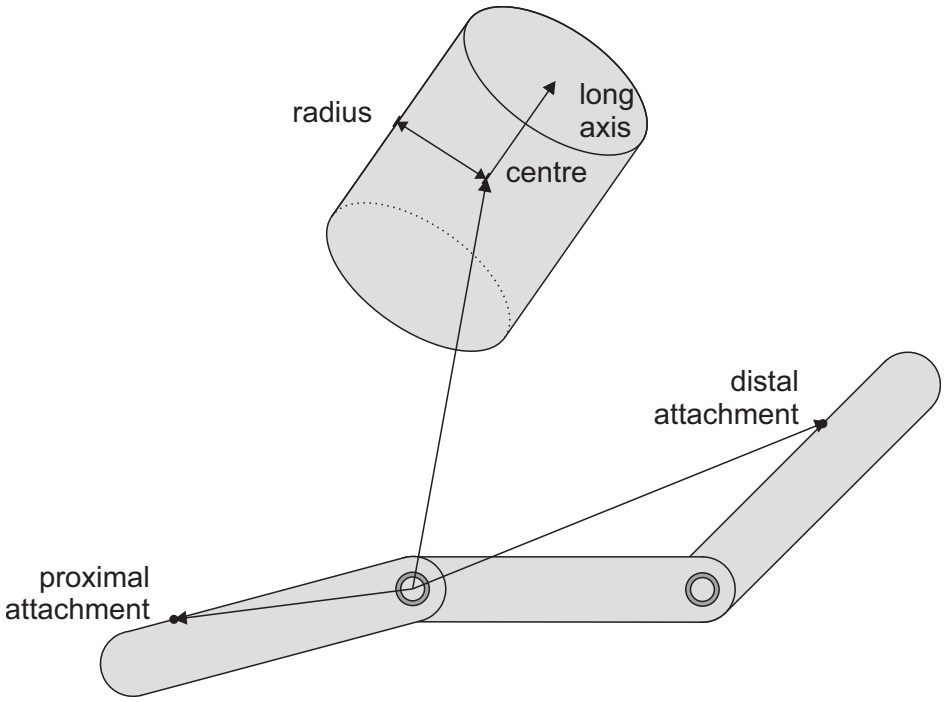

Figure 5.6: Points, dimensions, and directions of interest when modelling musculoskeletal geometry that includes a cylindrical wrapping constraint. Please refer to Appendix D for full details.

fine mathematically, and it will constrain the muscle to one side of the geometry in the musculoskeletal model which does not contain connective tissues found in the human body.

Without inclusion of the patella in the musculoskeletal model, the moment arms of the vasti and rectus femoris would have become negative within the natural range of knee motion, which is nonphysiological. Further anatomy requiring extra attention in musculoskeletal modelling was identified by driving the joints of the model through their full ranges of motion [76] and examining muscle geometry curves for anomalous behaviour. Iliopsoas and gastrocnemius were also found to produce negative moment arms at larger ranges of joint motions, and gastrocnemius had discontinuities in length where its wrap point is activated or deactivated. The alternate approach of representing anatomical constraints using three-dimensional cylindrical geometries was implemented for these muscles

also, as described in Appendix C. The mathematical model of the muscle path wrapping freely over the surface of a frictionless cylinder of infinite length is derived and presented in Appendix D.

5.1.3 Optimization of musculoskeletal geometry

Of the muscles included in the model, iliopsoas, vasti, gluteus maximus, hamstrings, and gastrocnemius are equivalent muscles and representative of a group of muscles in the Carhart model. The geometry of these equivalent muscles was determined as the weighted average of their comprising parts where individual muscles are weighted by their maximum isometric force, as described in Appendix C.

After scaling the White model to the stature of the rigid-link model, mapping the more detailed Carhart geometry to that model, adding cylindrical wrapping constraints, and combining muscle groups, this Frankenstein model contains no musculoskeletal component exactly as described in its source. Although known inaccuracies in modelling were addressed by this scheme, discrepancies were also introduced. Therefore, the model was tuned next to mitigate these discrepancies. In the tuning of the musculoskeletal model, the locations of via points and geometries of the cylindrical constraints were optimized to best match experimentally determined flexion-extension moment arms and muscle lengths reported in the literature. Details of this tuning are included in Appendix C. The resulting moment arms are shown in Figure 5.7.

The final model expresses a point of interest in a local coordinate system, specified by the frame in Table 5.1. The principal axes of these frames are defined using the anatomical landmarks and scheme proposed by Mansour and Pereira [138], although the origins have been relocated. In this model, the origin of both the pelvis and thigh frames are defined at the hip joint centre, the origin of the leg frame is the knee joint centre, and the origin of the foot frame is the ankle joint centre, as shown in Figure 5.8. The final model is included as Table 5.1 and shown in Figure 5.8.

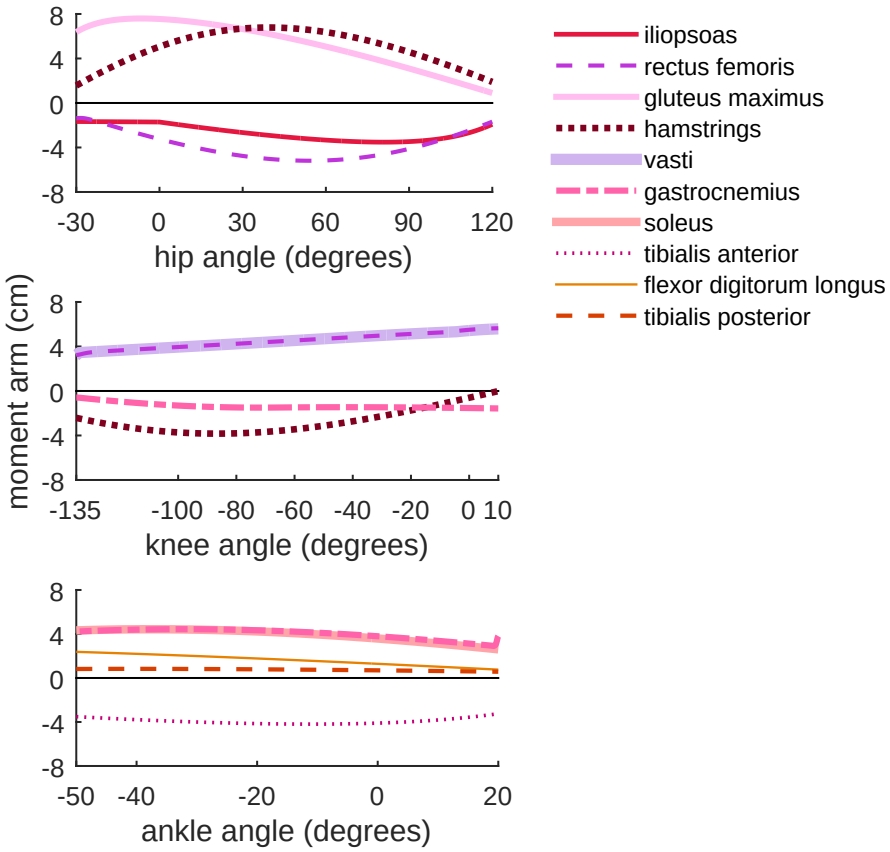

Figure 5.7: Muscle moment arms. Moment arms of biarticulate muscles are shown for a configuration with the alternate joint at 0 degrees.

Table 5.1: Musculoskeletal geometry.

Muscle	Type	Frame	Location (m)/Direction/Radius (m)
Iliopsoas	proximal attachment	pelvis	(-0.0718, 0.0183, 0.1032)
	via point	pelvis	(0.0316, 0.0048, 0.0364)
	via point	pelvis	(0.0318, 0.0013, 0.0151)
	cylinder centre	thigh	(0.0000, 0.0000, 0.0000)
	cylinder long axis	thigh	(-0.0085, -0.0919, -0.0137)
	cylinder radius	-	0.0171
	distal attachment	thigh	(-0.0185, -0.0185, -0.0554)
Rectus femoris	proximal attachment	pelvis	(0.0319, -0.0190, 0.0410)
	cylinder centre	thigh	patella centre
	cylinder long axis	thigh	(-0.0100, 0.0385, -0.0100)
	cylinder radius	-	0.0146
	via point	leg	(0.0560, -0.0169, -0.0072)
	via point	leg	(0.0515, -0.0107, -0.0341)
	distal attachment	leg	(0.0444, -0.0012, -0.0759)
Vasti	proximal attachment	thigh	(0.0209, -0.0406, 0.1773)
	via point	thigh	(0.0263, -0.0313, -0.2376)
	cylinder centre	thigh	patella centre
	cylinder long axis	thigh	(-0.0100, 0.0385, -0.0100)
	cylinder radius	-	0.0159
	via point	leg	(0.0560, -0.0117, -0.0011)
	via point	leg	(0.0507, -0.0069, -0.0355)
	distal attachment	leg	(0.0444, -0.0012, -0.0759)

Table 5.2: Musculoskeletal geometry. Continued.

Muscle	Type	Frame	Location (m)/Direction/Radius (m)
Gluteus maximus	proximal attachment	pelvis	(-0.1011, 0.0333, 0.0277)
	via point	pelvis	(-0.0740, 0.0333, -0.0172)
	via point	thigh	(-0.0488, -0.0542, -0.0890)
	distal attachment	thigh	(-0.0114, -0.0542, -0.0890)
Hamstrings	proximal attachment	pelvis	(-0.0448, 0.0174, -0.0509)
	distal attachment	leg	(-0.0015, -0.0009, -0.0383)
Tibialis anterior	proximal attachment	leg	(0.0199, -0.0077, -0.1575)
	via point	leg	(0.0385, 0.0302, -0.4219)
	distal attachment	foot	(0.0708, 0.0152, -0.0290)
Gastrocnemius	proximal attachment	thigh	(-0.0030, -0.0125, -0.3539)
	cylinder centre	thigh	(0.0009, -0.0003, -0.3703)
	cylinder long axis	thigh	(0.0076, -0.0480, -0.0023)
	cylinder radius	-	0.0178
	via point	leg	(-0.0270, 0.0081, -0.1175)
	distal attachment	foot	(-0.0388, 0.0230, -0.0215)
Soleus	proximal attachment	leg	(-0.0005, -0.0021, -0.1474)
	distal attachment	foot	(-0.0388, 0.0230, -0.0215)
Flexor digitorum longus	proximal attachment	leg	(-0.0073, 0.0100, -0.1991)
	via point	leg	(-0.0282, 0.0189, -0.4125)
	via point	foot	(0.0000, 0.0318, -0.0277)
	via point	foot	(0.0298, 0.0251, -0.0021)
	distal attachment	foot	(0.1049, -0.0319, -0.0647)

Table 5.3: Musculoskeletal geometry. Concluded.

Muscle	Type	Frame	Location (m)/Direction/Radius (m)
Tibialis posterior	proximal attachment	leg	(-0.0069, 0.0028, -0.1282)
	via point	leg	(-0.0083, 0.0468, -0.4385)
	via point	foot	(0.0000, 0.0254, -0.0127)
	distal attachment	foot	(0.0345, 0.0254, -0.0310)

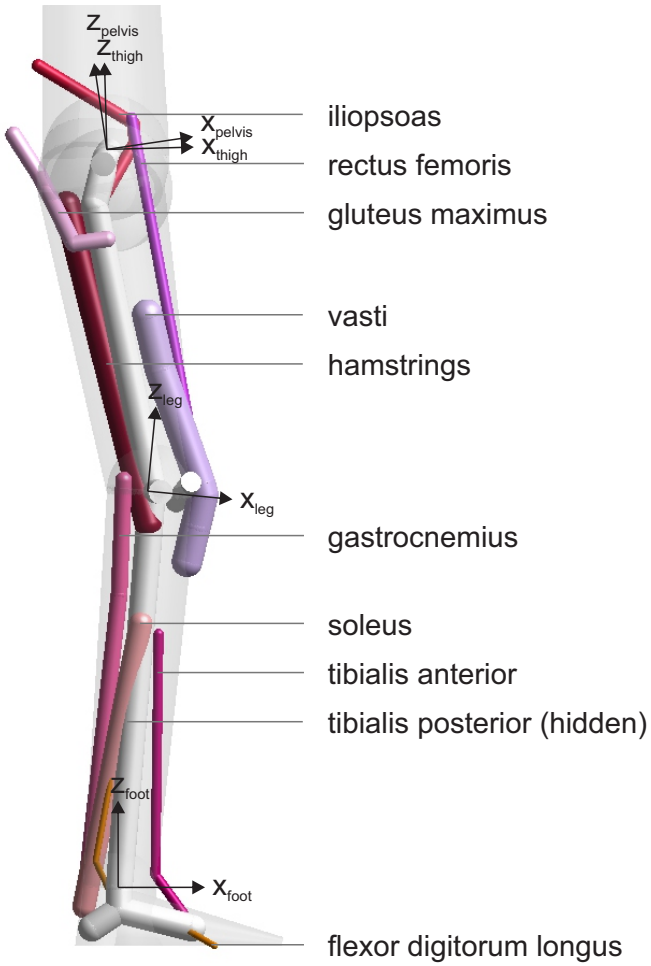

Figure 5.8: The optimized musculoskeletal geometry.

Constructing a musculoskeletal model from component parts is a labourious exercise, but the finished model provides reliable muscle geometry for any sagittal plane pose or motion of interest, which is important for this application because the motions are not predetermined and their possible ranges are large. With the musculoskeletal system defined, the next sections investigate the influence of muscles on STS.

5.2 Optimal control framework

In Chapters 3 and 4, a candidate motion (i.e. a motion that begins in sitting and ends in standing) was evaluated in terms of its feasibility and required joint torques. These torques were calculated by solving the equations of motion of the human system using inverse dynamics, as in the schematic of Figure 2.6. With the knowledge of musculoskeletal geometry gained in Section 5.1, it is possible to hypothesize the muscle forces that created these joint torques and to then consider these forces when evaluating the cost of a candidate motion. This Section details the changes made to the optimal control framework of the previous Chapters such that the solver may benefit from the biologically relevant information gained from the musculoskeletal model of this Chapter in predicting STS.

5.2.1 The inverse muscle force approach

In the human system, muscles contract and, in accordance with their geometry, produce moments about joints to move the body, as in Figure 2.6. Joint moments may be accurately estimated given a sufficiently accurate estimation of muscle forces, from an electromyography (EMG)-driven model [139] or from direct [140] or indirect measurement [141], and a sufficient representation of the geometry of the system. From these joint moments, the biomechanical problem may be solved forward and the resulting motions calculated. The inverse problem, going from kinematics to muscle forces, introduces a problem of mechanical indeterminacy where there are multiple combinations of muscle forces capable of

generating a given net joint moment. Fortunately, this indeterminacy problem has been tackled by many researchers although there is no perfect solution.

In this Chapter, the indeterminacy problem is managed using an optimization approach after adopting four simplifying assumptions to the model [59]. The first three assumptions made in this Chapter are non-ideal in that they simplify the human system beyond what is physiological, but they make the problem substantially more manageable (by not incorporating models of the corresponding phenomena.) The first assumption is that are there are no pre-defined patterns of co-contraction for the modelled muscles. The second assumption is that maximum muscle forces are unaffected by the muscle length or rate of change in length [142]. The third assumption is that muscles may generate force or relax instantaneously [142], that is there are no muscle dynamics in the model. The fourth assumption, which is physiological, is that the musculoskeletal system works in ways that are efficient. This efficiency is not fully understood, but has been proposed as a minimization of a function of muscle forces, muscle stresses, or muscle activations, as in Equations 2.10 to 2.12, for example.

After applying these assumptions to the model, the following static optimization problem may be solved to find a set of muscle forces, F, from the known net joint moments, Q, at any instant,

$$\min \sum_{i=1}^{10} \left(\frac{F_i}{PCSA_i} \right)^2 \text{ such that } \begin{cases} \mathbf{J}^T F = Q \\ F_{min} \leq F \leq F_{max} \end{cases} \tag{5.9}$$

where $\mathbf{J}^T$ is the (Jacobian) matrix of moment arms, F_{min} are the minimum and F_{max} are the maximum allowable muscle forces at that time. In this problem, F_{min} is set to $5\% F_{max}$ where,

$$F_{max} = \Gamma PCSA \tag{5.10}$$

where $PCSA$ are the physiological cross sectional areas of the muscles. In accordance with Arnold et al. [114], a specific tension (Γ) of 61 N/cm^2 was used for all muscles.

Minimization of muscle stresses squared was chosen for the cost function because of its popularity in the literature and because Anderson and Pandy showed, in their gait prediction work, that it resulted in the greatest similarity between static and dynamic predictions [142]. Alternate functions are available for use but have not been implemented at this time.

Now, having defined minimization problem 5.9, it is possible to estimate the muscle forces that would produce a candidate STS motion. It is also possible to evaluate the required effort of that motion in terms of these muscle forces.

5.2.2 Objective function construction for optimal sit-to-stand

Again, as in Chapters 3 and 4, candidate motions are evaluated for optimality and feasibility. In this Chapter, optimality is considered using a weighted sum of the time history of active joint torques determined by inverse dynamics, as in Equation 3.15 reproduced as Equation 5.11,

$$cost_{torque} = \int_0^5 A_M^2 \mathrm{d}t + \int_0^5 K_M^2 \mathrm{d}t + \int_0^5 H_M^2 \mathrm{d}t \tag{5.11}$$

and the time history of muscle stresses determined from these torques. Here, the equality constraint of Equation 5.9 is relaxed such that the effort of a motion in terms of its muscular requirements is

$$cost_{muscles} = w_m \int_0^5 \|\mathbf{J}^T F - Q\|^2 + \rho^2 \sum_{i=1}^{10} \left(\frac{F_i}{PCSA_i} \right)^2 \mathrm{d}t \tag{5.12}$$

where the weighting factor ρ is assigned a value of 10^{-3} m^2, as per Ou [143] such that the first term dominates and discriminates against physically infeasible "solutions". The entire $cost_{muscles}$ term is given a weight of $w_m = 10^{-4}$.

The $cost_{muscles}$ term is now added to the terms of Equation 3.16 and the overall cost of a candidate STS motion becomes

$$cost = cost_{torque} + cost_{muscles} + cost_{error} \tag{5.13}$$

where,

$$cost_{error} = w_h \int_0^5 error_h^2 \mathrm{d}t + w_t \int_0^5 error_t^2 \mathrm{d}t + w_l \int_0^5 error_l^2 \mathrm{d}t + w_s \int_0^5 error_s^2 \mathrm{d}t \quad (5.14)$$

as was defined as Equation 3.14 in Section 3.2 with the weighting factors defined in Chapter 4.

5.2.3 Computation of optimal controls

As in Chapter 3, an initial optimization problem is solved to establish a feasible STS starting-point. The initial motion, the same as described in Section 3.2, is passed to the model, and errors in feasibility are calculated from Equation 5.14. Bézier curve control point locations are adjusted by *fmincon* in MATLAB [129] to decrease errors and the first solution with zero associated error is used to seed the solver in a second optimization. The second optimization problem is new to this Chapter. It is solved to establish a feasible STS with plausible muscular demands. That is, the optimization routine of Section 3.2 is run until a candidate motion is found with zero associated error (according to Equation 5.14) where there is a solution to Equation 5.9 at all points in time. Whereas the solution of the first optimization problem, used in previous Chapters, is (theoretically) mechanically feasible, the solution of the second optimization problem, used in this Chapter, is also (theoretically) biomechanically feasible. This solution is used to seed the solver in the iterative dynamic optimization routine.

The iterative dynamic optimization routine is shown in Figure 5.9 and with further detail in Appendix E. The backbone of this routine is the same as in Section 3.2, while the difference between the two is the addition of muscular considerations for this Chapter, highlighted using dashed borders. In this optimization routine, the initial motion is passed to the model along with feasible and optimized muscle forces, calculated using Equation 5.9. Control point locations are adjusted by *fmincon* to decrease cost (Equation 5.13), which now includes adjusted muscle forces optimized using Equation 5.12. The optimal control

points are those that minimize cost with zero associated error. The cost of this candidate motion is recorded when the routine terminates. This process is repeated after elevating the degree of each Bézier curve by one, giving increased freedom to possible solutions. This process is iterated until successive solutions demonstrate convergence. The solution at the end of this process is purely predictive STS for the musculoskeletal model.

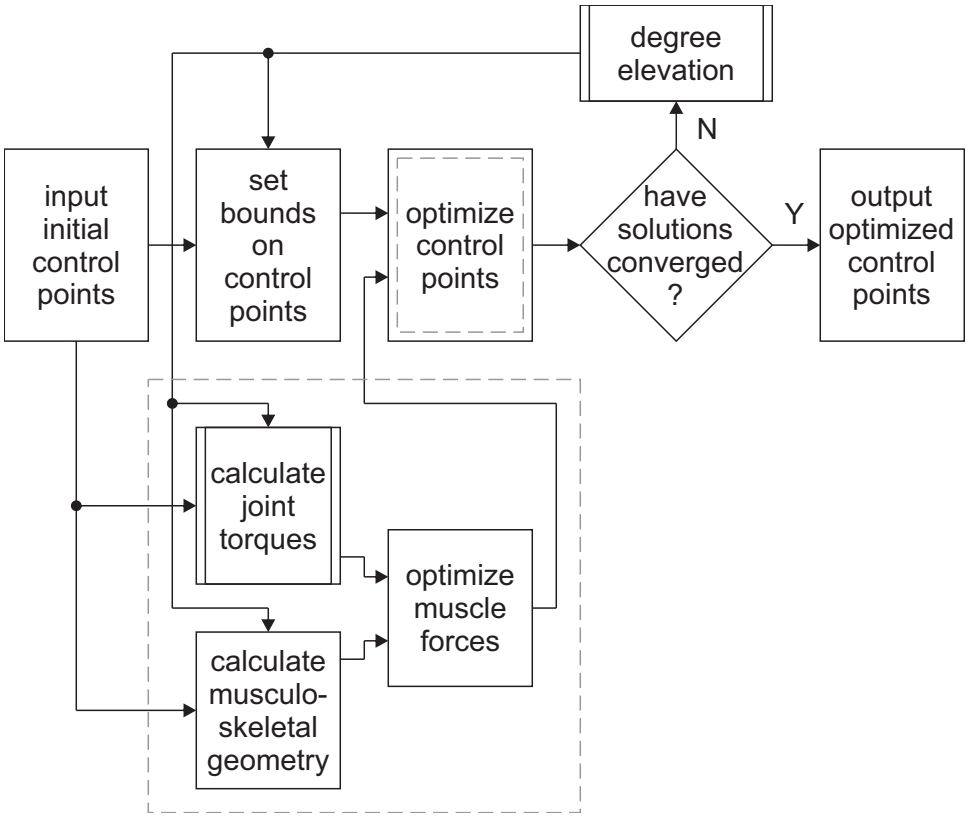

Figure 5.9: The iterative routine to determine an optimal sit-to-stand for the musculoskeletal model. Components that are new from previous Chapters are highlighted using a dashed border. Further detail is included in Appendix E.

5.3 Sit-to-stand prediction for a musculoskeletal model

The purpose of developing this musculoskeletal model is to use it in a biomechanical model for STS prediction. The results of this Section demonstrate to what extent incorporating muscular contributions in the motion prediction problem facilitates its solution. In this Chapter, the biomechanical model of Chapter 4 was augmented with the iliopsoas, rectus femoris, vasti, gluteus maximus, hamstrings, tibialis anterior, gastrocnemius, soleus, flexor digitorum longus, and tibialis posterior muscles. To incorporate these muscles in the optimal control problem, the cost function and iterative routine to determine an optimal STS, introduced in previous Chapters, were updated to include considerations of muscle forces and muscle stresses as in Equation 5.14 and Figure 5.9. The STS prediction routine was run for the new musculoskeletal model. The resulting motion is shown as a series of snapshots in Figure 5.10. As before, the gross motions predicted are consistent with healthy STS.

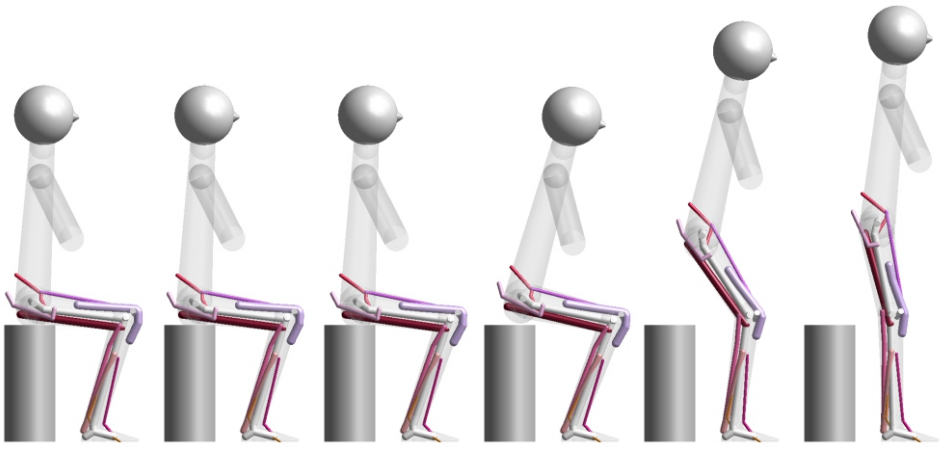

Figure 5.10: Evenly spaced snapshots of predicted sit-to-stand.

5.3.1 Comparison with the prediction using the Chapter 4 model

The optimal coordinate paths of STS are shown in Figure 5.11 for models without and with muscles. The STS motions predicted using each model are comparable, with a major difference being STS duration and four minor differences in kinematics. As can be observed, the prediction reshapes the paths of the generalized coordinates and lengthens the duration of STS to 2.00 s with the musculoskeletal model, compared to 1.55 s with the Chapter 4 model. The first minor difference is that the musculoskeletal model lends itself to a STS with a prolonged sitting phase, as can also be seen by comparing Figure 5.10 and Figure 4.13. The second and third minor differences are that the HAT of the musculoskeletal model moves more moderately, in terms of range of inclination, and the hips of the musculoskeletal model rise more abruptly than the model without muscles. The fourth, and last, minor difference is that the hips of the musculoskeletal model tend to be more anterior than the hips of the torque-driven model for the duration of motion.

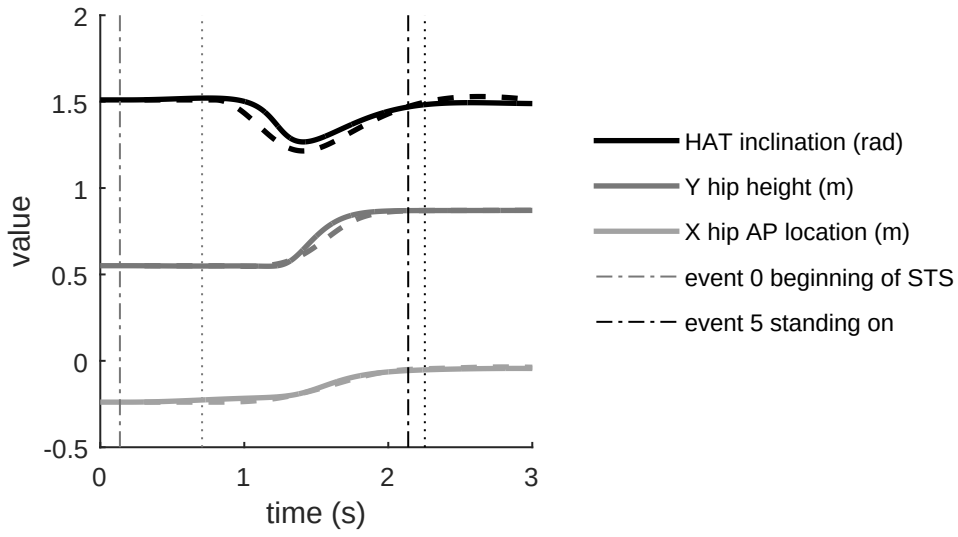

Figure 5.11: Optimal sit-to-stand from a 46 cm chair with the new musculoskeletal model, compared to the results of Chapter 4 (dashed curves and dotted vertical lines).

Although the STS motions are similar, there are differences in the joint torques associated with the optimal STS of each model, as seen in Figure 5.12. Generally, the musculoskeletal model tends towards a STS motion that demands smaller flexion torques, but larger extension torques for a shorter period of time. This preference for extension torques is consistent with Figure 5.7, because the bulk of muscle mass and largest moment arms are in the modelled extensor muscles. Also, looking to Figure 5.12, the musculoskeletal model tends towards a motion with less demand to the ankles, which again seems reasonable given that the modelled ankle muscles are generally smaller with smaller moment arms than muscles crossing the knee and hip.

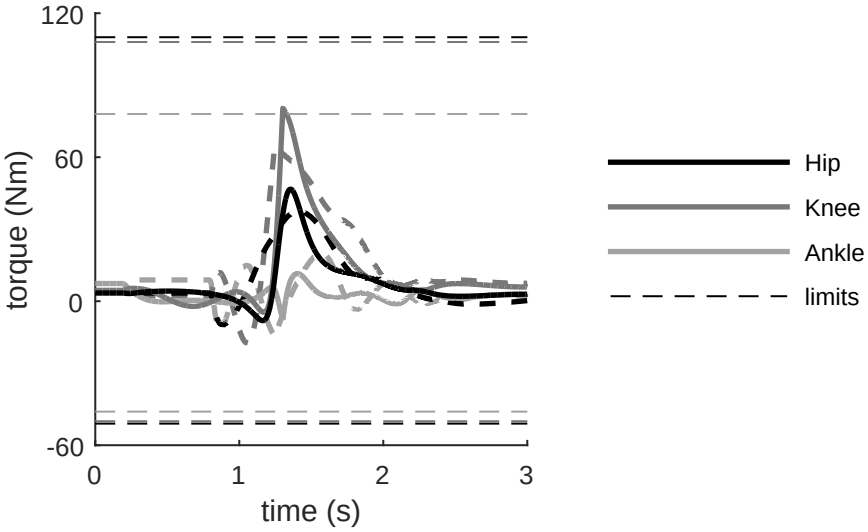

Figure 5.12: Joint torques for optimal sit-to-stand from a 46 cm chair with the musculoskeletal model (solid curves), compared to the results of Chapter 4 (dashed curves), compared to joint torque strengths, reported in Schultz et al. [113].

Comparing the results according to Equation 3.15, the optimal STS of the musculoskeletal model has a lesser cost, and requires less exertion, than the torque-driven model of Chapter 4 (and, in fact, the Chapter 3 model). It is particularly interesting that account-

ing for muscular demands in a motion's cost drives the prediction problem to a solution that is the most economizing of all STS predictions made in this thesis.

5.3.2 Comparison with healthy sit-to-stand

As in previous Chapters, the predicted STS is compared to normative STS data from the literature. It is also compared to the temporal information from STS experiments as reported in Section 4.4. In this Chapter, the predicted STS muscle forces are also compared to the experimental findings of Roebroeck et al. [144]. It must be stressed that this last comparison is a) to results of a descriptive study, rather than a normative one and b) to experimentally measured EMG, which is related to, but not the same thing as, muscle force.

The muscle forces found from the STS prediction are first divided by their maximum possible muscle force, determined from Equation 5.10, before being compared with normalized EMG, when available, in Figure 5.13. Three of the muscles, iliopsoas, flexor digitorum longus, and tibialis posterior, investigated in this Chapter do not have corresponding EMG data, which is not unexpected because their activity is impractical if not impossible to capture via surface EMG. The comparison of activity in the remaining seven muscles neglects the complexities of the relationship between motor unit action potentials, the origins of EMG, and muscle force (see Figure 2.6) and, therefore, analysis of these results is best limited to observing on/off patterns in the muscles. Comparing the normalized muscle forces and normalized EMG leads to two conclusions. First, of the seven muscles with recorded EMG activity, the prediction correctly identifies six as producing force, with the outlier being rectus femoris. Second, onset and offset patterns between the measured EMG and predicted muscle forces are not always consistent. The most likely reasons for this discrepancy and mitigating factors are discussed in the next Section.

Next, to examine the validity of the STS prediction, it is compared to normative data from the literature in Figures 5.14 and 5.15; the temporal information reported in Fig-

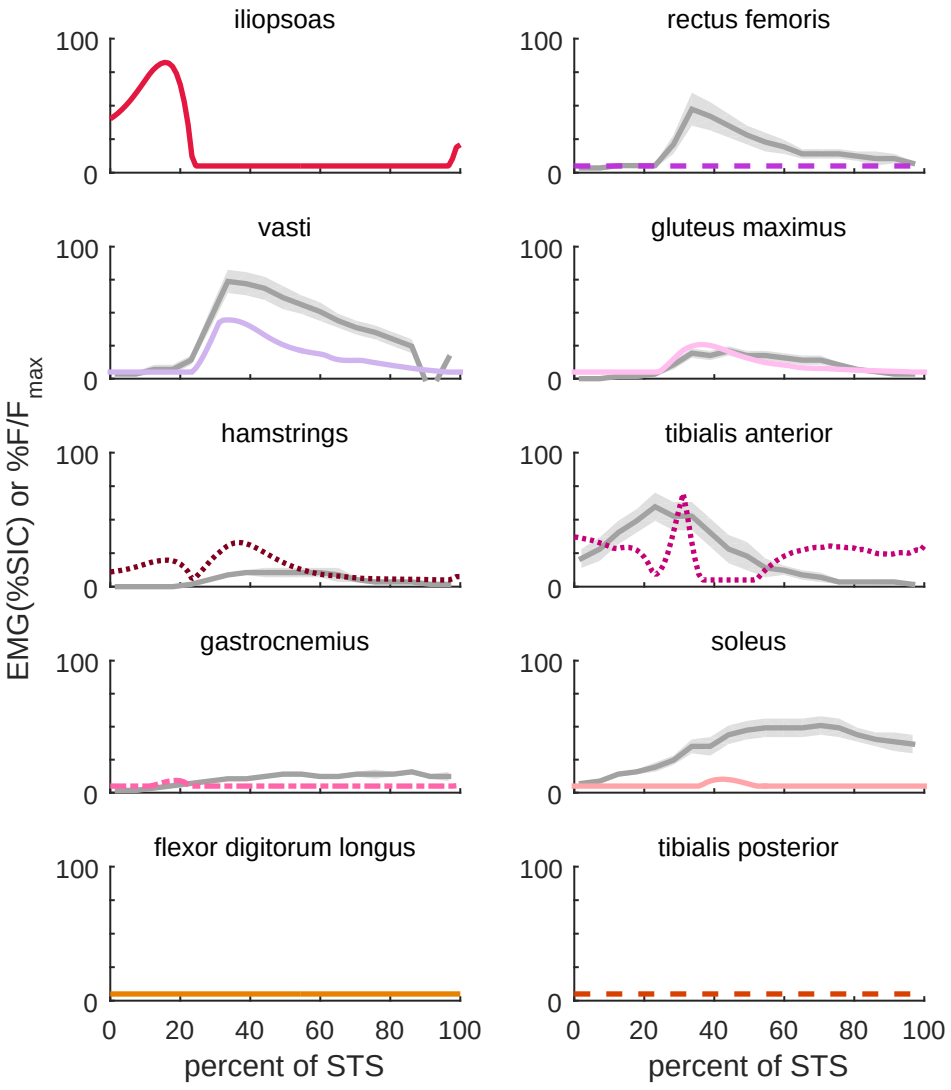

Figure 5.13: Normalized predicted muscle forces compared to normalized EMG (EMG divided by maximum EMG from static isometric contraction trials) from the experiments of Roebroeck et al. (in gray) [144]. Note that only normalized predicted muscle forces are presented for the iliopsoas, flexor digitorum longus, and tibialis posterior muscles as their activity was not measured experimentally.

ure 5.15 is from the STS experiment in this thesis. The predicted angles closely follow the normative trends during STS, although, as before, the hip appears particularly flexed in sitting and standing and the knee is particularly flexed in sitting. STS is predicted to take longer with the musculoskeletal model, and now five of the six events of STS are predicted within a standard deviation of what was observed in experiment, with the remaining event well within the range of times observed.

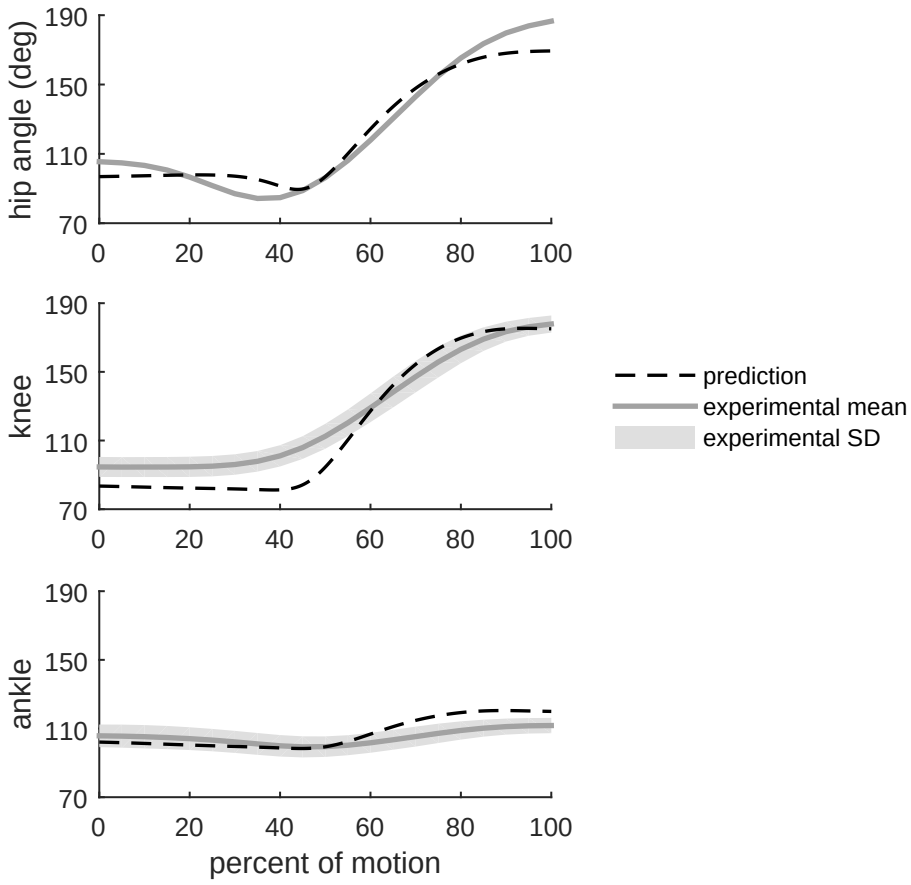

Figure 5.14: Predicted sit-to-stand joint angles profiles compared to experimental sit-to-stand, measured by Nuzik et al. [58]. Seat-off of the prediction is aligned to 47 percent motion. The root mean square errors are 8.0 deg, 11.6 deg, and 6.2 deg at the hip, knee, and ankle, respectively.

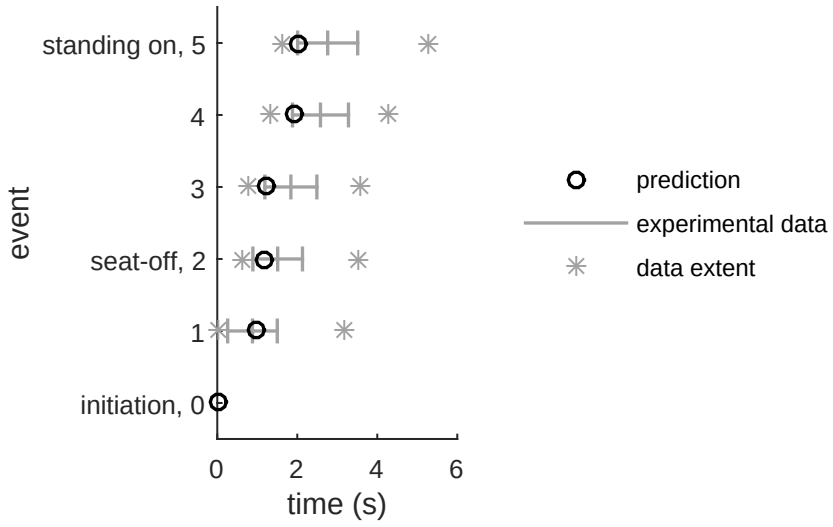

Figure 5.15: Predicted sit-to-stand event timing compared to means, standard deviations, and ranges, measured in the experiments of Chapter 4.

5.4 Discussion

In this Chapter, muscles were added to the STS prediction problem. This work builds on the recommendations of Garner, to include more uniarticular muscles when modelling STS [104], and extends the torque-driven model of Chapter 4 to incorporate muscles forces into the optimal control routine for predicting STS. By comparing the results of this Chapter with the prediction results of Chapter 4 and to normative STS data from the literature, it is possible to emphasize that not all joint torques are created equal, as they were quantified in the earlier cost function, 3.16, but that a torque generated using a relatively longer moment arm is mechanically efficient and a torque generated by a relatively larger muscle is physiologically efficient, as is captured in the cost function 5.13. Including muscles in the STS prediction problem and the cost function of this Chapter, makes it possible to optimize around the muscular origins of joint torques, and is important to the biofidelity of the resulting solution.

Section 5.1 of this Chapter detailed the construction of a musculoskeletal model built upon the rigid link model of the previous Chapters. The challenges of musculoskeletal model mapping and scaling were addressed as were the challenges of modelling muscle geometry over large ranges of joint angles. Tackling these challenges meant updating the patellar pulley model [18] to reframe it as a three-dimensional model with reasonable kinematic tracking in deep knee flexion. It also meant designing a validated model of lower extremity flexors and extensors for the popular deLeva model of female anthropometry [19]. The construction of this musculoskeletal model was, however, limited to the sagittal plane. If, in future studies, other muscles or planes of motion are of interest, use of modelling and validation strategies similar to that of Section 5.1 and Appendix C is strongly encouraged.

Incorporating muscles into the motion prediction problem was done in harmony with the fundamental theory of Crowninshield and Brand that people move in ways that minimize a function of muscle forces over time [99]. As is discussed in Section 5.2, no full muscle

models were used when incorporating these muscles. This simplification has influenced the solution space; for example, by neglecting muscle dynamics, non-physiological jumps in muscle force or non-physiological magnitudes of muscle force at a given geometry are possible. However, the magnitude of muscle force of a candidate solution is required to be below its maximum force in idealized conditions, as in Equation 5.10. The possibility of adding muscle activation dynamics and muscle contraction dynamics to the model is discussed later in this Section.

In this Chapter, a cost function minimizing both torques and muscle stresses was implemented (Equation 5.13). In previous formulation attempts, cost functions replacing joint torques with muscle forces entirely (i.e. removing the $cost_{torque}$ term in Equation 5.13 completely) were tested; however the solver failed to progress from the initial seed and this strategy was rejected. It is suspected that the optimizer did not progress because the initial guess is particularly inefficient, and because the cost was measured by a variable (muscle stress) even farther removed than torques from the control (kinetics), which resulted in a poorly conditioned solution space. This response of the system, where the solver fails to progress from the initial seed, is also evoked when the weight of the $cost_{muscles}$ term, w_m in Equation 5.12, is increased by an order of magnitude or more. Including muscles in the STS prediction resulted in slower and more normative timing. However, the static optimization routine that solves for muscle forces increased computation time drastically, from finding a final solution within hours using the Chapter 4 model to days using the Chapter 5 model. Nevertheless, muscular contributions have proven influential to predicting realistic STS, and therefore, more efficient strategies of including these muscles and resolving their contributions in a motion prediction routine should be investigated to obtain a more efficient optimal control solution.

The muscle contributions predicted in this Chapter are similar to those found by previous researchers. For example, like Daigle, this study finds the uniarticular hip extensor, iliopsoas, and the vasti primarily influential to STS [105]. Judging by the magnitude of

the muscle force traces in Figure 5.13, if an ankle muscle is to be added to this list, it should be tibialis anterior. There are, however, differences to predicted muscle contributions compared to those measured in the STS experiments of Roebroeck et al. [144]. These are because of differences between the model and physiology and there are at least three changes that may help to mitigate these discrepancies. The first possible change is to include muscle synergies in the inverse muscle force problem, which may be reasonable between the modelled quadriceps - rectus femoris and vasti, for example - and may force reasonable activity in rectus femoris when none was predicted in this Chapter.

The second possible change is re-defining the cost function in stance. It has been true in previous Chapters as in this one that the model assumes a standing posture demanding a particularly low ankle joint torque (to minimize the defined cost function). Upon further investigation differences between the predicted soleus muscle force and measured soleus EMG in stance as displayed in Figure 5.13, evidence was found that healthy people tend to stand with their centre of mass aligned more closely with the middle of the foot than through the ankle [145]. It has been hypothesized that this phenomenon exists because it economizes a person's potential to ambulate from stance, even though it is not the most economical in terms of muscular effort [146]. The origins of this phenomenon could be tapped into directly if predicting a "Get Up and Go" motion [147], which could be achieved by building a composite motion of STS followed by gait using Chapter 3 of this thesis as a framework.

The third change is adding muscle activation dynamics and muscle contraction dynamics to the model. This change would immediately address the physiologically inappropriate abrupt changes in predicted hamstrings and tibialis anterior muscle forces. It would also, likely, increase the duration of the predicted STS motion to make it even more in line with observed STS timing. However, incorporating these dynamics adds considerable complexity to the model that requires added validation and is therefore left as future work. On a last, minor, note, judging by the inactivity of the flexor digitorum longus and tibialis

posterior muscles, their inclusion in this model was likely superfluous, especially considering that the other uniarticular plantarflexor, soleus, has a superior moment arm and force production potential.

Inclusion of muscle geometry and forces in the STS motion prediction problem has been beneficial to finding a more human-like motion. In previous Chapters, STS motions with gross motion patterns characteristic of healthy STS were predicted and normative STS events were synthesized. In this Chapter, because of the addition of muscles, the STS motion predicted also exhibits timing within healthy variability seen in experiments.

The musculoskeletal model designed in this Chapter allows for investigation into the origins of STS. It is known anecdotally, and is represented in Figure 2.6, that changes to the musculoskeletal geometry and muscle dynamics can impact STS. Including muscles in this model makes it more useful for investigating pathology, progression of pathology, and adaptation to intervention as they relate to STS, which will be important for future work in STS prediction.

6

Conclusion

This thesis presents a biomechanical model and motion prediction routine for discovering purely predictive sit-to-stand (STS) motions. The model designed is the most comprehensive planar model for predicting STS to date. The motion prediction routine is built on the fundamental assumption that healthy people naturally prioritize mechanical efficiency in motion. The resulting motion is convincing when compared to experimental kinetics and kinematics of STS.

6.1 Previous state of the field

The body of research exploring healthy STS prediction is particularly small. In Chapter 2, the five major works of STS prediction were introduced. Two of the five, by Daigle and Domire, used models largely based on the model of Garner, but instead employed a minimum time criterion to predict STS [24, 105] and subsequently solved for the fastest possible STS motion, rather than an every-day STS motion. The work of Mombaur and Ho Hoang used a geriatric model and focused on the interaction between that model and a modelled assistive device. The remaining two works, by Garner and Ozsoy, provided the most appropriate starting point for the research presented in this thesis. Garner built a

musculoskeletal model for rising from seated [104]. He controlled his model through muscle excitations to find a STS motion minimizing a function of muscle stresses and peak muscle force rates. Ozsoy, instead, broke the STS motion into 5 phases. In each phase the joint angles of the digital human model were represented as quartic B-splines with adjustable knots. He implemented a multi-objective cost function in a highly constrained optimization problem to optimize the knots and predict a STS motion [52]. The approaches of researchers attempting to predict STS are unique, and, as was lamented in Chapter 2, it is very difficult, if not impossible, to discuss which research decisions hold most merit as validation attempts have been oversimplified in all of these works.

One research question that remained unresolved was how to model the buttocks. Garner's buttocks model was the most useful of previous predictive STS researchers. He modelled vertical contact forces between the buttocks and chair with a Kelvin-Voigt element with an exponential spring and linear damper [104]. However, as proved to be a shortcoming with all investigated lumped parameter buttocks models, including those outside of this application, it didn't provide physically plausible force values for the range of natural tissue deformations in STS [71]. There are finite element models of adipose [74] and muscle [75] tissues built from studies of pigs that are promising for use in human buttocks modelling; however finite element models are too time-consuming for use in a dynamic optimization routine of STS prediction. The most appropriate buttocks model for STS prediction, previous to this thesis, was a Kelvin-Voigt model built by Wan and Schimmels [73] to model off-road vehicle operators while seated. It models the buttocks as a Kelvin-Voigt element with linear spring and linear damper, and is the model used in Chapter 3 of this thesis.

With respect to musculoskeletal modelling, it is the nature of the field that there are an abundance of non-validated, application-specific models of musculoskeletal geometry. Garner included eight muscles, modelled for gait [18], in his biomechanical model and recommended the inclusion of additional muscles [104]. Ozsoy excluded muscles from his

model altogether but made their inclusion a primary recommendation for future work. Two of the most well known and accepted musculoskeletal models in the literature are the White [80] model and Carhart [81] model. The White model is designed for use in gait analysis and gives details on how to scale the musculoskeletal geometry to models of different stature. The Carhart model is designed for use over larger ranges of joint angles. However, neither of these models were able to accurately represent musculoskeltal geometry for the large range of joint angles in STS, but they did provide the foundation of the model of musculoskeletal geometry designed in Chapter 5 of this thesis.

6.2 Summary of thesis work

The goal of this thesis is to predict healthy STS. To this end the following work was completed: in Chapter 3 the biomechanical model and optimal control problem were defined, in Chapter 4 the buttocks was modelled and STS was redefined, and in Chapter 5 musculoskeletal geometry was modelled and the optimal control problem was recast to include muscular effort. The remainder of this Section provides a more detailed summary of the work produced in each chapter of this thesis.

In Chapter 3, a motion pattern imitating STS was synthesized and it was compared to normative descriptions of healthy STS. First, the human was represented as three rigid links in the sagittal plane. This model captures aspects of joint, foot, and buttocks physiology, which makes it the most comprehensive planar model for predicting STS to date. Second, candidate STS trajectories were described geometrically by a set of Bézier curves which seem well suited to predictive biomechanical simulations. Third, with the assumption that healthy people naturally prioritize mechanical efficiency, disinclination to a motion was described as a cost function of joint torques, and for the first time, physical infeasibility including slipping and falling. Using these models and optimal control strategy together

has produced gross motion patterns characteristic of healthy STS when compared with normative data from the literature.

Chapter 4 detailed the analysis of experimentally collected buttocks force-deformation behaviour and the construction and evaluation of a constitutive model of buttocks for STS prediction. Four candidate models of buttocks were characterized and it was determined that the Kelvin-Voigt model with Mooney-Rivlin spring best matched experimental results. This buttocks model was used in the remainder of the STS predictions in the thesis.

The temporal STS data collected in the Chapter 4 experiment provided evidence that healthy young adults, such as the 15 participants in the study, complete STS an average of 0.57 s more quickly than what was reported in Kralj et al. [27]. Given this information, modifications to two of five STS event descriptions and updated temporal data were proposed for use in describing normative STS of healthy young people from a standard chair.

In Chapter 5, 10 muscles were added to the rigid link model of the previous Chapters and a STS motion was again predicted and compared to healthy STS. This model of musculoskeletal geometry was built with attention to the modelling work of previous biomechanists and was strongly motivated by studies of human anatomy and physiology to provide realiable muscle moment arms and muscle lengths for the natural range of sagittal plane joint motions. Maintaining the assumption that healthy people naturally prioritize mechanical efficiency, disinclination to a motion was described as a cost function of muscle stresses, rather than joint torques, in this chapter. Using these new models and the new optimal control strategy together produces gross motion patterns and normative events characteristic of healthy STS.

6.3 Contributions to the field

In summary, this thesis has made significant contributions to the fields of biomechanical modelling and predictive simulation of STS in four main areas: validating STS predictions, modelling the biomechanics of STS, modelling the musculoskeletal system, and proposing a dynamic optimization routine for STS prediction.

First, gains were made in STS prediction validation in two areas. The first area is in comparing predicted motions to normative STS data in the literature for the first time, thereby establishing a benchmark for future work in STS prediction. This changes the tide of the research where for 25 years researchers have not been able to say which decisions in STS prediction produced better results. The comparisons made in this thesis make it possible and desirable for a future researcher to compare their prediction to the predictions made in this thesis, using these models and optimal control strategies. The second area is in the updated definitions and timing of STS events for the purpose of describing healthy STS. The new definitions supersede the seminal work of Kralj et al. [27] and are based on visual motion capture and force plate data from 15 healthy young adults standing from a 46 cm chair. Notably, the time-scale information presented in this thesis is more consistent with the notion that healthy young adults take less than 3 seconds to stand from seated [6], making this update even more acceptable to the biomechanics community.

Second, significant advancements were made in biomechanical modelling for STS. This thesis describes the most comprehensive planar model of a female human in STS prediction. This is particularly relevant for a goal of predicting pathological STS because women have proportionally more difficulty performing STS according to self-reporting studies [7]. Also, for the first time, the buttocks model used in this STS prediciton work was characterized by measured STS force-deformation buttocks behaviour. Lastly, the implications of fixing the feet to the ground in STS prediction was acknowledged by describing disinclination to

a motion as a cost function of physical infeasibility including slipping and falling, for the first time.

Third, a minor contribution and a major contribution were made in the general area of musculoskeletal modelling. The minor contribution is the extension of Brand's patellar pulley model for consistency with deep knee flexion and for a three-dimensional patella. The major contribution is the creation of a model of musculoskeletal geometry for the popular deLeva female anthropometric data set that is validated with respect to experimentally determined moment arms published in the literature.

The fourth contribution is in proposing a dynamic optimization routine for STS prediction. In this routine, candidate STS trajectories are described geometrically by a set of Bézier curves that seem well suited to predictive biomechanical simulations. This new dynamic optimization routine allows for motions of gradually increasing complexity while the model's performance is improving and has produced gross motion patterns characteristic of healthy STS when compared with normative data from the literature.

6.4 Recommendations for future research

There are at least three categories of future work that will add to and complement the research reported in this thesis: work that addresses limitations of the research presented, work that further develops the research as presented to make it more applicable to general use, and work to expand on this thesis to approach a vision of a future where modelling and simulation of biomechanical systems is inherent when discussing pathology and assessing medical treatment options. The work that is recommended to address limitations of this research is discussed first.

First, before applying the biomechanical models and motion prediction routines developed in this thesis to new research questions, it is advised that computation time be decreased, for example by investigating direct collocation techniques, implementing code

optimization, or moving this problem to a more powerful server. The optimization routine, described in Chapter 5, is slow and increasing its speed would make it considerably more practical for exploratory research.

Next, it would be prudent to explore more cost function forms when developing the performance criteria for the STS motion. The ones used in this thesis, minimizing functions of torque and muscle stress, produce realistic results but there are possibly others that would be more representative of how people control a STS motion. It may be a worthwhile exercise to apply an inverse optimal control approach to identify more optimal criteria [20] and weighting factors. Along this line, it would also be relevant to look for cost functions able to predict not only kinematics, but also muscle excitations that could be compared to experimental EMG.

The results of Chapter 5 of this thesis support the notion that muscles are important to the development and execution of motion patterns. While the muscles modelled in Chapter 5 are validated in terms of the sagittal-plane moment arms across the natural range of motion, they are not validated in terms of their lengths or moment arms in alternate planes. If this model of musculoskeletal geometry is to be used to calculate muscle activations or excitations, it will need to be tuned to account for these 3D effects and will need to include muscle dynamics. If this model is to be used in a study interested in joint moments in alternate planes, it should be tuned to known moment arms in those planes.

It would also be valuable to validate the scalability of the model, specifically if it can be used to predict subject-specific differences in STS motion patterns.

Depending on a future research question, it will be worth-while to expand on the three-link model to consider a four (or more) link model, by adding degrees of freedom at the spine (to free the pelvis) or the shoulder (to free the arms). If significantly non-symmetric motions are of interest, for example if there is an asymmetrical pathology, it will be important to extend the model to three dimensions by reducing the coupling between

the legs and changing the revolute joints to joints more complex and more representative of their anatomical counterpart.

This thesis proposed an iterative routine of STS "learning." It would be enlightening to investigate if this process is in harmony with theories of motor learning. If not, it would be interesting to remodel this routine to better match what is known about motor learning. However, if is relevant to theories of motor learning, it would be logical to apply this strategy to more motions learned in this way.

This research direction gets particularly exciting if it becomes possible to model motor learning, because it seems natural to adopt those theories to motion adaptation to changes in biomechanics or the environment. For example, a subset of age-related changes may be incorporated in the biomechanical model by adjusting the body segment parameters, and in the control routine by increasing the cost of falling to investigate alterations in STS with age. Other avenues of exploration include modelling the progression of degenerative diseases and the effects of therapeutic intervention. Then, at the intersection of this research work, it will be possible to examine when and how to intervene to promote health and well being through modelling and predictive simulation of human motion.

References

[1] R. W. Bohannon, S. R. Barreca, M. E. Shove, C. Lambert, L. M. Masters, and C. S. Sigouin, "Documentation of daily sit-to-stands performed by community-dwelling adults," *Physiotherapy Theory and Practice*, vol. 24, no. 6, pp. 437–442, 2008.

[2] World Health Organizatio, "International classification of functioning, disability and health," 2001. Available online: `www.who.int/classifications/icf/`.

[3] S. Katz, T. D. Downs, H. R. Cash, and R. C. Grotz, "Progress in development of the index of ADL," *The Gerontologist*, vol. 10, no. 1, pp. 20–30, 1970.

[4] E. Odding, *Locomotor disability in the elderly: an epidemiological study of its occurrence and determinants in a general population of 55 years and over: the Rotterdam study*. PhD thesis, Erasmus University Rotterdam, Rotterdam, Netherlands, October 1994.

[5] N. B. Alexander, A. B. Schultz, and D. N. Warwick, "Rising from a chair: Effects of age and functional ability on performance biomechanics," *Journal of Gerontology*, vol. 46, no. 3, pp. M91–M98, 1991.

[6] M. A. Hughes, D. K. Weiner, M. L. Schenkman, R. M. Long, and S. A. Studenski, "Chair rise strategies in the elderly," *Clinical Biomechanics*, vol. 9, no. 3, pp. 187–192, 1994.

[7] W. G. Janssen, H. B. Bussmann, and H. J. Stam, "Determinants of the sit-to-stand movement: A review," *Physical Therapy*, vol. 82, no. 9, pp. 866–879, 2002.

[8] H. Hatze, "A comprehensive model for human motion simulation and its application to the take-off phase of the long jump," *Journal of Biomechanics*, vol. 14, no. 3, pp. 135–142, 1981.

[9] F. E. Zajac, "Muscle and tendon: properties, models, scaling, and application to biomechanics and motor control," *Critical Reviews in Biomedical Engineering*, vol. 17, no. 4, pp. 359–411, 1989.

[10] M. L. Schenkman, R. A. Berger, P. O. Riley, R. W. Mann, and W. A. Hodge, "Whole-body movements during rising to standing from sitting," *Physical Therapy*, vol. 70, no. 10, pp. 638–651, 1990.

[11] B. J. Fregly, T. F. Besier, D. G. Lloyd, S. L. Delp, S. A. Banks, M. G. Pandy, and D. D. D'Lima, "Grand challenge competition to predict in vivo knee loads," *Journal of Orthopaedic Research*, vol. 30, no. 4, pp. 503–513, 2012.

[12] A. L. Kinney, T. F. Besier, D. D. D'Lima, and B. J. Fregly, "Update on grand challenge competition to predict *in Vivo* knee loads," *Journal of Biomechanical Engineering*, vol. 135, no. 021012, pp. 1–4, 2013.

[13] M. P. Murray, "Gait as a total pattern of movement," *Americal Journal of Physical Medicine*, vol. 46, no. 1, pp. 290–333, 1967.

[14] D. A. Winter, *The Biomechanics and Motor Control of Human Gait.* Waterloo, Ontario: University of Waterloo Press, 1987.

[15] C. A. Stevermer and J. C. Gillette, "Kinematic and kinetic indicators of sit-to-stand," *Journal of Applied Biomechanics*, vol. 32, no. 1, pp. 7–15, 2016.

[16] J. G. Zwicker and S. R. Harris, "A reflection on motor learning theory in pediatric occupational therapy practice," *Canadian Journal of Occupational Therapy*, vol. 76, no. 1, pp. 29–37, 2009.

[17] R. A. Schmidt, T. D. Lee, C. J. Winstein, G. Wulf, and H. N. Zelaznik, *Motor control and learning: a behavioural emphasis*. Champaign, Illinois: Human Kinetics, 6th ed., 2019.

[18] R. A. Brand, R. D. Crowninshield, C. E. Wittstock, D. R. Pedersen, C. R. Clark, and F. M. van Krieken, "A model of lower extremity muscular anatomy," *Journal of Biomechanical Engineering*, vol. 104, pp. 304–310, November 1982.

[19] P. de Leva, "Adjustments to Zatsiorsky-Seluyanov's segment inertia parameters," *Journal of Biomechanics*, vol. 29, no. 9, pp. 1223–1230, 1996.

[20] D. Clever, Y. Hu, and K. Mombaur, "Humanoid gait generation in complex environments based on template models and optimality principles learned from human beings," *The International Journal of Robotics Research*, pp. 1–21, 2018. DOI: 10.1177/0278364918765620.

[21] S. L. Whitney, D. M. Wrisley, G. F. Marchetti, M. A. Gee, M. S. Redfern, and J. M. Furman, "Clinical measurement of sit-to-stand performance in people with balance disorders: validity of data for the five-times-sit-to-stand test," *Physical Therapy*, vol. 85, no. 10, pp. 1034–1045, 2005.

[22] J. S. Munton, M. I. Ellis, and V. Wright, "Use of electromyography to study leg muscle activity in patients with arthritis and in normal subjects during rising from a chair," *Annals of the Rheumatic Diseases*, vol. 43, pp. 63–65, 1984.

[23] K. Turcot, S. Armand, D. Fritschy, P. Hoffmeyer, and D. Suvà, "Sit-to-stand alterations in advanced knee osteoarthritis," *Gait and Posture*, vol. 36, no. 1, pp. 68–72, 2012.

[24] Z. J. Domire, *A biomechanical analysis of maximum vertical jumps and sit-to-stand*. PhD thesis, Pennsylvania State University, State College, Pennsylvania, August 2004.

[25] S. S. Coghlin and B. J. Mcfadyen, "Transfer strategies used to rise from a chair in normal and low back pain subjects," *Clinical Biomechanics*, vol. 9, pp. 85–92, 1994.

[26] F. Sibella, M. Galli, M. Romei, A. Montesano, and M. Crivellini, "Biomechanical analysis of sit-to-stand movement in normal and obese subjects," *Clinical Biomechanics*, vol. 18, pp. 745–750, 2003.

[27] A. Kralj, R. Jaeger, and M. Munih, "Analysis of standing up and sitting down in humans: Definitions and normative data presentation," *Journal of Biomechanics*, vol. 23, no. 11, pp. 1123–1138, 1990.

[28] F. Bahrami, R. Riener, P. Jabedar-Maralani, and G. Schmidt, "Biomechanical analysis of sit-to-stand transfer in healthy and paraplegic subjects," *Clinical Biomechanics*, vol. 15, pp. 123–133, 2000.

[29] M. K. Y. Mak, O. Levin, J. Mizrahi, and C. W. Y. Hui-Chan, "Joint torques during sit-to-stand in healthy subjects and people with Parkinson's disease," *Clinical Biomechanics*, vol. 18, no. 3, pp. 197–206, 2003.

[30] M. K. Y. Mak and C. W. Y. Hui-chan, "The speed of sit-to-stand can be modulated in Parkinson's disease," *Clinical Neurophysiology*, vol. 116, pp. 780–789, 2005.

[31] L. M. Inkster and J. J. Eng, "Postural control during a sit-to-stand task in individuals with mild Parkinson's disease," *Experimental Brain Research*, vol. 154, no. 1, pp. 33–38, 2004.

[32] C. Cachia, "A biomechanical analysis of the sit-to-stand transfer in Parkinson's disease," msc thesis, Queen's University, Kingston, Ontario, January 2008.

[33] D. M. Cameron, R. W. Bohannon, G. E. Garrett, S. V. Owen, and D. A. Cameron, "Physical impairments related to kinetic energy during sit-to-stand and curb-climbing following stroke," *Clinical Biomechanics*, vol. 18, pp. 332–340, 2003.

[34] P. Cheng, M. Liaw, M. Wong, and F. Tang, "The sit-to-stand movement in stroke patients," *Archives of Physical Medicine and Rehabilitation*, vol. 79, pp. 1043–1046, 1998.

[35] D. Brunt, B. Greenberg, S. Wankadia, and M. A. Trimble, "The effect of foot placement on sit to stand in healthy young subjects and patients with hemiplegia," *Archives of Physical Medicine and Rehabilitation*, vol. 83, pp. 924–929, 2002.

[36] C. Monger, W. Private, J. H. Carr, and V. Fowler, "Evaluation of a home-based exercise and training programme to improve sit-to-stand in patients with chronic stroke," *Clinical Rehabilitation*, vol. 16, pp. 361–367, 2002.

[37] L. Ada and P. Westwood, "A kinematic analysis of recovery of the ability to stand up following stroke," *Australian Journal of Physiotherapy*, vol. 38, no. 2, pp. 135–142, 1992.

[38] S. Barreca, C. S. Sigouin, C. Lambert, and B. Ansley, "Effects of extra training on the ability of stroke survivors to perform an independent sit-to-stand: A randomized controlled trial," *Journal of Geriatric Physical Therapy*, vol. 27, no. 2, pp. 59–64, 2004.

[39] P. Silva, J. Franco, A. Gusmão, J. Moura, L. Teixeira-Salmela, and C. Faria, "Trunk strength is associate with sit-to-stand performance in both stroke and healthy subjects," *European Journal of Physical and Rehabilitation Medicine*, vol. 51, no. 6, pp. 717–724, 2015.

[40] D. M. O'Meara and R. M. Smith, "The effects of unilateral grab rail assistance on the sit-to-stand performance of older aged adults," *Human Movement Science*, vol. 25, pp. 257–274, 2006.

[41] A. N. Spring, J. Kofman, and E. D. Lemaire, "Design and evaluation of an orthotic knee-extension assist," *IEEE Transactions on Neural Systems and Rehabilitation Engineering*, vol. 20, no. 5, pp. 678–687, 2012.

[42] F. C. Su, K. A. Lai, and W. H. Hong, "Rising from chair after total knee arthroplasty," *Clinical Biomechanics*, vol. 13, no. 3, pp. 176–181, 1997.

[43] R. L. Mizner and L. Snyder-mackler, "Altered loading during walking and sit-to-stand is affected by quadriceps weakness after total knee arthroplasty," *Journal of Orthopaedic Research*, vol. 23, pp. 1083–1090, 2005.

[44] R. Davoodi and B. J. Andrews, "Optimal control of FES-assisted standing up in paraplegia using genetic algorithms," *Medical Engineering and Physics*, vol. 21, pp. 609–617, 1999.

[45] A. Kralj and T. Bajd, *Functional Electrical Stimulation: Standing and Walking after Spinal Cord Injury*. Boca Raton, Florida: CRC Press, 1989.

[46] R. Kamnik, T. Bajd, and A. Kralj, "Functional electrical stimulation and arm supported sit-to-stand transfer after paraplegia: A study of kinetic parameters," *Artificial Organs*, vol. 23, no. 5, pp. 413–417, 1999.

[47] H. Kagaya, Y. Shimada, K. Ebata, M. Sato, and K. Sato, "Restoration and analysis of standing-up in complete paraplegia utilizing functional electrical stimulation," *Archives of Physical Medicine and Rehabilitation*, vol. 76, no. September, pp. 876–881, 1995.

[48] K. Mombaur, "Optimization of sit to stand motions of elderly people for the design and control of physical assistive devices," in *Proceedings in Applied Mathematics and Mechanics* (P. Steinmann and G. Leugering, eds.), vol. 14, (Erlangen, Germany), pp. 805–806, 2014.

[49] M. Geravand, P. Z. Korondi, C. Werner, K. Hauer, and A. Peer, "Human sit-to-stand transfer modeling towards intuitive and biologically-inspired robot assistance," *Autonomous Robots*, vol. 41, no. 3, pp. 575–592, 2017.

[50] R. K. Prinz, S. Neville, and N. J. Livingston, "Development of a fuzzy-based sit-to-stand controller," in *Canadian Conference on Electrical and Computer Engineering*, (Vancouver, British Columbia), pp. 1631–1634, Institute of Electrical and Electronics Engineers, 2007.

[51] R. K. Prinz, "Synthesizing the sit-to-stand movement using fuzzy logic-based control and a simple biomechanical model," MASc thesis, University of Victoria, Victoria, British Columbia, August 2010.

[52] B. Ozsoy and J. Yang, "Simulation-based unassisted sit-to-stand motion prediction for healthy young individuals," in *International Design Engineering Technical Conferences & Computers and Information in Engineering Conference*, (Buffalo, New York), American Society of Mechanical Engineers, August 2014.

[53] International Society of Biomechanics, "Proceedings of the 16th International Symposium on Computer Simulation in Biomechanics," in *Technical Group on Computer Simulation*, (Gold Coast, Australia), July 2017.

[54] J. Wheeler, C. Woodward, R. L. Ucovich, J. Perry, and J. M. Walker, "Rising from a chair: Influence of age and chair design," *Physical Therapy*, vol. 65, no. 1, pp. 22–26, 1985.

[55] S. Kawagoe, N. Tajima, and E. Chosa, "Biomechanical analysis of effects of foot placement with varying chair height on the motion of standing up," *Journal of Orthopaedic Science*, vol. 5, no. 2, pp. 124–133, 2000.

[56] M. M. Khemlani, J. H. Carr, and W. J. Crosbie, "Muscle synergies and joint linkages in sit-to-stand under two initial foot positions," *Clinical Biomechanics*, vol. 14, no. 4, pp. 236–246, 1999.

[57] C. A. M. Doorenbosch, J. Harlaar, M. E. Roebroeck, and G. J. Lankhorst, "Two strategies of transferring from sit-to-stand; the activation of monoarticular and biarticular muscles," *Journal of Biomechanics*, vol. 27, no. 11, pp. 1299–1307, 1994.

[58] S. Nuzik, R. Lamb, and A. Vansant, "Sit-to-stand movement pattern: A kinematic study," *Physical Therapy*, vol. 66, no. 11, pp. 1708–1713, 1986.

[59] D. A. Winter, *Biomechanics and motior control of human movement*. Hoboken, New Jersey: John Wiley & Sons, 4th ed., 2009.

[60] W. T. Dempster, "Space requirements of the seated operator," Tech. Rep. 55-159, United States Air Force, July 1955.

[61] R. Drillis, R. Contini, and M. Bluestein, "Body segment parameters," Tech. Rep. 1166.03, Department of Health, Education, and Welfare, 1966.

[62] S. Pheasant, *Bodyspace: anthropometry, ergonomics and design*. London, United Kingdom: Taylor & Francis, 1986.

[63] S. Yoshioka, A. Nagano, D. C. Hay, and S. Fukashiro, "The minimum required muscle force for a sit-to-stand task," *Journal of Biomechanics*, vol. 45, no. 4, pp. 699–705, 2012.

[64] T. S. Buchanan, D. G. Lloyd, K. Manal, and T. F. Besier, "Neuromusculoskeletal modeling: Estimation of muscle forces and joint moments and movements from measurements of neural command," *Journal of Applied Biomechanics*, vol. 20, no. 4, pp. 367–395, 2004.

[65] M. Damsgaard, J. Rasmussen, S. Torholm Christensen, E. Surma, and M. de Zee, "Analysis of musculoskeletal systems in the anybody modeling system," *Simulation Modelling Practice and Theory*, vol. 14, pp. 1100–1111, 2006.

[66] V. M. Zatsiorsky, V. N. Seluyanov, and L. G. Chugunova, "Methods of determining mass-inertial characteristics of human body segments," in *Contemporary Problems of Biomechanics* (C. G. G. and S. A. Regirer, eds.), pp. 272–291, CRC Press, 1990.

[67] H. M. Reynolds, C. C. Snow, and J. W. Young, "Spatial geometry of the human pelvis," Tech. Rep. ADA118238, Federal Aviation Administration, Washington DC, March 1982.

[68] Y. C. Fung, *Biomechanics*. New York, New York: Springer-Verlag, 1981.

[69] S. S. Sandhu and J. McPhee, "A two-dimensional nonlinear volumetric foot contact model," in *International Mechanical Engineering Congress & Exposition*, (Vancouver, British Columbia), pp. 703–710, American Society of Mechanical Engineers, November 2010.

[70] P. Brown and J. McPhee, "A 3D ellipsoidal volumetric footground contact model for forward dynamics," *Multibody System Dynamics*, vol. 42, no. 4, pp. 447–467, 2018.

[71] E. Linder-Ganz, N. Shabshin, Y. Itzchak, and A. Gefen, "Assessment of mechanical conditions in sub-dermal tissues during sitting: A combined experimental-MRI and finite element approach," *Journal of Biomechanics*, vol. 40, no. 7, pp. 1443–1454, 2007.

[72] C. C. Liang and C. F. Chiang, "A study on biodynamic models of seated human subjects exposed to vertical vibration," *International Journal of Industrial Ergonomics*, vol. 36, no. 10, pp. 869–890, 2006.

[73] Y. Wan and J. M. Schimmels, "Optimal seat suspension design based on minimum "simulated subjective response"," *Journal of Biomechanical Engineering*, vol. 119, no. 4, pp. 409–416, 1997.

[74] M. Geerligs, G. W. M. Peters, P. A. J. Ackermans, C. W. J. Oomens, and F. P. T. Baaijens, "Linear viscoelastic behavior of subcutaneous adipose tissue," *Biorheology*, vol. 45, no. 6, pp. 677–688, 2008.

[75] A. Palevski, "Stress relaxation of porcine gluteus muscle subjected to sudden transverse deformation as related to pressure sore modeling," *Journal of Biomechanical Engineering*, vol. 128, no. 5, pp. 782–787, 2006.

[76] Committee for the Study of Joint Motion, *Joint Motion*. Chicago, Illinois: American Academy of Orthopaedic Surgeons, 1965.

[77] M. P. Murray, A. B. Drought, and R. C. Kory, "Walking patterns of normal men," *Journal of Bone and Joint Surgery*, vol. 46, pp. 335–360, March 1964. cited in [78].

[78] D. A. Winter, A. O. Quanbury, D. A. Hobson, H. G. Sidwall, G. Reimer, B. G. Trenholm, T. Steinke, and H. Shlosser, "Kinematics statistical of normal locomotion-a study based on T.V. data," *Journal of Biomechanics*, vol. 7, pp. 479–486, 1974.

[79] S. L. Delp, *Surgery simulation: a computer graphics system to analyze and design musculoskeletal reconstructions of the lower limb*. PhD thesis, Stanford University, Stanford, California, August 1990.

[80] S. C. White, H. J. Yack, and D. A. Winter, "A three-dimensional musculoskeletal model for gait analysis. anatomical variability estimates," *Journal of Biomechanics*, vol. 22, no. 8-9, pp. 885–893, 1989.

[81] M. R. Carhart, *Biomechanical analysis of compensatory stepping: Implications for paraplegics standing via FNS*. PhD thesis, Arizona State University, Tempe, Arizona, August 2000.

[82] V. Norman-Gerum and J. McPhee, "Comparison of cylindrical wrapping geometries to via points for modeling muscle paths in the estimation of sit-to-stand muscle forces," in *9th International Conference on Multibody Systems, Nonlinear Dynamics, and Control*, (Portland, Oregon), August 2013.

[83] C. K. Chow and D. H. Jacobson, "Locomotion via optimal programming," *Mathematical Biosciences*, vol. 10, no. 3-4, pp. 239–306, 1971.

[84] T. K. Ghosh and W. H. Boykin, "Analytic determination of an optimal human motion," *Journal of Optimization Theory and Applications*, vol. 19, no. 2, pp. 327–346, 1976.

[85] H. Hatze, "The complete optimization of a human motion," *Mathematical Biosciences*, vol. 28, no. 1-2, pp. 99–135, 1976.

[86] B. R. Umberger and R. H. Miller, "Optimal control modeling of human movement," in *Handbook of Human Motion* (W. S. Müller, Bertram Wolf, Sebastian I. Brueggemann, Gert-Peter Deng, Zhigang McIntosh, Andrew Miller, Freeman Selbie, ed.), pp. 1–22, Springer Nature, 2017.

[87] A. V. Rao, "A survey of numerical methods for optimal control," *Advances in Astronautical Sciences*, vol. 135, pp. 497–528, 2010.

[88] M. Diehl, "Optimal control - an overview," 2015. Available online: `www.syscop.de/files/2015ss/events/tempo/OptimalControl.pdf`.

[89] R. E. Bellman, *Dynamic Programming*. Princeton, New Jersey: Princeton University Press, 1957.

[90] G. T. Yamaguchi and F. E. Zajac, "Restoring unassisted natural gait to paraplegics via functional neuromuscular stimulation: A computer simulation study," *IEEE Transactions on Biomedical Engineering*, vol. 37, no. 9, pp. 886–902, 1990.

[91] M. G. Pandy, F. C. Anderson, and D. G. Hull, "A parameter optimization approach for the optimal control of large-scale musculoskeletal systems," *Journal of Biomechanical Engineering*, vol. 114, no. 4, pp. 450–460, 1992.

[92] M. G. Pandy, B. A. Garner, and F. C. Anderson, "Optimal control of non-ballistic muscular movements: a constraint-based performance criterion for rising from a chair," *Journal of Biomechanical Engineering*, vol. 117, pp. 15–26, 1995.

[93] S. Porsa, Y. C. Lin, and M. G. Pandy, "Direct methods for predicting movement biomechanics based upon optimal control theory with implementation in OpenSim," *Annals of Biomedical Engineering*, vol. 44, no. 8, pp. 2542–2557, 2016.

[94] A. J. Meyer, I. Eskinazi, J. N. Jackson, A. V. Rao, C. Patten, and B. J. Fregly, "Muscle synergies facilitate computational prediction of subject-specific walking motions," *Frontiers in Bioengineering and Biotechnology*, vol. 4, October 2016.

[95] M. Ezati, B. Ghannadi, N. Mehrabi, and J. McPhee, "Optimal vertical jump of a human," in *4th International Conference On Control Dynamic Systems, And Robotics*, (Toronto, Ontario), pp. 103–1, August 2017.

[96] H. Celik and S. J. Piazza, "Simulation of aperiodic bipedal sprinting," *Journal of Biomechanical Engineering*, vol. 135, no. 8, pp. 1–8, 2013.

[97] E. Todorov and M. I. Jordan, "Optimal feedback control as a theory of motor coordination," *Nature Neuroscience*, vol. 5, no. 11, pp. 1226–1235, 2002.

[98] N. Mehrabi, R. Sharif Razavian, B. Ghannadi, and J. McPhee, "Predictive simulation of reaching moving targets using nonlinear model predictive control," *Frontiers in Computational Neuroscience*, vol. 10, pp. 1–12, January 2017.

[99] R. D. Crowninshield and R. A. Brand, "The prediction of forces in joint structures," *Exercise & Sport Sciences Reviews*, vol. 9, no. 1, pp. 159–182, 1981.

[100] W. Weber and E. Weber, *Mechanik der Menschlichen Gehwerkzeuge*. Göttingen, Germany: Dietrich, 1836. quoted in [99].

[101] Y. Nubar and R. Contini, "A minimal principle in biomechanics," *The Bulletin of Mathematical Biophysics*, vol. 23, no. 4, pp. 377–391, 1961.

[102] K. N. An, B. M. Kwak, E. Y. Chao, and B. F. Morrey, "Determination of muscle and joint forces: a new technique to solve the indeterminate problem," *Journal of biomechanical engineering*, vol. 106, no. 4, pp. 364–367, 1984.

[103] A. Pedotti, V. V. Krishnan, and L. Stark, "Optimization of muscle-force sequencing in human locomotion," *Mathematical Biosciences*, vol. 38, no. 1-2, pp. 57–76, 1978.

[104] B. A. Garner, "A dynamic musculoskeletal computer model for rising from a squatting or sitting position," MSc in Engineering thesis, The University of Texas at Austin, Austin, Texas, August 1992.

[105] K. E. Daigle, "The effect of muscle strength on the coordination of rising from a chair in minimum time," MA thesis, The University of Texas at Austin, Austin, Texas, August 1994.

[106] A. M. Mughal and K. Iqbal, "Fuzzy optimal control of sit-to-stand movement in a biomechanical model," *Journal of Intelligent and Fuzzy Systems*, vol. 25, pp. 247–258, 2013.

[107] N. A. Bakar and A. R. Abdullah, "Dynamic simulation of sit to stand exercise for paraplegia," in *International Conference on Control System, Computing and Engineering*, (Penang, Malaysia), pp. 114–118, Institute of Electrical and Electronics Engineers, November 2011.

[108] F. C. Wang, C. H. Yu, Y. L. Lin, and C. E. Tsai, "Optimization of the sit-to-stand motion," in *International Conference on Complex Medical Engineering*, (Beijing, China), pp. 1248–1253, Institute of Electrical and Electronics Engineers, May 2007.

[109] B. Ozsoy, *Three-dimensional sit-to-stand motion prediction*. PhD thesis, Texas Tech University, Lubbock, Texas, May 2014.

[110] K. Mombaur and K. L. Ho Hoang, "How to best support sit to stand transfers of geriatric patients: Motion optimization under external forces for the design of physical assistive devices," *Journal of Biomechanics*, vol. 58, pp. 131–138, 2017.

[111] Z. J. Domire and J. Challis, H, "The influence of seat height on sit to stand in the elderly," in *International Society of Biomechanics XXth Congress - American Society of Biomechanics 29th Annual Meeting*, (Cleveland, Ohio), p. 659, August 2005.

[112] C. C. Gordon, T. Churchill, C. E. Clauser, B. Bradtmiller, J. T. McConville, I. Tebbetts, and R. A. Walker, "1988 anthropometric survey of U.S. army personnel: Methods and summary statistics," Tech. Rep. 89/027, United States Army Natick Research, Development and Engineering Center, 1989.

[113] A. B. Schultz, N. B. Alexander, and J. A. Ashton-Miller, "Biomechanical analyses of rising from a chair," *Journal of Biomechanics*, vol. 25, no. 12, pp. 1383–1391, 1992.

[114] E. M. Arnold, S. R. Ward, R. L. Lieber, and S. L. Delp, "A model of the lower limb for analysis of human movement," *Annals of Biomedical Engineering*, vol. 38, no. 2, pp. 269–279, 2010.

[115] B. Garner and M. Pandy, "The obstacle-set method for representing muscle paths in musculoskeletal models," *Computer methods in biomechanics and biomedical engineering*, vol. 3, no. 1, pp. 1–30, 2000.

[116] P. Favre, C. Gerber, and J. G. Snedeker, "Automated muscle wrapping using finite element contact detection," *Journal of Biomechanics*, vol. 43, no. 10, pp. 1931–1940, 2010.

[117] A. Scholz, I. Stavness, M. Sherman, S. Delp, and A. Kecskeméthy, "Improved muscle wrapping algorithms using explicit path-error Jacobians," in *Computational Kinematics* (F. Thomas and A. Perez Gracia, eds.), vol. 15, (Barcelona, Spain), pp. 395–403, Springer, 2013.

[118] V. Norman-Gerum and J. McPhee, "Constrained dynamic optimization of sit-to-stand motion driven by Bézier curves," *Journal of Biomechanical Engineering*, vol. 140, pp. 121011 1–7, December 2018.

[119] Waterloo Maple, Waterloo, Ontario, *MapleSim*, 2016.2 ed.

[120] G. T. Yamaguchi, *Dynamic Modeling of Musculoskeletal Motion: A Vectorized Approach for Biomechanical Analysis in Three Dimensions*. New York, New York: Springer Science & Business Media, 2006.

[121] R. Riener and T. Edrich, "Identification of passive elastic joint moments in the lower extremities," *Journal of Biomechanics*, vol. 32, no. 5, pp. 539–544, 1999.

[122] V. Norman-Gerum and J. McPhee, "What is sit-to-stand without a chair?," in *8th ECCOMAS Thematic Conference on Multibody Dynamics*, (Prague, Czech Republic), June 2017.

[123] "ElastoGap." Modelica Standard Library, 2012. Available online: `reference.wolfram.com/system-modeler/libraries/Modelica/Modelica.Mechanics.Translational.Components.ElastoGap.html`.

[124] B. Weir, "Guideline on office ergonomics," Tech. Rep. Z412-00, Canadian Standards Association International, Toronto, Ontario, 2016.

[125] Engineers Edge, "Coefficient of friction equation and table chart," 2000. Available online: `www.engineersedge.com/coeffients_of_friction.htm`.

[126] "30-second chair stand." Stopping Elderly Accidents, Deaths & Injuries, 2017.

[127] M. E. Mortenson, *Geometric Modeling*. New York, New York: Industrial Press, 3rd ed., 2006.

[128] D. A. Winter, F. Prince, J. S. Frank, C. Powell, and K. F. Zabjek, "Unified theory regarding A/P and M/L balance in quiet stance," *Journal of Neurophysiology*, vol. 75, no. 6, pp. 2334–2343, 1996.

[129] The MathWorks, Natick, Massachusetts, *MATLAB*, R2015a ed.

[130] M. L. Schenkman, P. O. Riley, and C. Pieper, "Sit to stand from progressively lower seat heights - alterations in angular velocity," *Clinical Biomechanics*, vol. 11, no. 3, pp. 153–158, 1996.

[131] C. W. J. Oomens, O. F. J. T. Bressers, E. M. H. Bosboom, C. V. C. Bouten, and D. L. Bader, "Can loaded interface characteristics influence strain distributions in muscle adjacent to bony prominences?," *Computer Methods in Biomechanics and Biomedical Engineering*, vol. 6, no. 3, pp. 171–180, 2003.

[132] E. M. H. Bosboom, M. K. C. Hesselink, C. W. J. Oomens, C. V. C. Bouten, M. R. Drost, and F. P. T. Baaijens, "Passive transverse mechanical properties of skeletal muscle under in vivo compression," *Journal of Biomechanics*, vol. 34, no. 10, pp. 1365–1368, 2001.

[133] C. W. J. Oomens and G. Peters, "Mechanical behavior and properties of adipose tissue," in *The Mechanobiology of Obesity and Related Diseases* (A. Gefen and D. Benayahu, eds.), vol. 16, pp. 3–9, Springer International Publishing, 2015.

[134] M. K. Patil, M. S. Palanichamy, and D. N. Ghista, "Dynamic response of human body seated on a tractor and effectiveness of suspension systems," *SAE Transactions*, vol. 86, pp. 3221–3235, 1977.

[135] M. E. Tinetti, "Performance-oriented assessment of mobility problems in elderly patients," *Journal of the American Geriatrics Society*, vol. 34, no. 2, pp. 119–126, 1986.

[136] OpenSim, Stanford, California, *Gait 2392 and 2354 Models*. Available online: `simtk-confluence.stanford.edu/display/OpenSim/Gait+2392+and+2354+Models`.

[137] S. Koo and T. P. Andriacchi, "A comparison of the influence of global functional loads vs. local contact anatomy on articular cartilage thickness at the knee," *Journal of Biomechanics*, vol. 40, no. 13, pp. 2961–2966, 2007.

[138] J. M. Mansour and J. M. Pereira, "Quantitative functional anatomy of the lower limb with application to human gait," *Journal of Biomechanics*, vol. 20, no. 1, pp. 51–58, 1987.

[139] S. J. Olney and D. A. Winter, "Predictions of knee and ankle moments of force in walking from EMG and kinematic data," *Journal of Biomechanics*, vol. 18, no. 1, pp. 9–20, 1985.

[140] P. Komi, M. Salonen, M. Jarvinen, and O. Kokko, "In vivo measurements of achilles tendon forces in man: I. methological development," *International Journal of Sports Medicine*, vol. 8 (supplement), pp. 3–8, 1987.

[141] J. A. Martin, S. C. Brandon, E. M. Keuler, J. R. Hermus, A. C. Ehlers, D. J. Segalman, M. S. Allen, and D. G. Thelen, "Gauging force by tapping tendons," *Nature Communications*, vol. 9, no. 1, pp. 2–10, 2018.

[142] F. C. Anderson and M. G. Pandy, "Static and dynamic optimization solutions for gait are practically equivalent," *Journal of Biomechanics*, vol. 34, no. 2, pp. 153–161, 2001.

[143] Y. Ou, "An analysis of optimization methods for identifying muscle forces in human gait," Diplom-Ingenieur thesis, Universität Duisburg-Essen, Duisburg, Germany, January 2013.

[144] M. E. Roebroeck, C. A. M. Doorenbosch, J. Harlaar, R. Jacobs, and G. J. Lankhorst, "Biomechanics and muscular activity during sit-to-stand transfer," *Clinical Biomechanics*, vol. 9, no. July, pp. 235–244, 1994.

[145] M. Schieppati, M. Hugon, M. Grass, A. Nardone, and M. Galante, "The limits of equilibrium in young and elderly normal subjects and in parkinsonians," *Electroencephalography and clinical Neurophysiology*, vol. 93, pp. 286–298, 1994.

[146] C. Le Mouel and R. Brette, "Mobility as the purpose of postural control," *Frontiers in Computational Neuroscience*, vol. 11, pp. 1–11, July 2017.

[147] "Timed up & go (TUG)." Stopping Elderly Accidents, Deaths & Injuries, 2017.

[148] A. S. Arnold, S. Salinas, D. J. Asakawa, and S. L. Delp, "Accuracy of muscle moment arms estimated from MRI-based musculoskeletal models of the lower extremity," *Computer Aided Surgery*, vol. 5, pp. 108–119, 2000.

[149] W. Herzog and L. J. Read, "Lines of action and moment arms of the major force-carrying structures crossing the human knee joint," *Journal of Anatomy*, vol. 182, pp. 213–230, 1993.

[150] B. Hintermann, B. M. Nigg, and C. Sommer, "Foot movement and tendon excursion: An in vitro study," *Foot & Ankle International*, vol. 15, no. 7, pp. 386–395, 1994.

[151] M. Millard, M. Sreenivasa, and K. Mombaur, "Predicting the motions and forces of wearable robotic systems using optimal control," *Frontiers in Robotics and AI*, vol. 4, pp. 1–12, August 2017.

[152] G. Németh and H. Ohlsén, "In vivo moment arm lengths for hip extensor muscles at different angles of hip flexion," *Journal of Biomechanics*, vol. 18, no. 2, pp. 129–140, 1985.

[153] D. A. Neumann, "Kinesiology of the hip: A focus on muscular actions," *Journal of Orthopaedic & Sports Physical Therapy*, vol. 40, no. 2, pp. 82–94, 2010.

[154] C. W. Spoor, J. L. van Leeuwen, C. G. M. Meskers, A. F. Titulaer, and A. Huson, "Estimation of instantaneous moment arms of lower-leg muscles," *Journal of Biomechanics*, vol. 23, no. 12, pp. 1247–1259, 1990.

[155] G. Yamaguchi and F. Zajac, "A planar model of the knee-joint to characterize the knee extensor mechanism," *Journal of Biomechanics*, vol. 22, no. 1, pp. 1–10, 1989.

[156] R. W. Ogden, *Non-linear Elastic Deformations*. Mineola, New York: Dover Publications, Dover ed., 1997.

[157] H. Hermens and B. Freriks, "Recommendations for sensor locations on individual muscles." The SENIAM (Surface ElectroMyoGraphy for the Non-Invasive Assessment of Muscles) project. Available online: `www.seniam.org/`.

APPENDICES

Appendix A

Experiments Performed

This appendix provides details on the subjects, equipment used, and protocol of the performed experiments, the data from which informs the buttocks modelling in Chapter 4. The Office of Research Ethics at the University of Waterloo approved the experimental protocol and all participants gave informed consent to the study.

Subjects

Fifteen healthy subjects volunteered to participate in this study. The subjects had no pain when sitting, standing, walking or going between these activities in the six months prior to the study. Table A.1 summarizes the participants sex, age, height, mass and self-reported physical training status.

Table A.1: Summary of participant information.

Participant	Sex	Age (years)	Mass (kg)	Hip to floor (m)	Height (m)	Training Status
P01	male	29	80.0	0.90	1.79	average
P02	male	32	72.0	1.00	1.80	high
P03	male	25	83.9	0.96	1.83	average
P04	male	28	93.4	0.90	1.79	average
P05	female	24	72.6	0.88	1.73	average
P06	female	19	55.3	0.75	1.54	average
P07	female	26	54.0	0.86	1.64	average
P08	female	26	55.0	0.88	1.63	high
P09	female	19	59.2	0.81	1.67	average
P10	male	25	70.0	0.98	1.80	average
P11	female	21	61.4	0.96	1.60	low
P12	male	24	79.4	0.97	1.85	high
P13	male	23	83.9	1.02	1.91	high
P14	female	29	49.0	0.90	1.58	average
P15	male	23	70.3	0.92	1.80	high
Average		24.9	69.3	0.91	1.73	average
Standard deviation		3.6	12.8	0.07	0.11	n/a
Maximum		32	93.4	1.02	1.91	high
Minimum		19	49.0	0.75	1.54	low

Equipment

Figure A.1 is a block diagram of the experimental set-up. Calibrations of the motion capture and force platform systems were performed at the beginning of each collection day and occasionally between participants.

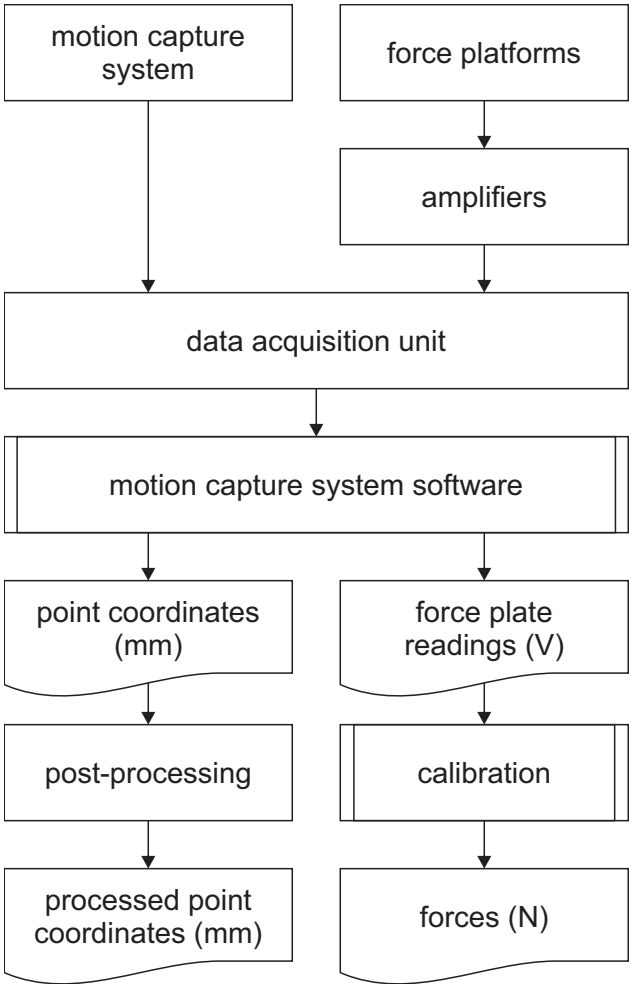

Figure A.1: Experimental data flow.

A pair of Advanced Mechanical Technology Inc. (AMTI) OR6-7 force platforms record ground reaction forces in this study. After amplification, this data travels to the Optotrak Data Acquisition Unit (ODAU). Six banks of Optotrak cameras captured the motions of 17

optical markers organized into five rigid body clusters in the calibrated collection volume. These markers are wired to a strober, which itself is wired to the ODAU.

The ODAU collects the force plate and Optotrak data, synchronously, in real time. Sampling and digitization of force plate data was set to happen at 2048 Hz while Optotrak data was collected at 100 Hz. From the ODAU, the data was passed to Northern Digital Incorporateds First Principles software on the desktop computer, which records, processes, and exports experimental data. This software also supports defining the global coordinate system, calibrating the collection volume, and defining virtual markers in the Optotrak system. Finally, the software is used to export the data as comma separated value files.

The motion capture data is exported as calibrated point coordinates in the global coordinate system while the force plate data is exported in Volts. With respect to the kinematic data, post processing included approximating the locations of markers that have been occluded during the experiment. Missing values were replaced using linear interpolation or, if not possible, by holding the last known value. Force plate data in Volts was calibrated to Newtons using calibration matrices provided by the original equipment manufacturer and certified calibration technician.

Experimental protocol

Throughout the experiment, participants wore a system of four marker clusters: one cluster of four on the right thigh, a cluster of four on the right leg, a cluster of four on the right foot, a cluster of five on the sacrum of the pelvis, and a fifth cluster of three on the chair. Adhesive tape and Velcro straps were used to hold these clusters in place. Palpation and digitization of bony landmarks created virtual markers on locations including: the right greater trochanter, each of the right medial and lateral femoral epicondyles, right medial malleolus, anterior superior iliac spines and posterior superior iliac spines.

A chair of 46 cm height was placed on one force plate. Sitting in that chair, the participants were asked to place their feet fully on the second force plate in a comfortable location where they would not need to move them to stand up. Participants were reminded to move as naturally as possible.

Each trial began with the participant sitting quietly for two minutes. On cue, they crossed their arms on their chest and sat quietly. The data collection was then initiated. On a second cue, approximately three seconds later, the participant stood up. Participants stood still for five seconds and then walked on the spot for one minute at a self-selected pace. During this time, ten seconds after initiation, the data collection terminates. 10 seconds of data was sufficient to capture quiet sitting and standing data for use as a baseline while allowing ample time for a sit-to-stand task of typical duration. On a final cue, the participant sat again. This sit-to-stand task was completed a maximum of ten times. Results of this experiment are included in Chapter 4.

Appendix B

Hyperelastic Spring Equations

Hyperelastic materials, by definition, have a stress-strain relationship derived from a strain energy density function. The three hyperelastic material models under investigation in Chapter 4 are the neo-Hookean material model, the Mooney-Rivlin material model, and the Ogden material model. The derivation of the spring equations representing each of these models, given the assumptions stated herein, is provided in this Appendix.

Background

The strain energy density function (W) of a material relates the strain energy density of the material to the deformation gradient (F)

$$W = W(F) \tag{B.1}$$

where

$$F = \begin{bmatrix} \frac{\partial x_1}{\partial X_1} & \frac{\partial x_1}{\partial X_2} & \frac{\partial x_1}{\partial X_3} \\ \frac{\partial x_2}{\partial X_1} & \frac{\partial x_2}{\partial X_2} & \frac{\partial x_2}{\partial X_3} \\ \frac{\partial x_3}{\partial X_1} & \frac{\partial x_3}{\partial X_2} & \frac{\partial x_3}{\partial X_3} \end{bmatrix} \tag{B.2}$$

When aligned to the principal directions, that is the axes of a coordinate system in which the material undergoes pure stretch, the normal stretches are the principal stretches and

the off-axis stretches are zero, such that

$$F = \begin{bmatrix} \frac{\partial x_1}{\partial X_1} & 0 & 0 \\ 0 & \frac{\partial x_2}{\partial X_2} & 0 \\ 0 & 0 & \frac{\partial x_3}{\partial X_3} \end{bmatrix} \tag{B.3}$$

where, by definition, the diagonal elements are the principal stretch ratios (λ_1, λ_2, λ_3)

$$\lambda_1 = \frac{\partial x_1}{\partial X_1}, \quad \lambda_2 = \frac{\partial x_2}{\partial X_2}, \quad \lambda_3 = \frac{\partial x_3}{\partial X_3} \tag{B.4}$$

All of the models of interest are expressed in terms of these principal stretch ratios and are, in fact, Ogden type models. The strain energy density of an Ogden material model is

$$W = \sum_{j=1}^{N} \frac{\mu_j}{\alpha_j} \left(\lambda_1^{\alpha_j} + \lambda_2^{\alpha_j} + \lambda_3^{\alpha_j} - 3 \right) \tag{B.5}$$

where μ_j and α_j are material constants.

Constitutive relation

To relate the principal strains to the principal stretches, the strain energy density function is substituted into the equations of principal stresses for hyperelastic materials. The buttocks is assumed incompressible and therefore, as shown in [156], the principal Cauchy stresses are represented by

$$\sigma_i = p + \lambda_i \frac{\partial W}{\partial \lambda_i} \tag{B.6}$$

where p is the pressure enforcing incompressibility, $\lambda_1 \lambda_2 \lambda_3 = 1$.

Differentiating the partial derivative in Equation B.6 results in stresses of the form

$$\sigma_i = p + \sum_{j=1}^{N} \mu_j \lambda_i^{\alpha_j} \tag{B.7}$$

Buttocks loading is assumed to occur uniaxially in the vertical direction, making the off-axis principal stresses zero. On account of incompressibility, the principal stretches are

related such that

$$\lambda_1 = \lambda_1, \quad \lambda_2 = \lambda_1^{-\frac{1}{2}}, \quad \lambda_3 = \lambda_1^{-\frac{1}{2}} \tag{B.8}$$

and the deformation gradient becomes

$$F = \begin{bmatrix} \lambda & 0 & 0 \\ 0 & \lambda^{-\frac{1}{2}} & 0 \\ 0 & 0 & \lambda^{-\frac{1}{2}} \end{bmatrix} \tag{B.9}$$

where the subscript indicating the vertical direction has been dropped for brevity.

The pressure, p, is solved for using the relationships between the principal stretches and principal stresses such that

$$p = -\sum_{j=1}^{N} \mu_j \lambda_1^{-\frac{\alpha_j}{2}} \tag{B.10}$$

By substitution of the expression for pressure in Equation B.10 into Equation B.7, the Cauchy stress in the vertical direction may now be written as

$$\sigma = \sum_{j=1}^{N} \mu_j \left(\lambda^{\alpha_j} - \lambda^{-\frac{\alpha_j}{2}} \right) \tag{B.11}$$

where the subscript indicating the vertical direction has again been dropped.

Spring equations

Desiring a force-deformation constitutive model of the buttocks, it is advantageous to consider the nominal stress as it is work conjugate to the deformation gradient. The relationship between the nominal stress (P) and Cauchy stress is

$$P = JF^{-1} \cdot \sigma \tag{B.12}$$

The vertical component of this nominal stress, for the deformation and Cauchy stress identified in the previous section, is

$$P = \frac{\sum_{j=1}^{N} \mu_j \left(\lambda^{\alpha_j} - \lambda^{-\frac{\alpha_j}{2}} \right)}{\lambda} \tag{B.13}$$

assuming a unit area for this application, the Ogden-type spring equation is found to be

$$F = \sum_{j=1}^{N} \mu_j \left(\lambda^{\alpha_j - 1} - \lambda^{-\frac{\alpha_j}{2} - 1} \right) \tag{B.14}$$

where F, in Equation B.14 and all equations to follow, is force.

A first order ($N = 1$) Ogden-type spring with $\alpha_1 = 2$ reduces to a neo-Hookean-type spring, while a second order ($N = 2$) Ogden-type spring with $\alpha_1 = 2$ and $\alpha_2 = -2$ reduces to a Mooney-Rivlin-type spring. The equations of these springs are provided in Chapter 4. Arbitrarily assigning the values of the μ_1, μ_2, and μ_3 of each spring model as 10N, 1N, and 1N, respectively and the value of α_3 as -1, the springs display the force-deformation behaviour shown in Figure B.1. Doubling each constant, in turn, produces the behaviours in Figure B.2. The constants that best model the force-deformation behaviour of the buttocks in sit-to-stand are determined in Chapter 4.

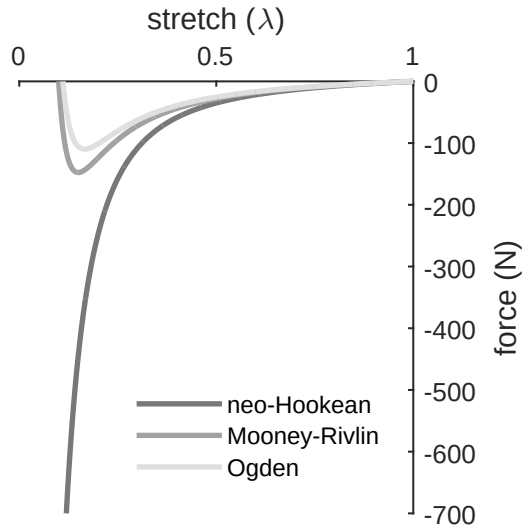

Figure B.1: Force-deformation behaviour of three hyperelastic springs.

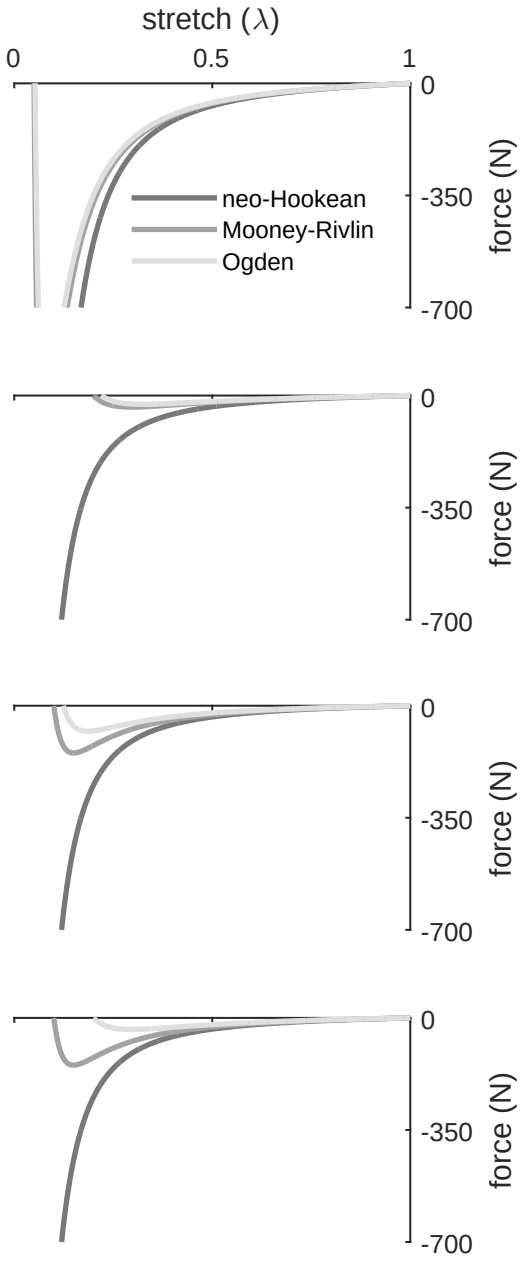

Figure B.2: Changes in force-deformation behaviour of the three springs from doubling each μ_1, μ_2, μ_3, and α_3 in turn.

Appendix C

Details of Musculoskeletal Geometry Optimization

Musculoskeletal geometry dictates muscle length, moment arms, and lines of action. This geometry in turn affects a muscles potential for force production, efficiency in producing joint torques, and resulting bone on bone forces. It is important to this work to appropriately capture these kinetics and, therefore, to appropriately represent a musculoskeletal geometry for this model.

The muscles of this model; iliopsoas, rectus femoris, vasti, gluteus maximus, hamstrings, tibialis anterior, gastrocnemius, soleus, flexor digitorum longus, and tibialis posterior, are represented using line segments connecting approximated centroids of the muscles proximal and distal attachment points according to the models of White et al. [80] and Carhart [81], as in Chapter 5. Via points (points the muscle is constrained to pass through) and wrap points (points the muscle is conditionally constrained to pass through) are included to account for interactions between muscles and, what are assumed to be, anatomical constraints such as retinacula or bone. Still, these models were not made for larger ranges of joint motions and have not been validated for this application. In this Appendix, the biomechanical model defined in Chapters 3 and 4 is actuated through the ranges of healthy

hip, knee, and ankle flexion and extension angles and a muscle model is tuned to better agree with descriptions of muscle geometry from the literature.

Defining equivalent muscle units

Of the muscles included in the model, iliopsoas, vasti, gluteus maximus, hamstrings, and gastrocnemius, are equivalent muscles and representative of a group of muscles as described by Carhart [81]. Iliopsoas is comprised of iliacus and psoas; vasti of vastus medialis, vastus intermedius, and vastus lateralis; gluteus maximus is made of its superior, middle, and inferior parts; hamstrings are comprised of semimembranosus, semitendinosus, and the long head of biceps femoris; and gastrocnemius is the combination of the medial gastrocnemius and lateral gastrocnemius. The geometry of the component parts can be seen in the model on the left of Figure C.1. The geometry of the equivalent muscles was determined as the weighted average of their comprising parts where the individual parts were weighted by their maximum isometric force capacity [114]. The hamstrings were a special case of this application where the geometries of semimembranosus and the long head of biceps femoris are described using proximal and distal attachment points alone while the geometry of semitendinosus includes two via points. These via points of semitendinosus were discarded before determining the hamstrings equivalent muscle unit. The geometry of the resulting equivalent muscle units is seen in the model on the right in Figure C.1.

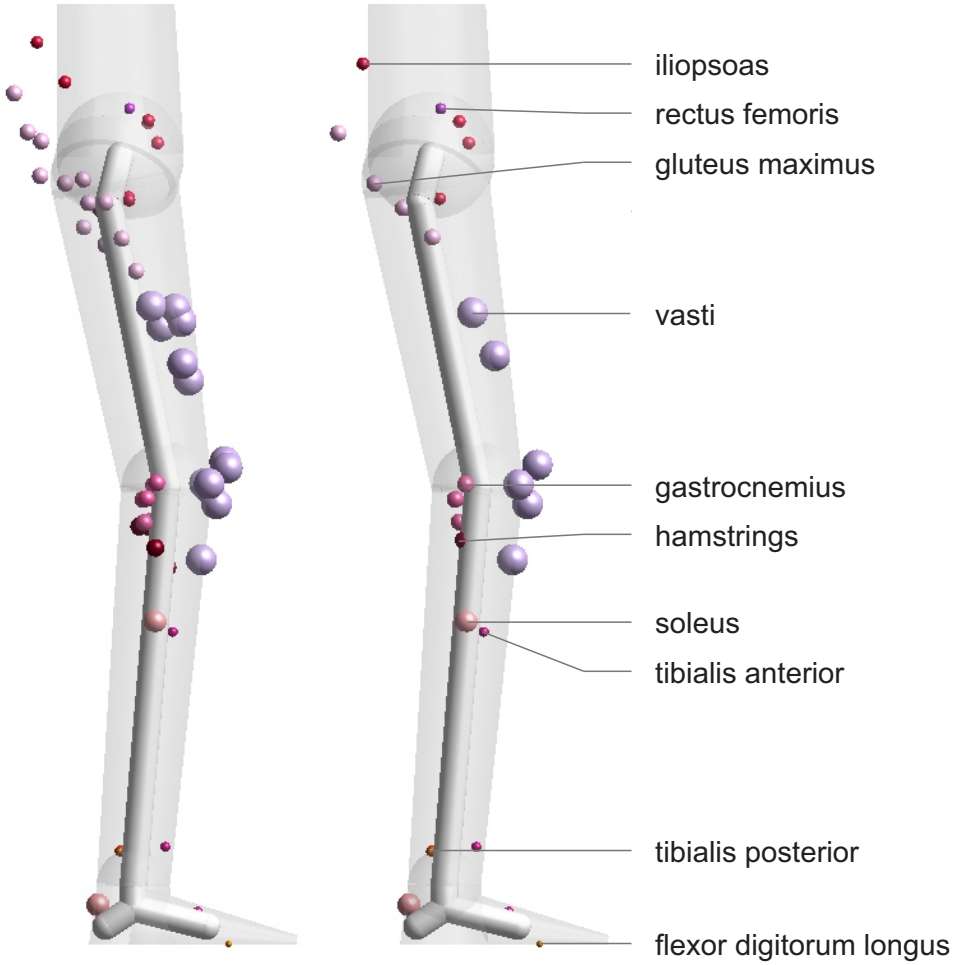

Figure C.1: Points describing musculoskeletal geometry initially (left) and after grouping equivalent muscle units (right).

Inclusion of muscle wrapping

Muscles naturally encounter anatomical constraints that influence their paths. These alterations are typically accounted for over limited ranges of motion using via points and wrap points. In addition to these points, White et al. endorse the use of a patellar pulley model for wrapping of the quadriceps over the patella across the knee joint [80]. Examination of the muscle geometry models from White et al. and Carhart indicate that this strategy of

muscle wrapping in muscle path modelling may be advantageous and possibly necessary for more muscles than the quadriceps. Strategic inclusion of muscle wrapping geometries in a musculoskeletal model alleviate issues in modelling including muscles folding back on themselves, crossing joint centres, and/or changing discontinuously in length. In the Chapter 5 model, cylindrical constraints have been included for iliopsoas, rectus femoris, vasti, and gastrocnemius according to Table C.1. The wrapping geometry about these constraints is described in Appendix D.

Table C.1: Evidence or prior modelling of anatomical obstacles.

Muscle	Cylinder	Evidence
iliopsoas	neck of the femur	iliopsoas bursa
rectus femoris	patella	patellar pulley model [18]
vasti	patella	patellar pulley model [18]
gastrocnemius	femoral condyles	gastrocnemius bursa

Cylinders in this model are defined by four values; their centre, the direction of their long axis, their radius, and sense, as described in Appendix D. The anatomy of the patella suggests a radius of 1.63 cm, which is the thickness of a patella reported in the literature [155], for the cylinders in the quadriceps models. Radii of the cylinders for the iliopsoas and gastrocnemius are more abstract and first defined as the minimum length from the nearest (via or wrap) point on the same segment to the long axis of the cylinder, as described in Equation C.1.

$$radius = \left\| point - centre - long\ axis\ \frac{(point - centre) \cdot long\ axis}{long\ axis \cdot long\ axis} \right\| \tag{C.1}$$

The cylinder about the neck of the femur was defined in the thigh frame. It was located at the centre of the femoral head and its long axis was defined in the direction of the greater trochanter. The initial radius of the cylinder was defined according to Equation C.1 as the

minimum length from the existing via point on the thigh to the long axis of the cylinder. This via point was then discarded as its contribution to the geometry of the iliopsoas is redundant by its inclusion in defining this cylinder.

The quadriceps are comprised of the rectus femoris and vasti. Their cylinders are located at the centre of the deep surface of the patella as defined in Chapter 5. Their initial long axes run medial-laterally as defined using the epicondyles of the femur.

The last cylinder is that of gastrocnemius. It is located at the midpoint between the medial and lateral femoral epicondyles, with long axis along the ray connecting these points. Its initial radius is the minimum length from the existing wrap point on the thigh to the long axis of the cylinder, found using Equation C.1.

All muscles whose geometry was described with wrap points have cylindrical constraints in the vicinity of those wrap points. It is assumed that these strategies of modelling muscle geometry are redundant and all wrap points are removed from the model. The muscle paths of this model now consist of proximal attachment points, via points, cylindrical constraints, and distal attachment points.

Optimization

All muscle geometries were optimized by the following routine, with deviations to follow. Via points, cylinder centres, cylinder long axis, and cylinder radii were varied to improve muscle moment arms without de-optimizing muscle lengths. This was accomplished by minimizing the difference between modelled moment arms and those measured experimentally as reported in the literature, while ensuring that changes to the muscle length brought the length closer to that reported in the literature [114]. Optimal muscle lengths were assumed to occur at the starting posture specified by the Surface Electromyography for the Non-Invasive Assessment of Muscles (SENIAM) project [157], when available. It was also assumed that proximal and distal attachments of the muscles are accurately described in

the model and were typically not varied. Therefore, the hamstrings and soleus are not included in this optimization because their models consist of only attachment points and are well behaved, even after mapping to this model.

The values optimized were bounded in this optimization routine. Locations of via points are allowed to vary so long as they remain within the three dimensional space defined by the maximum and minimum coordinates of the via point ± 1 cm and the next most proximal and next most distal point on the same segment. In absence of a next most proximal or distal point, the point describing the proximal or distal joint centre of the segment, respectively, was used as substitute. It was assumed that via points without influence on a moment arm are in reasonable locations and are further bound within a space extending 1 cm in all directions from their initial location. Cylinder centres and long axes were bound within 1 cm in all directions. Radii were allowed to vary between half and one and one half their initial value.

Considerations specific to each muscle are included in the sub-sections below as well as a comparison of experimental and optimized moment arms for the natural range of joint motions. For reference, the range of hip motion is 30 degrees extension to 120 degrees flexion, the range of knee motion is 135 degrees flexion to 10 degrees extension, and the range of ankle motion is 50 degrees plantar flexion to 20 degrees dorsiflexion [76] as introduced in Chapter 2.

Iiopsoas

The iliopsoas geometry had a cylinder added to it, as mentioned previously, to alleviate issues of the muscle bending over itself in deep flexion. As in the Table C.2, via points on the pelvis, the long axis, and the radius of the cylinder were optimized to best match experimental moment arms while achieving a length of 20.7 cm [114], without knowledge of the angle at which this length ought to occur.

Table C.2: Iliopsoas geometry optimized

Type	Frame	Optimized
proximal attachment	Pelvis	No
via point	Pelvis	Yes
via point	Pelvis	Yes
cylinder centre	Thigh	No
cylinder long axis	Thigh	Yes
cylinder radius	-	Yes
distal attachment	Thigh	No

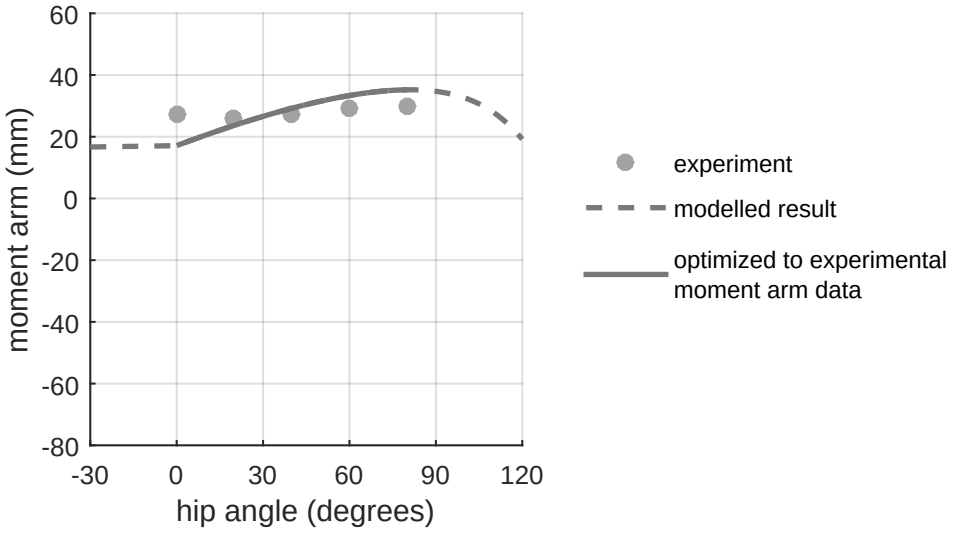

Figure C.2: Iliopsoas moment arm from experiment [148] and simulation. The root mean square error is 5.6 mm.

Rectus femoris

The rectus femoris geometry had a cylinder added to it in the location of the patella as specified by the modified patellar pulley model, described in Chapter 5. As in Table C.3, the long axis and radius of the cylinder were optimized, as well as the via points on the leg. The proximal attachment point of the rectus femoris was allowed to move up to 2 cm in all directions as, no matter the distal geometry, its original location produced negative moment arms at extreme joint angles. The length of the moment arm produced by rectus femoris at the hip has not been specified for a given joint angle, although a constant of 4.3 cm [153] was provided for a straight knee. In light of this lack of information the rectus femoris was only expected to achieve a moment arm of 4.3 cm at the hip at some hip angle while the knee was at 0 degrees. An optimal length of 42.2 cm [114] was ascribed with a knee in 'slight' flexion and the upper body 'slightly' bent backward. This length was assumed to occur when the knee was between 0 and 10 degrees flexion and the hip between 0 and 10 degrees extension.

Table C.3: Rectus femoris geometry optimized

Type	Frame	Optimized
proximal attachment	Thigh	No
cylinder centre	Thigh	No
cylinder long axis	Thigh	Yes
cylinder radius	-	Yes
via point	Leg	Yes
via point	Leg	Yes
distal attachment	Leg	No

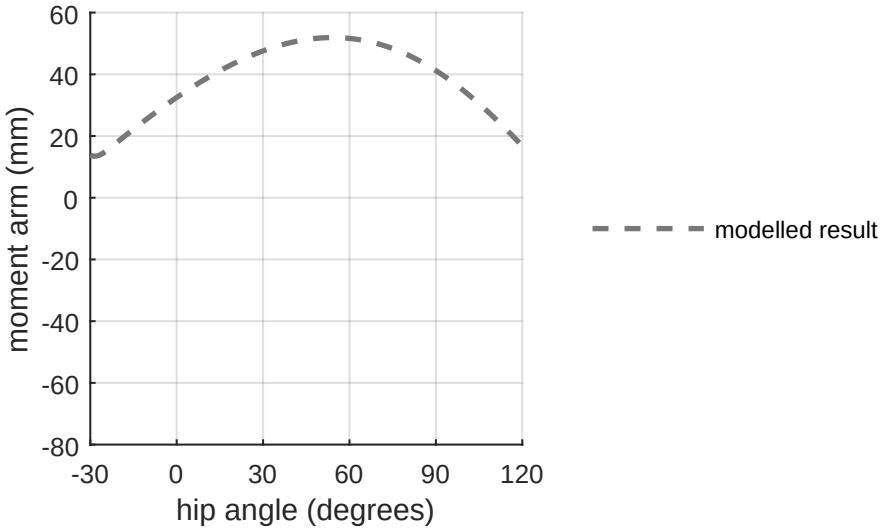

Figure C.3: Rectus femoris moment arm at the hip from simulation with a straight knee.

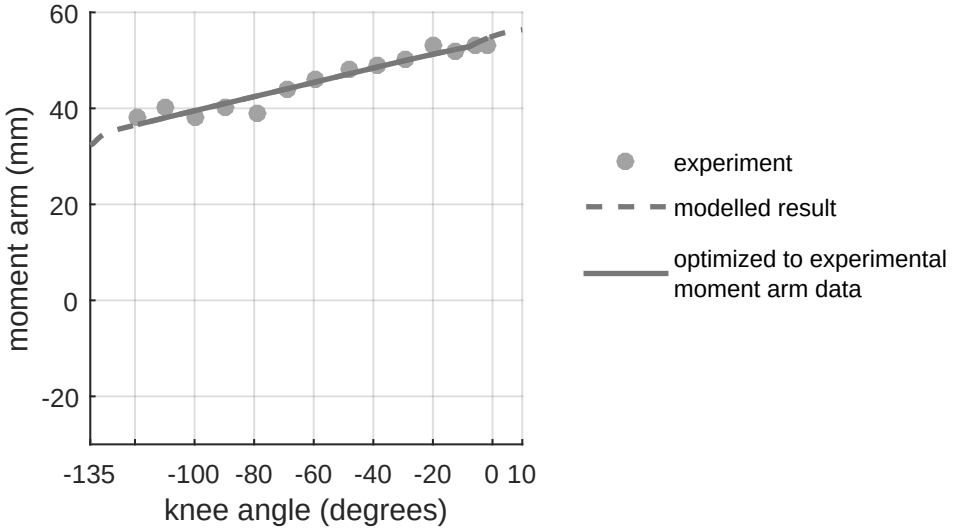

Figure C.4: Rectus femoris moment arm at the knee from experiment [149] and simulation with a straight hip. The root mean square error is 1.4 mm.

Vasti

The remaining quadriceps, the vasti, have a cylinder added to them in the location of the patella as specified by the modified patellar pulley model, described in Chapter 5. As in Table C.4, the via points on the thigh and leg as well as the long axis and radius of the cylinder were optimized to best match experimental moment arms while achieving a length of 21.8 cm [114] with the knee in 'slight' flexion, assumed between 0 and 10 degrees.

Table C.4: Vasti geometry optimized

Type	Frame	Optimized
proximal attachment	Thigh	No
via point	Thigh	Yes
cylinder centre	Thigh	No
cylinder long axis	Thigh	Yes
cylinder radius	-	Yes
via point	Leg	Yes
via point	Leg	Yes
distal attachment	Leg	No

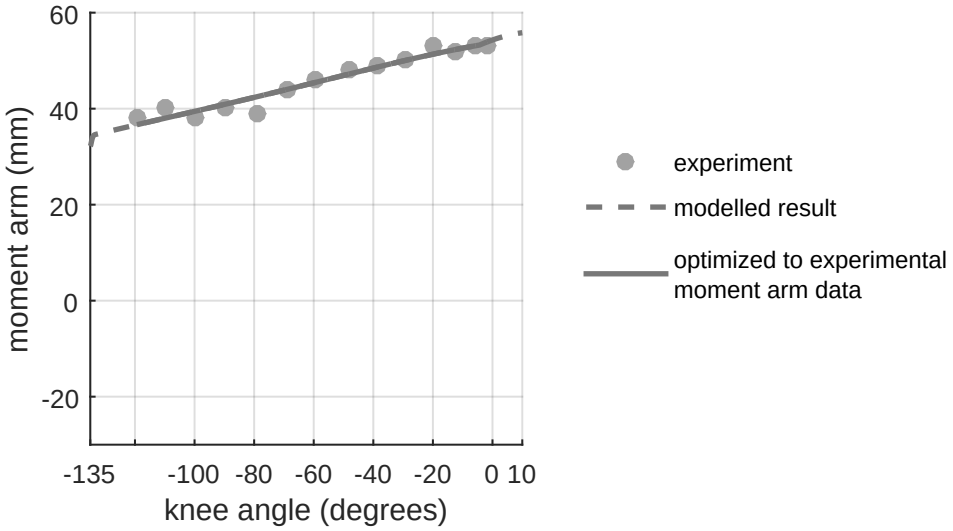

Figure C.5: Vasti moment arm from experiment [149] and simulation. The root mean square error is 1.4 mm.

Hamstrings

The hamstrings geometry was tuned to rectify the production flexion moment arms at the hip. As in Table C.5, the attachment points are optimized to best match experimental moment arms while aiming for a length of 43.7 cm [114], with the hip straight and knee flexed no more than 90 degrees.

Table C.5: Hamstrings geometry optimized

Type	Frame	Optimized
proximal attachment	Pelvis	Yes
distal attachment	Leg	Yes

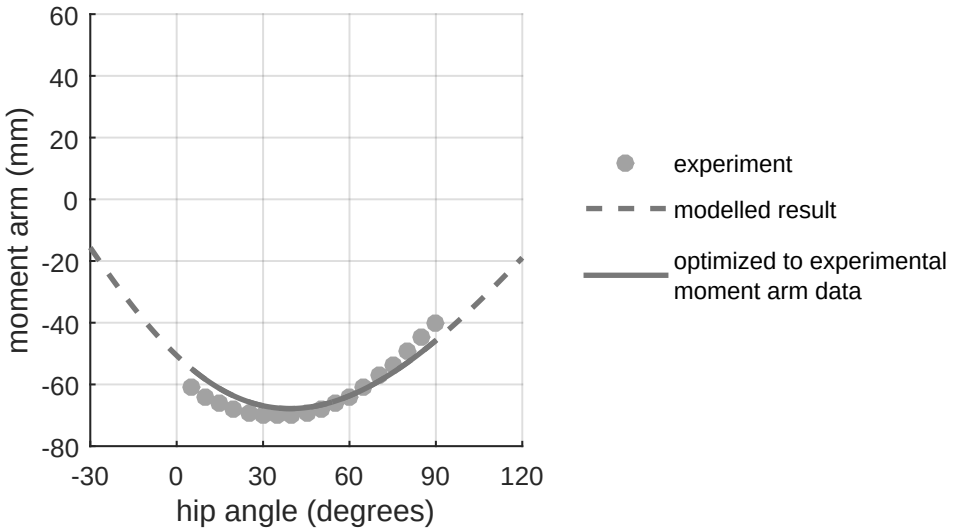

Figure C.6: Hamstrings moment arm at the hip from experiment [152] and simulation with a straight knee. The root mean square error is 3.5 mm.

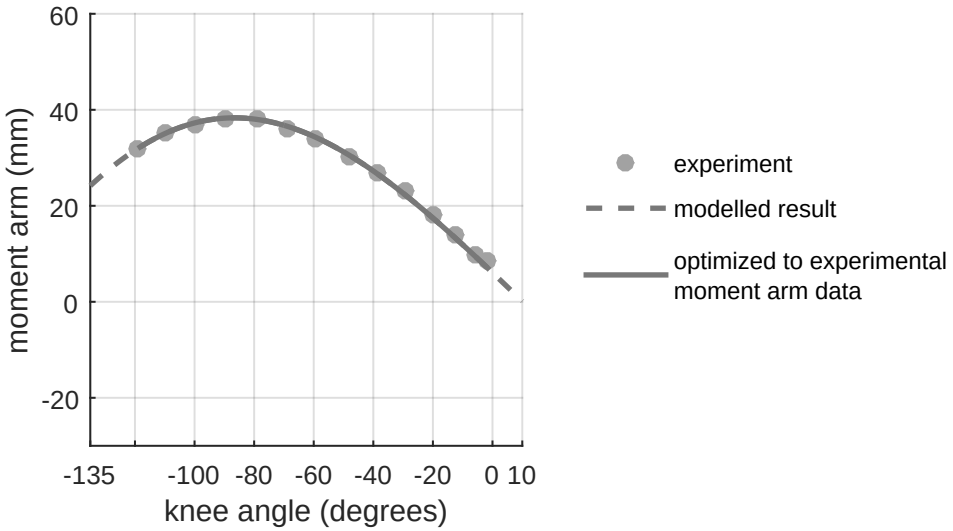

Figure C.7: Hamstrings moment arm at the knee from experiment [149] and simulation with a straight hip. The root mean square error is 0.6 mm.

Gluteus maximus

The two via points of gluteus maximus are optimized to best match the moment arm data from the literature while aiming for a length of 22.2 cm [114] in prone, assumed 0 degrees.

Table C.6: Gluteus maximus geometry optimized

Type	Frame	Optimized
proximal attachment	Pelvis	No
via point	Pelvis	Yes
via point	Thigh	Yes
distal attachment	Thigh	No

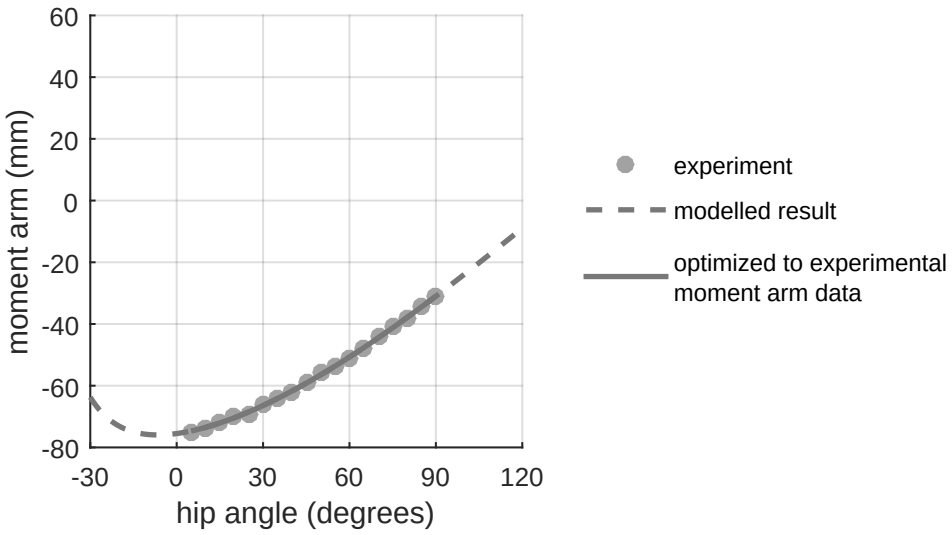

Figure C.8: Gluteus maximus moment arm from experiment [152] and simulation. The root mean square error is 0.3 mm.

Tibialis anterior

The via point of tibialis anterior was optimized to so that the moment arm produced fell within the moment arm data from the literature while aiming for a length of 31.5 cm [114] in dorsiflexion.

Table C.7: Tibialis anterior geometry optimized

Type	Frame	Optimized
proximal attachment	Leg	No
via point	Leg	Yes
distal attachment	Foot	No

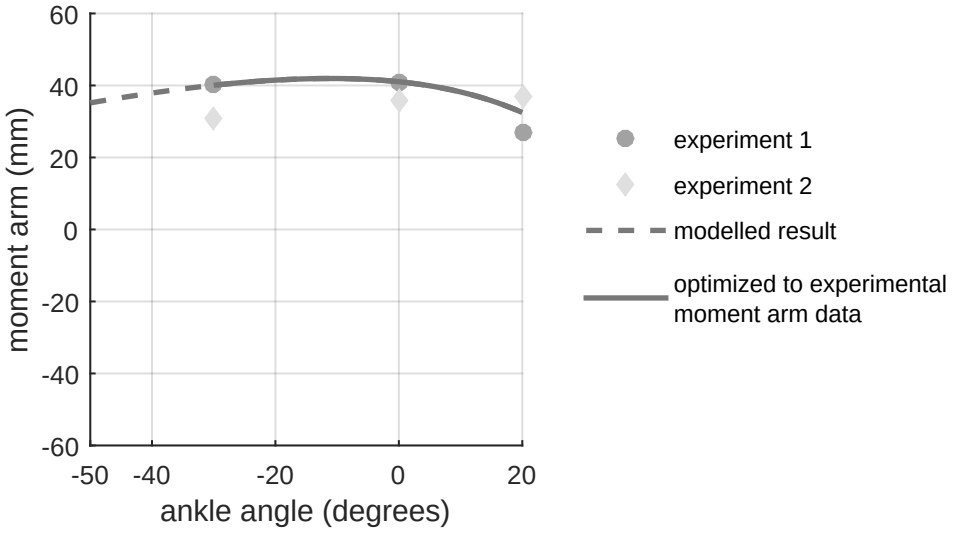

Figure C.9: Tibialis anterior moment arm from experiments 1 [154] and 2 [150] and simulation. The root mean square error is less than 0.1 mm.

Gastrocnemius

The gastrocnemius geometry had a cylinder added to it to alleviate issues of the muscle bending over itself in deep flexion. As in Table C.8, all variables other than the distal attachment point are optimized to best match experimental moment arms while achieving a length of 44.9 cm [114], with the knee straight and ankle in a neutral posture.

Table C.8: Gastrocnemius geometry optimized

Type	Frame	Optimized
proximal attachment	Thigh	Yes
cylinder centre	Thigh	Yes
cylinder long axis	Thigh	Yes
cylinder radius	-	Yes
via point	Leg	Yes
distal attachment	Foot	No

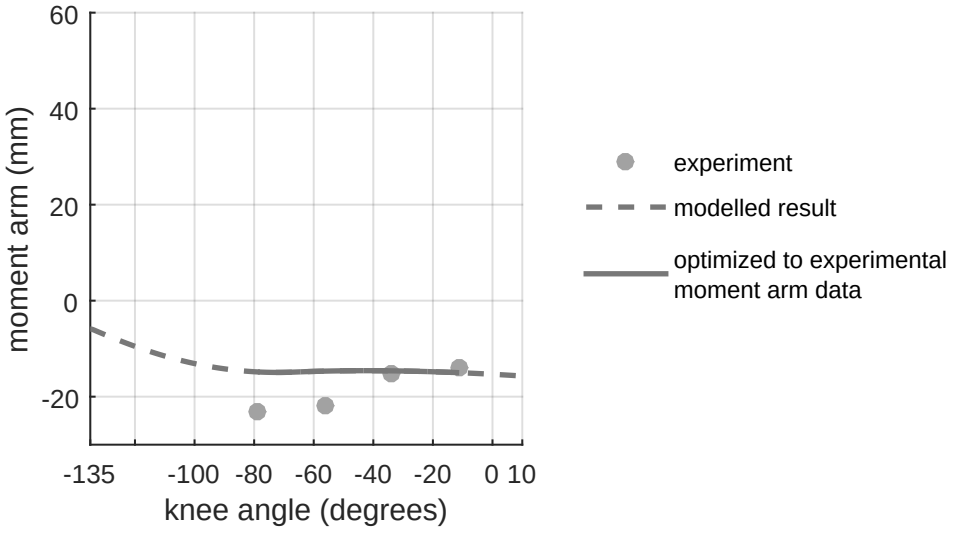

Figure C.10: Gastrocnemius moment arm at the knee from experiment [149] and simulation. The root mean square error is 5.5 mm.

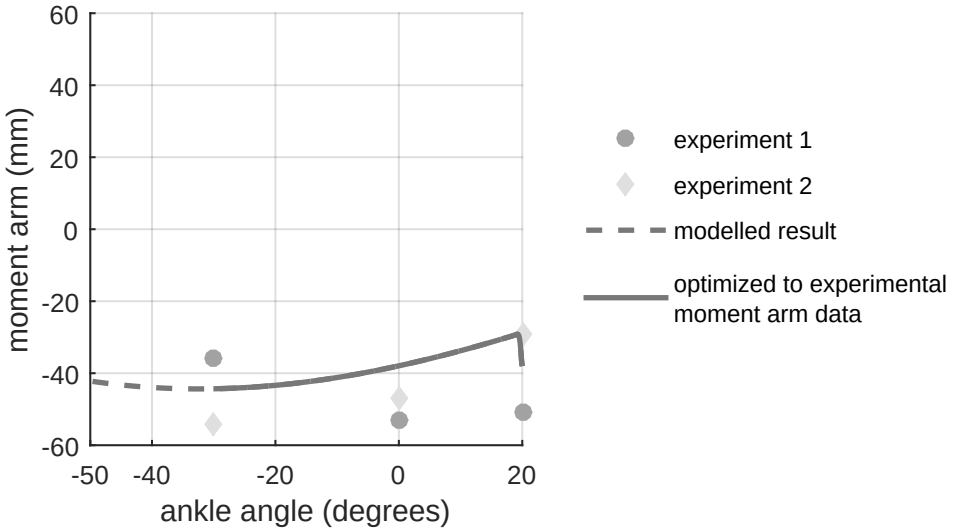

Figure C.11: Gastrocnemius moment arm at the ankle from experiments 1 [154] and 2 [150] and simulation. The root mean square error is 5.2 mm.

Flexor digitorum longus

The via points of flexor digitorum longus were optimized so that the moment arm produced fell within the moment arm data from the literature while aiming for a length of 42.3 cm [114], without knowledge of where this length ought to occur.

Table C.9: Flexor digitorum longus geometry optimized

Type	Frame	Optimized
proximal attachment	Leg	No
via point	Leg	Yes
via point	Foot	Yes
via point	Foot	Yes
distal attachment	Foot	No

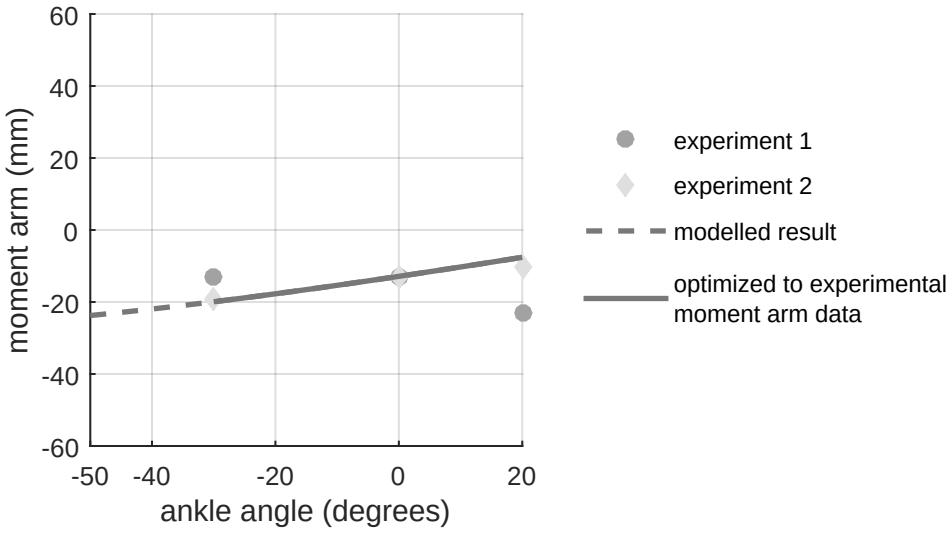

Figure C.12: Flexor digitorum longus moment arm from experiments 1 [154] and 2 [150] and simulation. The root mean square error is 1.5 mm.

Tibialis posterior

The via points of tibialis posterior were optimized to fall within the moment arm data from the literature while aiming for a length of 32.0 cm [114], without knowledge of where this length ought to occur.

Table C.10: Tibialis posterior geometry optimized

Type	Frame	Optimized
proximal attachment	Leg	No
via point	Leg	Yes
via point	Foot	Yes
distal attachment	Foot	No

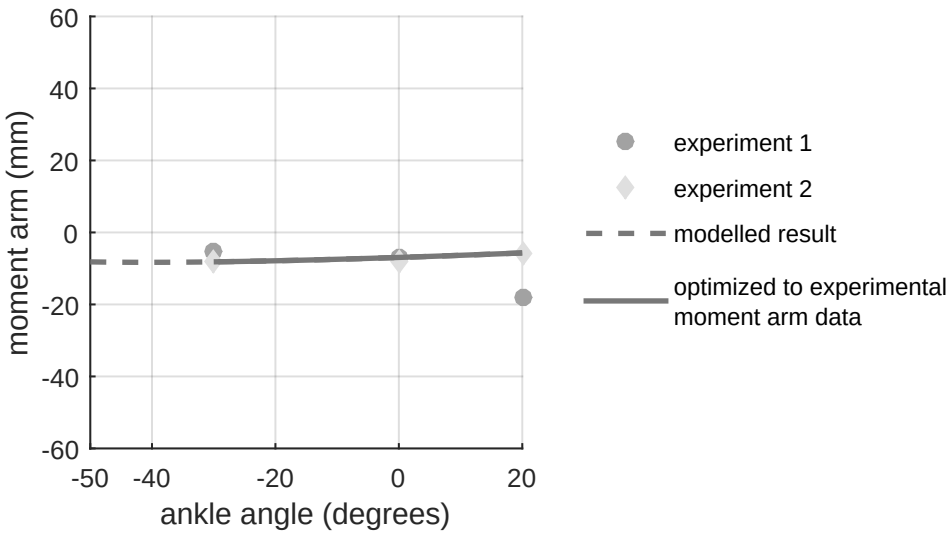

Figure C.13: Tibialis posterior moment arm from experiments 1 [154] and 2 [150] and simulation. The root mean square error is 0.2 mm.

Summary

The model identified from this optimization of musculoskeletal geometry can be seen in Figure C.14 and are provided in Table 5.1. As an improvement to the initial geometry of this model, and other models in the literature, muscles do not fold back on each other, they do not have negative moment arms, and they do not have discontinuous length profiles. In addition, the moment arms and muscle lengths produced by this model are in better agreement to experimental data reported in the literature.

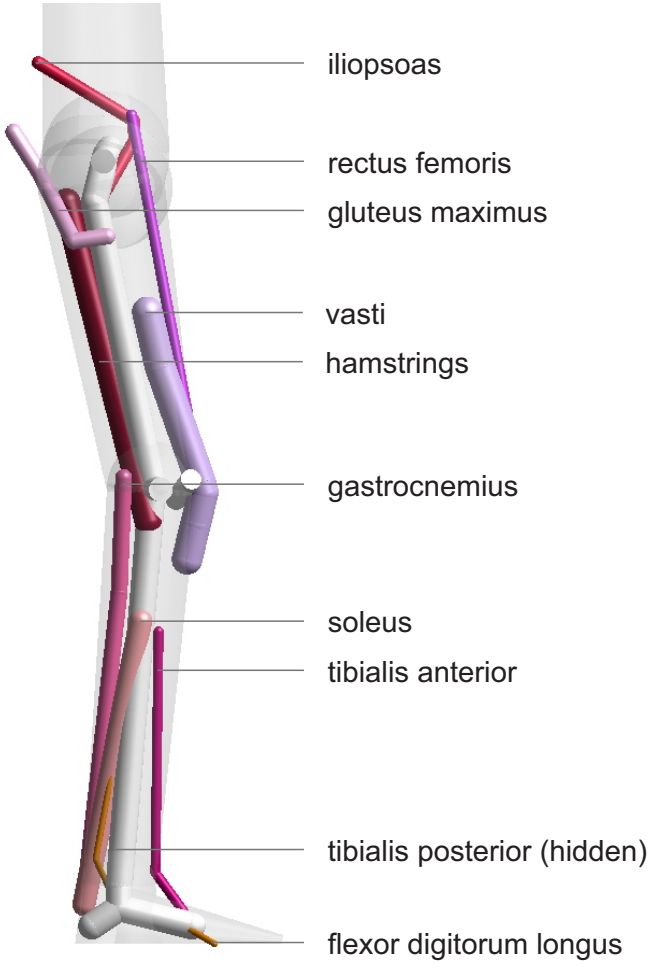

Figure C.14: The optimized musculoskeletal geometry.

Appendix D

Geometry of Wrapping a Cylindrical Constraint

One way of computationally modelling the effect of an anatomical constraint on the path of a muscle is by inclusion of a geometric obstacle in that path. The geometry of a muscle allowed to wrap freely over the surface of a frictionless cylinder of infinite length is determined as the minimum length path from the nearest proximal attachment point to the nearest distal attachment point. If the path of the muscle includes a portion wrapped over the surface of the cylinder, as seen in Figure D.1, the locations of the points of contact between the muscle and cylinder are calculated according to the equations in this Appendix.

For these calculations, the nearest proximal and distal attachment points to the cylinder are required as well as the centre of the cylinder, the long axis of the cylinder and radius of the cylinder and the sense of the wrapping geometry, as in Figure D.2. The requirement that the sense of the wrap be defined is a consequence of defining cylinders of infinite length it must be decided which side of the cylinder the muscle is to reside on. For the muscles of this work, this information is found in Table 5.1 and all cylinders lie between the muscle and the joint centre spanned. Although the vectors in the table are expressed in different body frames, they should be transformed to the same frame; for the purpose

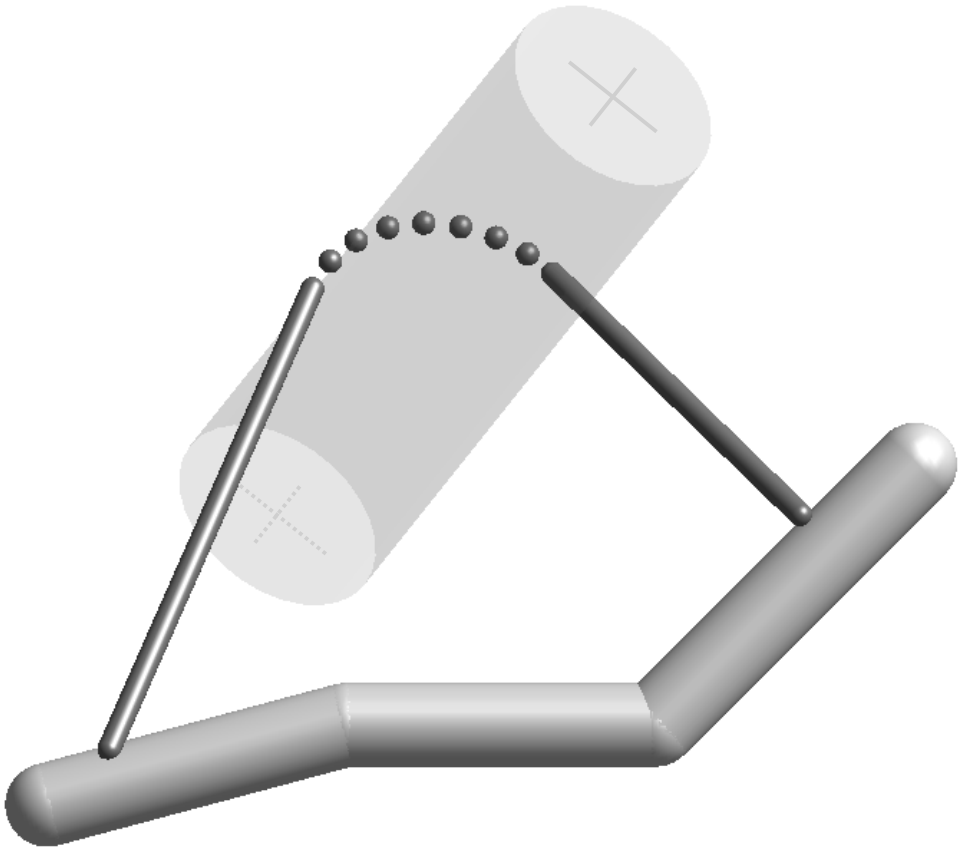

Figure D.1: The minimum length path around a cylinder. The portion of the path represented as spheres indicates where the path is on the surface of the cylinder.

of this Appendix, they are expressed in what has been called the obstacle frame, i.e. the frame where the cylinder is originally defined, as in Figure D.2.

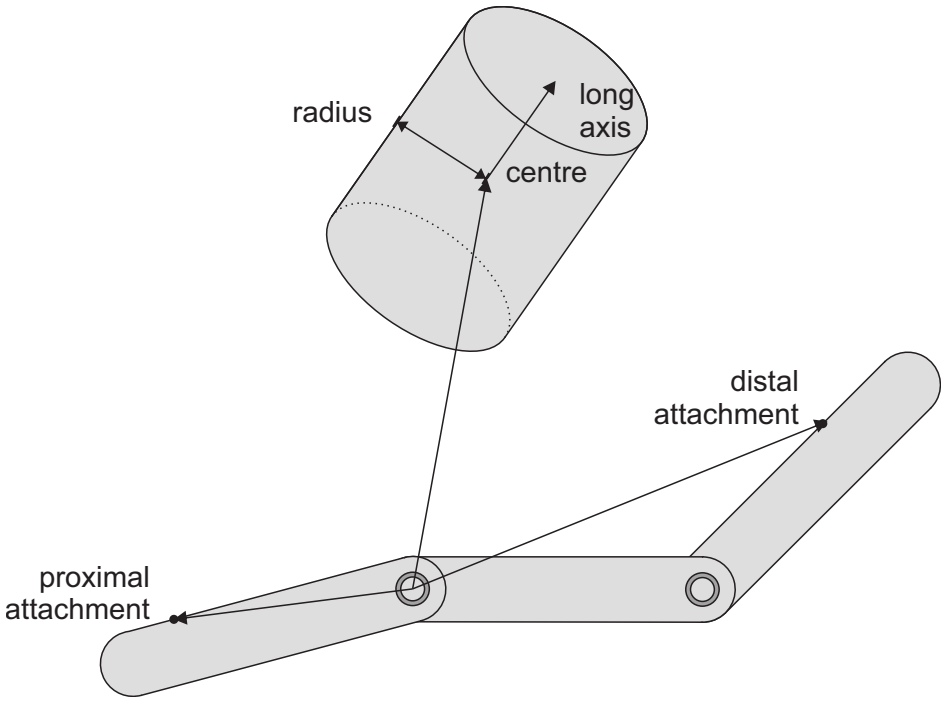

Figure D.2: Points, dimensions, and directions of interest when wrapping a cylinder.

In two-dimensions

Looking down the long axis of the cylinder, there is symmetry between a) the proximal attachment point and point of arrival to the cylinder and b) the distal attachment point and point of departure from the cylinder. These points of arrival and departure are each referred to as a point of contact in Figure D.3. Two parallel planes were conceived such that the intersection of each plane and the cylinder is a circle, the first plane passing through the proximal attachment point and the second plane passing through the distal attachment point. The geometry of each plane was evaluated separately, as follows.

First, proximal and distal cylinder local coordinate systems were defined. The z-direction is coincident with the long axis of the cylinder, as in Equation D.1. The x-direction was defined along the vector from the centre of the cylinder to the attachment

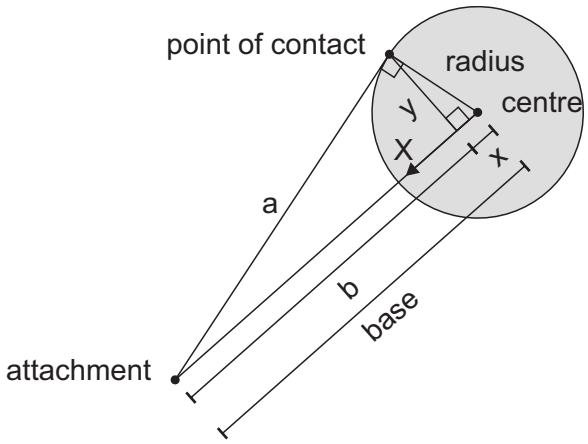

Figure D.3: The geometry at a point of contact with the cylinder.

point and the y-direction is defined to make a right-handed orthonormal system, as in Equations D.2 and D.3.

$$\hat{z} = \frac{long\ axis}{\|long\ axis\|} \tag{D.1}$$

$$\hat{y} = \frac{\hat{z} \times (attachement - centre)}{\|\hat{z} \times (attachement - centre)\|} \tag{D.2}$$

$$\hat{x} = \hat{y} \times \hat{z} \tag{D.3}$$

Assuming wrapping occurs, the muscle contacts the cylinder tangent to the surface of the cylinder, and the geometry of Figure D.3 is defined.

The point of arrival to (or departure from) the cylinder is at (x, y). These coordinates were found via Pythagorean Theorem,

$$x^2 + y^2 = radius^2 \tag{D.4}$$

$$y^2 + b^2 = a^2 \tag{D.5}$$

and a simple geometric relationship from Figure D.3,

$$x + b = base \tag{D.6}$$

Re-arranging these equations, x and y are known given the sense of the wrap which determines the sign of y.

$$x = \frac{radius^2}{base} \tag{D.7}$$

$$y = \sqrt{radius^2 - x^2} \tag{D.8}$$

Once the point of arrival, the point of departure, and the base lengths are known, both the proximal and distal sides of the wrapping geometry are considered together.

In three-dimensions

The point of arrival and the point of departure were next expressed in the same cylinder frame (either the proximal cylinder frame or distal cylinder frame). Let the points of arrival and departure be (x_a, y_a, z_a) and (x_b, y_b, z_b), respectively, where the x and y components are known.

It is next determined for which geometric arrangements wrapping will occur. Assuming the current frame is the proximal cylinder frame, wrapping occurs when $x_b < x_a$. When $x_b \geq x_a$, the muscle does not contact the cylinder and its path is a straight line from proximal to distal attachment points. When there is wrapping, the z components of the point of arrival and point of departure are determined.

Looking down the long axis of the cylinder again, the two-dimensional (2D) length of the muscle from proximal attachment point to point of arrival is $base_a$ and the 2D length of the muscle from distal attachment point to point of departure is $base_b$. The 2D length

of the muscle wrapping over the cylinder is the arc length from the point of arrival to the point of departure, where the arc angle, θ, is calculated using either Equation D.9 or D.10. The choice of arc angle equation was made to avoid small angle calculations. The muscle segments found were arrayed to form the base of the triangle in Figure D.4.

$$\theta = \arccos\left(\frac{x_b}{radius}\right) - \arccos\left(\frac{x_a}{radius}\right) \tag{D.9}$$

$$\theta = 2\ radius \sin\left(\frac{\sqrt{(x_b - x_a)^2 + (y_b - y_a)^2}}{2\ radius}\right) \tag{D.10}$$

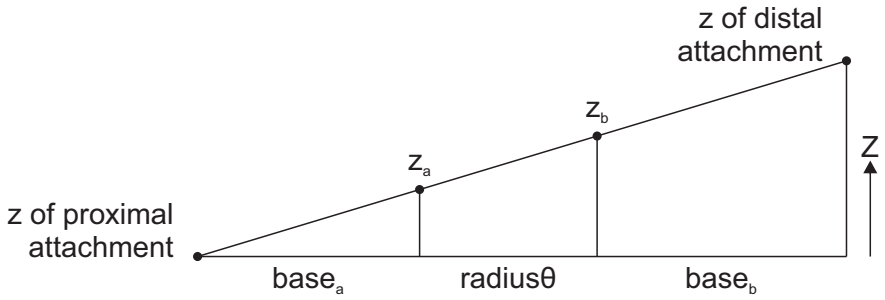

Figure D.4: Relating the two- and three-dimensional wrap through similar triangles.

Allowing the z components of the proximal and distal attachment points to be z_p and z_d, respectively, z_a and z_b are found using Equations D.11 and D.12. These equations are derived from the similar triangle relationships in Figure D.4.

$$z_a = \frac{z_d\ base_a + z_p\ radius\ \theta + z_p\ base_b}{base_a + radius\ \theta + base_b} \tag{D.11}$$

$$z_b = \frac{z_d\ base_a + z_d\ radius\ \theta + z_p\ base_b}{base_a + radius\ \theta + base_b} \tag{D.12}$$

With these final calculations the points of arrival and departure are known in a cylinder frame of reference and may be transformed to other useful frames, as in Chapter 5, to better understand the geometry of the musculoskeletal system as a whole.

Appendix E

The Routine to Determine an Optimal Sit-to-Stand

There are two itereative dynamic optimization routines used in this thesis. The first is presented in Chapter 3 and is appropriate for the torque-driven model of Chapters 3 and 4. The second routine is built on the first. It is presented in Chapter 5 and is appropriate for the muscle-driven model of that Chapter. This second routine was presented in Chapter 5 as Figure 5.9 and is presented in further detail in this Appendix as Figure E.1.

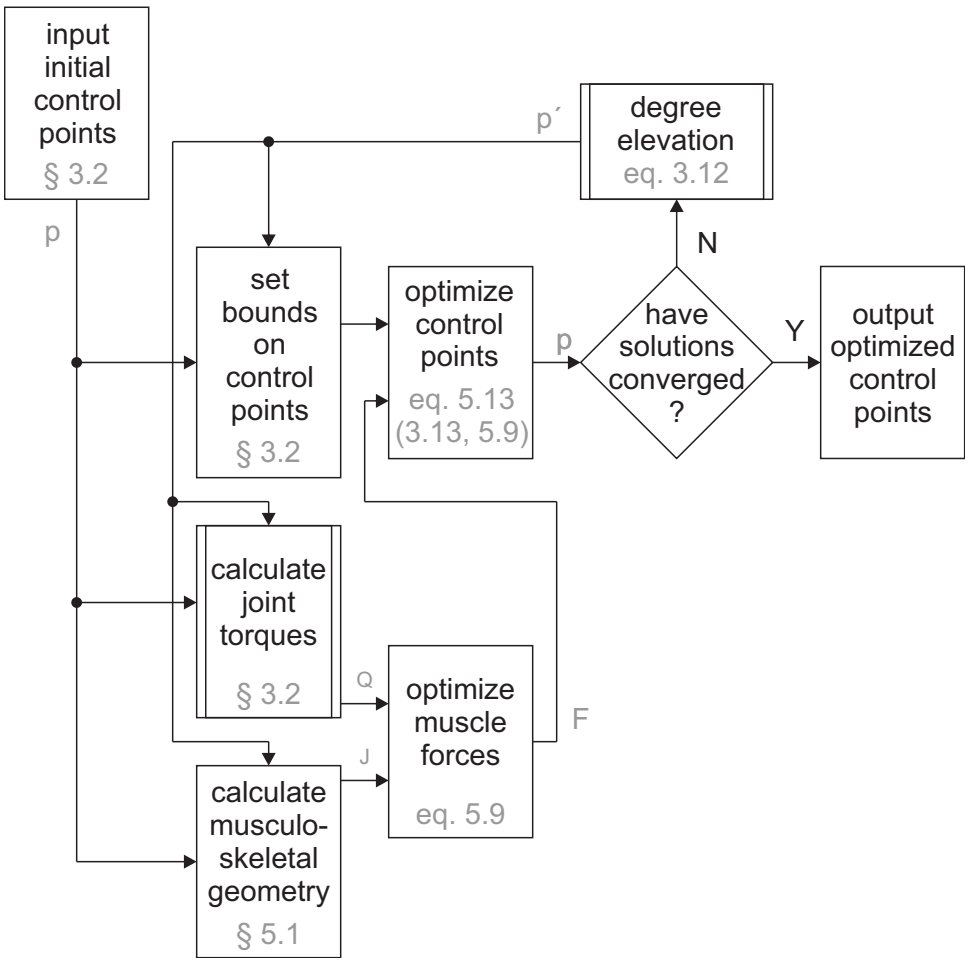

Figure E.1: The iterative routine to determine an optimal sit-to-stand for the musculoskeletal model. The thesis sections and equations most relevant to execution of this routine are provided in gray. Routine signals are labelled along arrows in gray.